University of Venda

SCHOOL OF ENVIRONMENTAL SCIENCES

DEPARTMENT OF MINING AND ENVIRONMENTAL GEOLOGY

EVALUATION OF POTENTIAL ACID MINE DRAINAGE: A CASE STUDY OF THE ALBERT SILVER MINE, MPUMALANGA PROVINCE, SOUTH AFRICA

BY

NGOMANE STANELY SIMON

STUDENT NUMBER – 14005133

MASTER'S DISSERTATION SUBMITTED TO THE HIGHER DEGREES COMMITTEE, SCHOOL OF ENVIRONMENTAL SCIENCES, UNIVERSITY OF VENDA, AS A MINIMUM REQUIREMENT FOR MASTER OF EARTH SCIENCES IN MINING AND ENVIRONMENTAL GEOLOGY

SUPERVISOR: EMERITUS PROF. J.S. OGOLA

CO-SUPERVISOR: DR. H.R. MUNDALAMO

CO-SUPERVISOR: PROF. DR. HABIL. CH. WOLKERSDORFER

SEPTEMBER 2020

DECLARATION

I, **NGOMANE STANELY SIMON**, declare that this dissertation submitted to the Department of Mining and Environmental Geology, School of Environmental Sciences, University of Venda, for Master of Earth Sciences in Mining and Environmental Geology has not been submitted before for any degree or examination at this or any other institution and that it is my own work in design and Execution; and that all sources used in this study have been cited and acknowledged.

Student's Signature  Date: 2020/06/21

(Mr S.S. Ngomane)

Supervisor's Signature  Date: 2020/06/21

(Emeritus Prof. J.S. Ogola)

Co-Supervisor'Signature  Date: 2020/06/21

(Dr H.R. Mundalamo)

Co-Supervisor' Signature  Date 2020-06-16

(Prof. Dr. habil. Ch. Wolkersdorfer)

DEDICATION

This Dissertation is dedicated to my family at large especially my mother Elizabeth Taliyane Manikela and my cousin Thomas Mkhabela for their love, support and words of encouragement that gave me strength to keep moving.

ACKNOWLEDGEMENTS

Firstly, I would like to thank the Almighty God for stretching his love, giving me the opportunity and strength to make it up this far.

I would also like to pass my sincere appreciation to the Department of Mining and Environmental Geology at the University of Venda and the Mine Water Management Laboratory at TUT for the apparatuses that I used during the study. I would also like to extend my sincere gratitude to my supervisor Prof. J.S. Ogola and my co-supervisors Dr. H.R. Mundalamo and Prof. Ch. Wolkersdorfer for their immeasurable supervision, in estimated patience and constructive disparagement during the production of the dissertation.

Special thanks go to my family for their support and assistance during the study, my mother Elizabeth Taliyane Manikela and my cousin Thomas Mkhabela for their financial and emotional support not forgetting my friends for their spiritual upliftment.

I would like to convey my sincere appreciation to my research assistants; Dr. T. Mahlangu, Lutento Ramalata and Bridget Nemadodzi. I also appreciate the support from my friends throughout my time at the university.

Finally, the study was supported by the Thrip funding thus they are hereby dearly acknowledged. Opinions expressed and conclusions arrived at, are those of the author and not necessarily to be attributed to the sponsor.

ABSTRACT

Generally, mining produces mine wastes that contain sulfide minerals that have potential to produce acid mine drainage. Albert Silver Mine conducted mining of the silver-sulfide bearing ore from 1885 to 1914. However, at the time, little attention was being given to acid mine water generation. This study investigated the current status of acid mine drainage on the Moses river and the potential of the silver ore to produce acid mine drainage. This was achieved through investigating both sulfide and carbonate minerals in the silver ore. The sulfide and carbonate minerals were investigated using X-ray diffraction spectroscopy and petrographic studies. The current status of acid mine generation of the site was also studied through water quality analysis of the Moses River. Static and kinetic tests acid mine drainage prediction techniques were conducted to determine the acid generation potential of the silver ore.

The sulfide minerals discovered within the silver ore are pyrite, arsenopyrite, chalcopyrite and galena, the carbonate mineral discovered was calcite (5.6 wt%). The neutralisation capacity of the rock samples was high as confirmed by the values of NNP and NPR, ranging from 20.75 to 80.65 kg $CaCO_3$/t and 2.64 to 115.91 kg $CaCO_3$/t, NAG_{pH} ranged from 2.3 to 5.37 and the $NAG_{pH7.0}$ ranged from 0.1976 to 12.378 kgH_2SO_4/t. The kinetic tests yielded neutral pH values ranging from 5.98 to 8.02, electrical conductivities from 13.85 to 147.5 µS/cm, acidity from 0.04 to 0.25 mmol/L, alkalinity from 0.01 to 0.704 mmol/L, sulfate concentrations from 0 to 8 mg/L and ferrous iron concentrations from 0 to 0.18 mg/L. The water chemistry results from the Moses River yielded pH values from 7.00 to 7.78, electrical conductivities from 240 to 520 µS/cm and very low metal concentrations; lower than WHO and S.A. water quality guidelines.

Pyrite was framboidal in morphology, disseminated and with large surface areas. Mineralogically, the study discovered sulfide minerals and calcite was the only carbonate mineral. According to the water quality analysis there is no threat of acid mine drainage at the Moses river, the outcomes of the acid mine drainage prediction led to the conclusion that there is no potential acid mine drainage issue.

Keywords: *Albert Silver Mine, Acid Mine Drainage, Acid potential, Acid Neutralisation, Sulfide minerals, Carbonate minerals.*

TABLE OF CONTENTS

LIST OF FIGURES

LIST OF TABLES

LIST OF ACRONYMS AND ABBREVIATIONS

AAS	Atomic Absorption Spectrometer/Spectroscopy
ABA	Acid Base Accounting
AMD	Acid Mine Drainage
AP	Acid Potential
BIC	Bushveld Igneous Complex
CGS	Council for Geosciences
DO	Dissolved Oxygen
EC	Electrical Conductivity
GIS	Geographical Information System
GPS	Global Positioning System
IC	Ion Chromatography
LGS	Lebowa Granite Suite
NAG	Net Acid Generation
NP	Neutralisation Potential
NNP	Net Neutralising Potential
NPR	Net Potential Ratio
PPL	Plain Polarised Light
RGS	Rashoop Granophyre Suite
RLS	Rustenburg Layered Suite
TDS	Total Dissolved Solids
UK	United Kingdom
USA	United States of America
XPL	Crossed Polarised Light
XRD	X-Ray Diffraction Spectrometry
XRF	X-ray Fluorescence Spectrometry

1. CHAPTER ONE: INTRODUCTION

1.1 Background

Mining is important to the world economy and it is an important part of the advancement and improvement on the planet today. Generally, mining produces mine wastes that contain sulfide minerals such as pyrite and marcasite. These minerals have a high potential for acid mine drainage (AMD) generation due to oxidation reaction that takes place in the presence of water and oxygen. AMD has the ability to leach metals from the surrounding rocks. According to Hamilton *et al*. (1999), these metals have verifiably brought about ecological distruction with examples including Fly River, Papua New Guinea; Iron Mountain, California, USA; Kalgoorlie, Australia and Wheal Jane, UK. In South Africa, AMD is one of the major environmental effects as it renders water unfit for domestic, industrial and agriculture use (Steyl, 2012).

In the past, there were no legal frameworks or guidelines to protect the environment from the negative effects of mining. However, today there are legal frameworks to protect the environment from such effects. The legal frameworks have mandated the mining companies to come up with proactive strategies for the protection of the environment. One such strategy is to undertake predictive studies on AMD long before mining takes place. Laboratory leach tests involving both static and kinetic tests are one of the commonly utilised approaches in determining the drainage chemistry of the mine waste. Nevertheless, the weaknesses and vulnerabilities related to laboratory scale tests have prompted the development of geochemical models which can predict the time-related concentration profiles of leachates (Ferguson, 1986; Ferguson and Erikson 1987; Lawrence, 1989).

The focus of this study was to establish the AMD potential at the Albert Silver Mine in Mpumalanga Province of South Africa. This involved petrographic studies, geochemical analysis and AMD prediction tests of the mineralised host rocks. There are no known studies conducted at the site to ascertain the AMD potential.

1.2 Study Area

1.2.1 Location

Albert Silver Mine is found on the farm Roodepoortjie 250JR, at the Thembisile Hani Municipality. It is located approximately 28 km to the SE from the main Kwa-mhlanga location; the municipality frame shows the Thembisile Hani municipality (light blue) where the mine is located (red point) and the aerial view shows the Albert Silver mine area (purple frame) (Fig. 1.1). Geologically, it is found in the Verena granites along the Moses River.

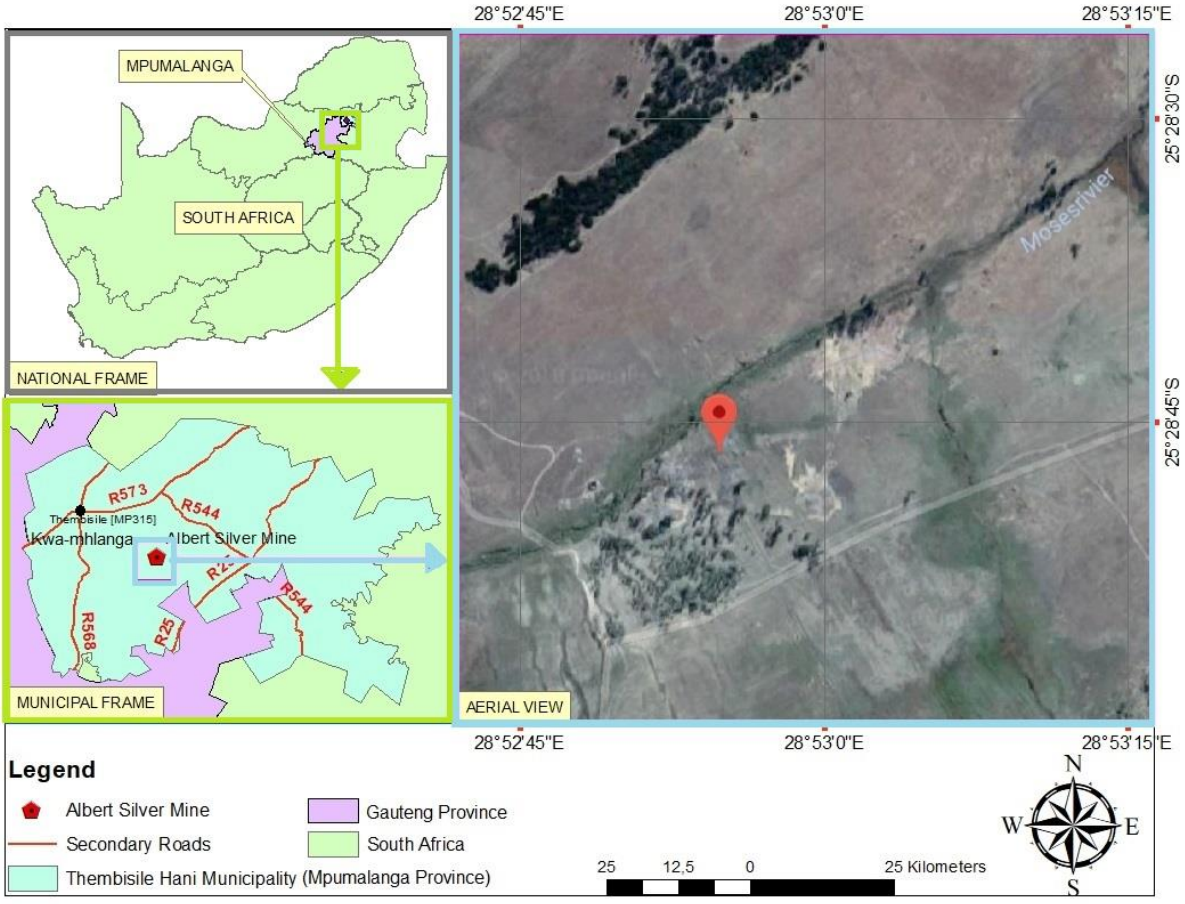

Figure 1.1: Location map of the study area.

1.2.2 Climate

The premises of the mine and other surrounding areas experience very hot summer days and cold nights. The temperature at this area is cold during winter seasons with temperature reaching below 0 °C (Fig. 1.2). The hot summer days are about 35 °C. It

has a relatively low rainfall that makes it to be classified as a dry area with rainfall estimated at 6 mm per annum. Summer is the only wet season in this area with rainfall occurring between November and March with an average rainfall of approximately 30 mm. The long periods of dryness lead to this place being classified as drought stricken area (Potop and Soukup, 2008).

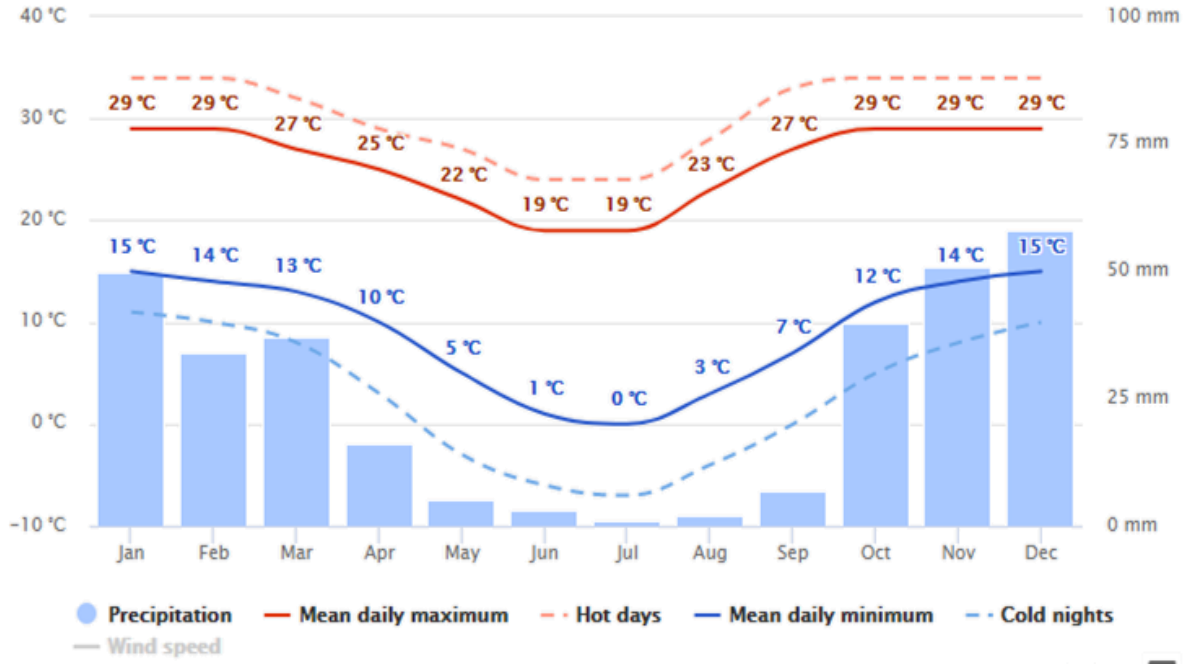

Figure 1.2: Climatic condition of the study area during summer and winter (Meteoblue, 2018).

1.2.3 Topography and Drainage

Topography is undulating farmland with delicate slopes and granitic outcrops, where surface depression is caused by dyke intrusions, for the most part. The mine is situated on and near the SE bank of the Moses River, which is a perennial river with water flow throughout the year due to numerous natural wetlands that feed into it.

1.2.4 Vegetation and Soil Cover

The study area is dominated by tall grasses as the dominating vegetation, while pine trees are the dominating tree type. The dispersed vegetation might result from historic farming taking place at and around the study area (Figure 1.3). The study area is dominated by sandy soil with gravel within the mining lease and this might be

due to past mining activities; while clay soils dominate the lower part of the area along the Moses River.

1.3 Problem Statement

Albert Silver Mine ended operations in 1914 with operations having taken place on the Albert lode which had a high content of sulfide minerals such as chalcopyrite, pyrite, galena, bornite, sphalerite and arsenopyrite. Some of these minerals might pose a high potential of AMD formation. Through the mine lease flows a perennial river known as Moses River, which potentially receives residual contaminants washed by rainfall from the mined area. The company called Lerama Resources indicated that if the Albert Silver Mine project receives sufficient funding, it might be re-opened again. According to the documented literature, the geological situation of the deposit is well studied by Champion (1970), Robb *et al.* (1994) and Meulenbeld *et al.* (2014). However, there was no study on the AMD potential so far.

(a) **(b)**

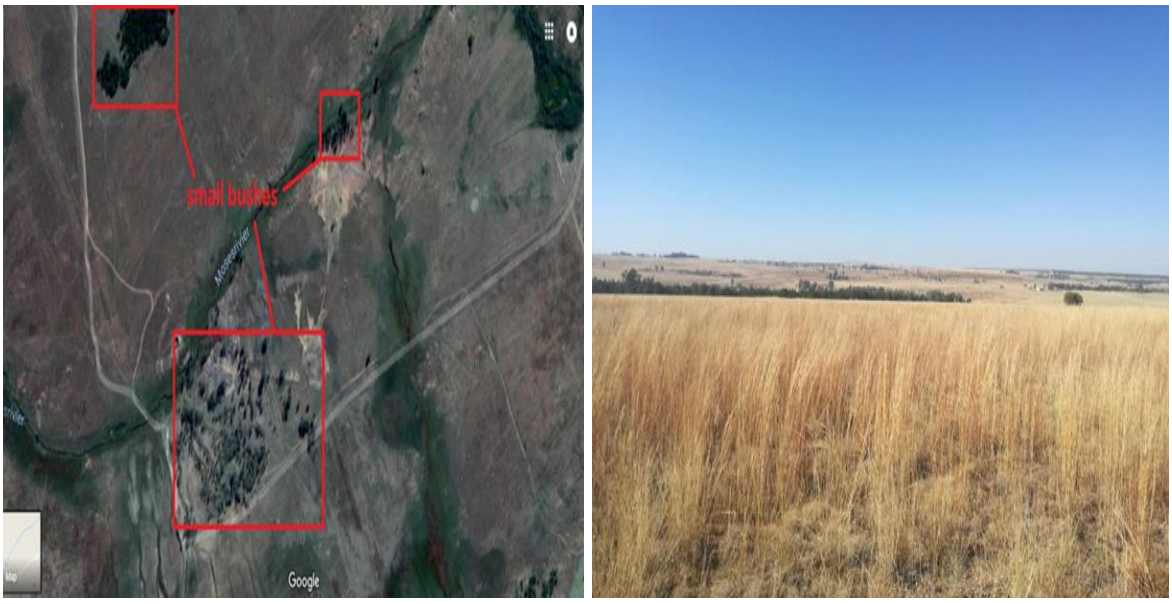

Figure 1.3: Vegetation cover of the study area; (a) sparsely distributed small bushes and (b) dominant grass.

1.4 Justification

This study has attempted to provide understanding and knowledge of possible contamination of the Moses River because of the effluents of the mine including any

metal loading. It provides sufficient information on the potential AMD in relation to future mining of the deposit. It is documented that there is still enough silver left underground and it is proposed that the site might be worked in the future. Thus, the findings of this study provided information on the potential for AMD generation from the Albert lode and mineralised host rocks. This will be beneficial to the mining company to develop a strategy of managing AMD prior to actual mining and will highly assist the mining company to avoid costs that comes with management of AMD.

1.5 Research Questions

- What is the nature of sulfide minerals in the silver ore mineralisation that may be responsible for the generation of acid mine drainage at the study area?
- What are the carbonate minerals and the extent of their occurrence in the silver ore mineralisation that may be responsible for the neutralisation of acid mine drainage at the study area?
- What is the current status of acid mine drainage at the Moses River?
- What is the potential of the silver ore to produce acid mine drainage at this deposit?

1.6 Objectives

The main objective of the study is to evaluate the potential of AMD at the Albert Silver Mine in Mpumalanga Province and the extent to which it might pollute Moses River.

Specific Objectives were to:

- determine the sulfide minerals and their characteristics in the silver ore that may be responsible for the AMD generation using X-ray diffraction (XRD) and petrographic studies;
- Identify the carbonate minerals in the silver ore that may be responsible for the neutralisation of AMD, using X-ray diffraction (XRD) and petrographic studies;

- evaluate the current status of AMD in the Moses River within the study area by conducting tailings geochemical analysis, water sample analysis and stream sediment geochemical analysis; and
- investigate the acid generation and neutralisation potential of the silver ore and mineralised host rock through prediction tests (static and kinetic).

2. CHAPTER TWO: LITERATURE REVIEW

2.1 Geology of the Bushveld Igneous Complex

2.1.1 Regional Geology

The rock sequence of the Bushveld Igneous Complex from the oldest to the youngest is as follows: Transvaal Supergroup, Rooiberg Group, Rustenberg Layered Suite (RLS), Rashoop Granophyre Suite (RGS), Lebowa Granite Suite (LGS), Alkaline intrusions (Fig. 2.1). According to a review conducted by Kinnaird (2005), it was stated that the Palaeoproterozoic Bushveld Igneous Province in South Africa is comprised of: a group of mafic sills that intruded the floor rocks of the Transvaal Supergroup. Bimodal but the Rooiberg Group volcanic rocks which are one of the biggest pyroclastic areas on earth covering approximately 50 000 km^2 with a thickness up to 3 km.

The Rustenburg Layered Suite (RLS) is the biggest and most seasoned mafic layered rock compared to other igneous complexes (Cawthorn and Walraven, 1997). This layered suite covers a region of roughly 65 000 km^2 and includes anorthosites as well as mafic and ultramafic cumulates (Harmer, 2000). The Rashoop Granophyre Suite was emplaced at the contact between the Lebowa Granite Suite and the Rustenburg Layered Suite. The Rashoop granophyre contained metamorphosed sediments and intrusive acidic rocks. The different satellite intrusions are the youngest lithologies and are of the same age including the Molopo Homesteads and Nkomati (Uitkomst).

The central portions of the Bushveld Complex consist of granites which fall under the LGS and also the granophyres of the RGS are found on the central portion (De Bruiyn, 1980). The LGS contains numerous granite types, with the Nebo Granite being the dominating type (Kleeman and Twist, 1989). Locally, the different types were differentiated by their colour, mineralogy or texture, where in all of them feldspars (orthoclase and plagioclase), quartz, biotite, hornblende and additional muscovite, zircon, apatite, titanite and minor oxides occured. According to Ferré *et al*. (1999), the granites occurred as laccolithic emplacement by roof uplift as sequential sheet-like intrusions of magma along the roof of the RLS. There are many

reasons regarding the origin of the granophyres, which includes its plutonic origin as an equivalence of the dacites.

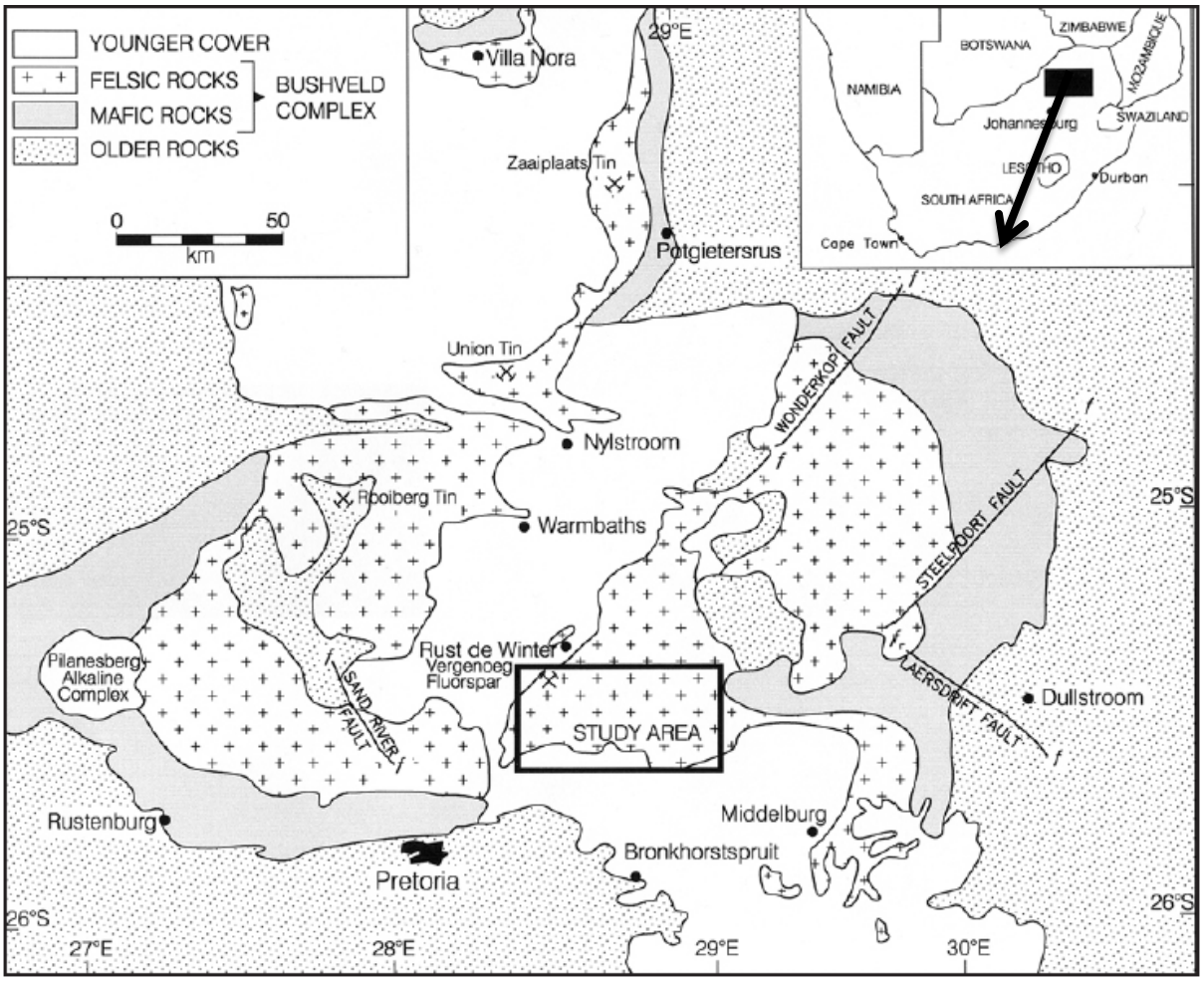

Figure 2.1: Simplified geological map of the Bushveld Igneous Complex (modified from Bailie and Robb, 2004).

A large number of these formations show localised contrasts, varieties and origins, with most granophyre being the intrusive hypabyssal reciprocals of the Rooiberg Group, and they began from magmatic forms (Walraven, 1987; Hatton and Schweitzer, 1995). The granophyres were dated to at Pb-Pb age of 2053 ± 12 Ma and have intermediate contacts with Rooiberg Group volcanic rocks (Viljoen, 2016). The Rooiberg Group progresses from dacites and rhyodacites below the sequence to rhyolites at the top (Schweitzer *et al*., 1995). Dating through Pb-Pb single zircon gives ages of approximately 2061 ± 2 Ma (Walraven, 1997), and it was noted that the granites intruded after the extrusion of the last Rooiberg Group rhyolite (Schweitzer *et al*., 1997).

2.1.2 Local Geological Situation

The mine lies within the SE flank of the granite phase of the Bushveld Igneous Complex. This granite is mainly a pink porphyritic variety and it is either coarse or fine-grained, corresponding to the Bobbejaankop and Lease granite phases respectively (Champion, 1970). The two varieties appear to occur in patches throughout the area and are interbedded in places. In addition, a few small patches of medium-grained grey granite were also encountered in the immediate vicinity of the mine (Robb *et al.,* 1994). Quartz-hematite veins are found throughout the entire area as well as to the S and N of Roodepoortjie (Robb *et al.,* 1994) (Fig. 2.2). All veins strike roughly EW and can be located as hard red-brown gossan outcroppings across the farm tracks. A large diabase dike traverses the area from SE to NW, cutting through both the Albert lode and the minor intermediate lodes N of it (Champion, 1970; Robb *et al.,* 1994; Bailie and Robb, 2004). The eastern sector of the Albert lode is displaced northwards relative to the western sector and the displacement was formed by the dyke (Champion, 1970).

According to Bailie and Robb (2004), the Albert silver deposit is type III: Sulfide-carbonate ore bodies (base and precious metal rich). This criterion was developed by Crocker (1979) and Crocker *et al*. (2001). The Cu-Pb-Zn-Ag-carbonate association is the major part of the criteria. The lodes on the Roodepoortjie farm comprise the Albert lode in the S which has been randomly divided into the western and the eastern sectors by the dyke. In addition to the Albert lode, there are minor intermediate lodes and the northern lode which has high uranium-hematite contents (Robb *et al*., 1994). Apart from the Albert lode, none of the other bodies possess wall rock alteration zones of any magnitude (Crocker *et al*., 2001). According to Champion (1970), the relatively limited alteration zone along the southern flank of the Albert lode considered in conjunction with the pronounced displacements encountered in the lode suggests that the lode strikes on an EW fault on its southern flank, this resulted in the erosion of part of the alteration zone during and after displacement. The Albert vein outcrops on the surface close to the Moses River. Along the southern edge of the deposit, the vein rises to 0.3 meters above surface level (Van Zijl, 1965). However, on the northern edge, the vein comprises of a

quartz-hematite mineralisation and ascends 2 m over the granite alteration zone which is weathered by the Moses River (Champion 1970).

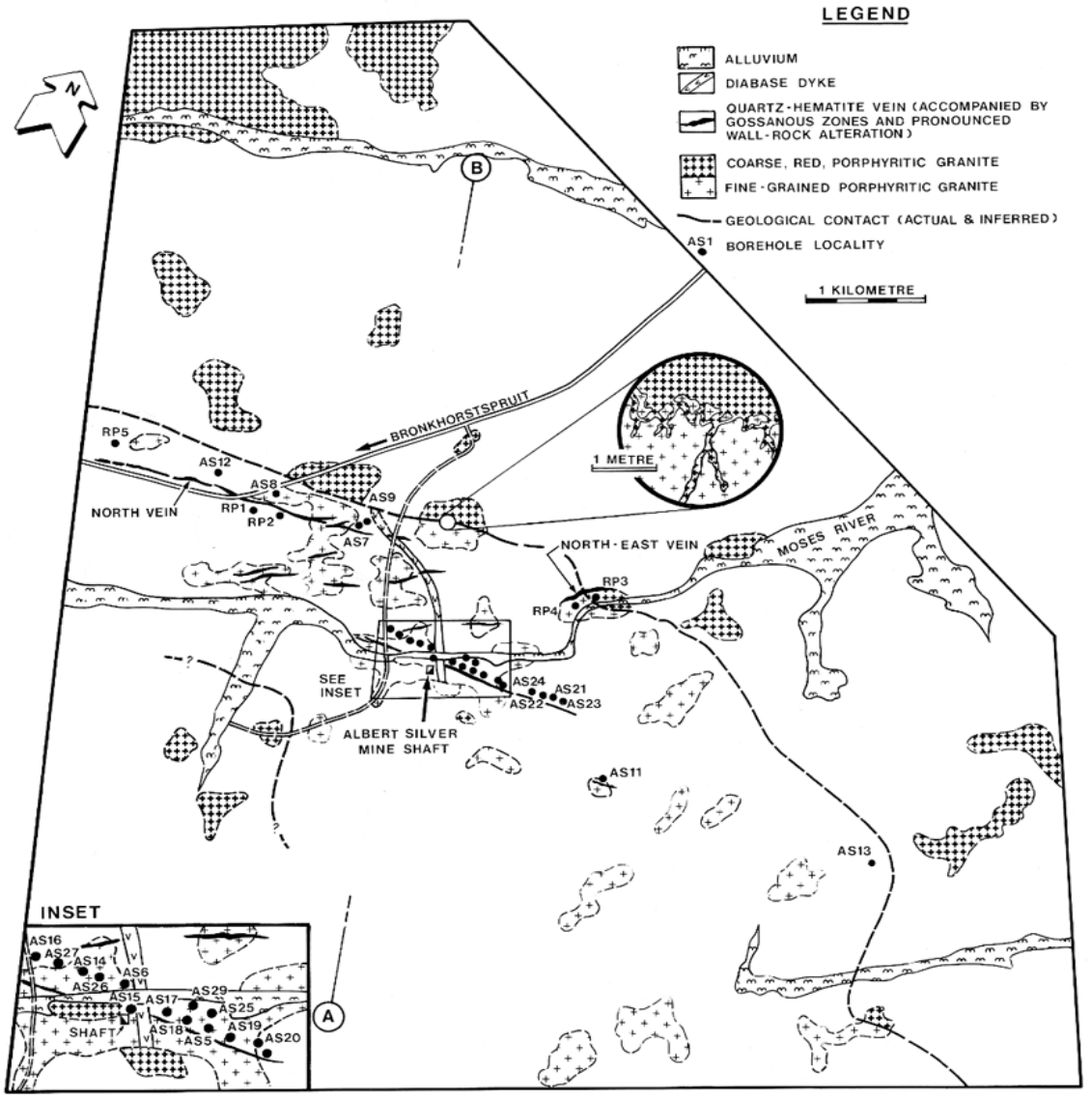

Figure 2.2: Geological map of the farm Roodepoortjie 250JR where the Albert Silver deposit is located (from Robb *et al*., 1994).

Using XRD, Meulenbeld *et al*. (2014), documented the presence of various primary and secondary copper minerals in relationship with sulfates and arsenates, such as linarite (Fig. 2.3). According to Van Zijl (1965), Champion (1970) and Cairncross and Dixon (1995) the contribution of sulfide and arsenic to the assemblage of secondary minerals was unclear. They further observed that mineral groupings show that the Albert Silver mine is additionally a source of arsenic, which is not regular in South Africa's mineral deposits (Table 2.1).

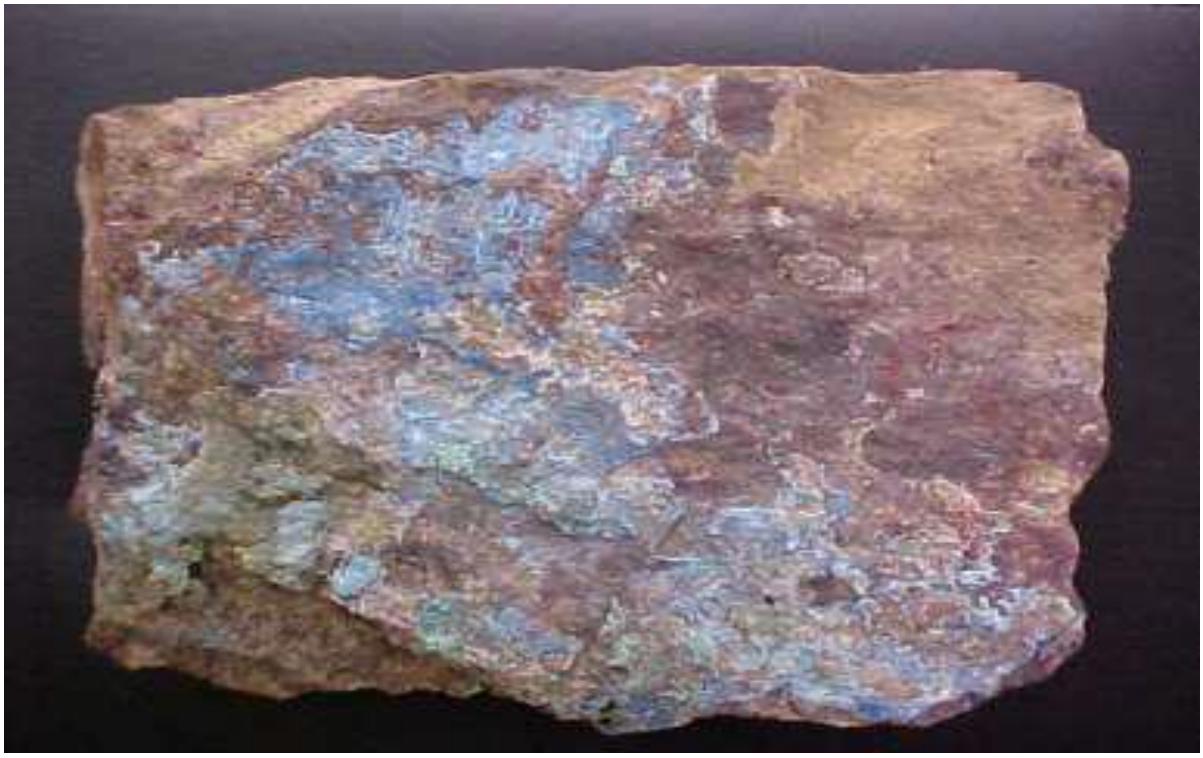

Figure 2.3: Linarite (light blue) and brochantite (light green) with minor clinoclase on a fragment of the Albert lode (from Meulenbeld *et al*., 2014).

Table 2.1: Mineral occurrences at the Albert Silver mine (from Meulenbeld *et al*., 2014).

Mineral	**Formula**	**Reference**
Acanthite	Ag_2S	Cairncross & Dixon, 1995
Anglesite	$PbSO_4$	XRD
Arsenopyrite	FeAsS	Van Zijl, 1965, Champion, 1970, XRD
Azurite	$Cu_3^{2+}(CO_3)_2(OH)_2$	Champion, 1970
Bornite	Cu_5FeS_4	Van Zijl, 1965, Champion 1970
Bronchantite	$Cu_4^{2+}(SO_4)(OH)_6$	XRD
Calcite	$CaCO_3$	Champion (1970)
Cassiterite (adjacent to the copper lode)	SnO_2	Cairncross & Dixon, 1995
Cerussite	$PbCO_3$	XRD
Chalcanthite	$Cu^{2+}SO_4.5H_2O$	Champion 1970
Chalcocite	Cu_2S	Van Zijl, 1965
Chalcopyrite	$CuFeS_2$	Van Zijl, 1965, Champion 1970, XRD
Chlorite	Group collective name	Champion 1970
Clinoclase	$Cu_3^{2+}(AsO_4)(OH)_3$	XRD

Mineral	Formula	Reference
Covellite	CuS	Champion 1970, XRD
Fluorite	CaF_2	Champion 1970
Galena	PbS	Van Zijl, 1965, Champion 1970
Gold	Au	Champion 1970, Cairncross and Dixon, 1995
Hematite/Specularite (oxidized portions of the lode)	α-Fe_2O_3	Van Zijl, 1965, Champion 1970, XRD
Jamesonite	$Pb_4FeSb_6S_{14}$	Van Zijl, 1965
Libethenite	$Cu_2^{2+}(PO_4)(OH)$	Cairncross & Dixon, 1995
Limonite	α-$Fe^{3+}O(OH)$	Champion, 1970
Linarite	$PbCu^{2+}(SO_4)(OH)_2$	XRD
Lindackerite-type	$H_2Cu_5^{2+}(AsO_4)_4.8\text{-}9H_2O$	Champion 1970
Malachite	$Cu_2^{2+}(CO_3)(OH)_2$	Champion 1970, Cairncross and Dixon,1995, XRD
Magnesite	$Fe^{2+}Fe_2^{3+}O_4$	Champion 1970
Marshite	CuI	XRD
Metatorbernite	$Cu^{2+}(UO_2)^2(PO_4)_2.8H_2O$	Cairncross & Dixon, 1995
Metazeunerite	$Cu^{2+}(UO_2)_2(AsO_4)_2.8H_2O$	Champion 1970, Cairncross and Dixon,1995
Molybdenite	MoS_2	Champion 1970
Muscovite	$KAl_2(Si_3Al)O_{10}(OH,F)_2$	XRD
Olivenite	$Cu_2^{2+}(AsO_4)(OH)$	Cairncross & Dixon, 1995
Onoratoite	$Sb_8O_{11}Cl_2$	XRD
Pitchblende	UO_2	Champion 1970
Pyrite	FeS_2	Van Zijl, 1965, Champion 1970
Quartz (Gauge; Jasperoid and milky	SiO_2	Van Zijl, 1965, XRD
Siderite	$Fe^{2+}CO_3$	Van Zijl, 1965
Silver	Ag	Cairncross and Dixon, 1995
Sphalerite	(Zn,Fe)S	Van Zijl, 1965, Champion 1970
Sulfantimonides	Yellow complex Bi, As, Sb, Pb, oxides	Champion 1970
Tennantite	$(Cu,Ag,Fe,Zn)_{12}As_4S_{13}$	Cairncross and Dixon, 1995, XRD
Tetrahedrite	$(Cu,Ag,Fe,Zn)_{12}As_4S_{13}$	Van Zijl, 1965, Champion 1970, Cairncross and Dixon, 1995
Torbernite	$Cu^{2+}(UO_2)_2(PO_4)_2.8\text{-}12H_2O$	Cairncross and Dixon, 1995
Trippkeite	$CuAs_2O_4$	XRD
Uraninite	UO_2	Cairncross and Dixon, 1995
Zeunerite	$Cu^{2+}(UO_2)_2(AsO_4)_2.10\text{-}16H_2O$	Cairncross and Dixon, 1995

The supergene enhanced silver mineralisation at the Albert silver deposit is comparable to that of the western deposits in the United States, Mexico, Central America and along the western slopes of the South American Andes (Maulenbeld *et al*., 2014). According to Champion (1970), the silver-bearing at of the Albert Silver mine at present do not yield high silver compared to the production obtained by Albert Silver Mine in 1914. The discovery of argentite and native silver by Champion (1970) proposes that silver properties experienced are of supergene enrichment.

According to Park and McDiarmid (1963), the mineralization style of the Albert Silver deposit is similar to that of the supergene enrichment silver deposit of the western hemisphere, such as that of Zacatecas, Mexico and Chañarcillo in Chile. It has structural sequences similar to Chañarcillo in the ore bearing veins of hypogene nature. The supergene leaching and enrichment are found in pyrite-bearing silver and copper deposits (Park and McDiarmid, 1963).

2.2 Mining History of Albert Silver Mine

Around 1885, the mineral deposit of the Albert Silver mine was discovered, and production proceeded irregularly until 1914 (Robb *et al.,* 1994) as an underground mine (Figure 2.4). Detailed surface geophysical investigations of the ore bodies were conducted by Van Zijl (1965). The old workings appeared as two development drives along the strike of the vein at the 23-meter and 47-meter levels below the surface, together with several raises and winzes which passed the mineral alteration zone (Champion 1970). The deposit was proven by three shafts with the deepest estimated at a depth of 122 m and drives occurred with a distance of 416 m. The development was undertaken from 1886 to 1891. At shaft number 3, according to the plan, there was intensive development, and this might have incorporated some mining stopes (Reeks, 2012).

The mine produced high grades of silver from 1885 till 1899 and afterwards until 1914 (Robb *et al.,* 1994). During mine operation, the ore was highly-evaluated and yielded approximately 20 000 t of ore containing 1.14 kg/t of silver and 10% copper (Robb *et al.,* 1994). The deposit was categorised as uneconomic in 1994 due to market status, even though results from investigations after the 1950's indicated mineral reserves to a depth of 150 m to be around 1.2 Mt at 73 g/t of silver, 0.42%

copper, 0.27% lead and 100 ppm of U_3O_8 (Robb *et al.,* 1994). The history of the mine is well documented by Reeks (2012). At present, the mine workings are flooded and the Department of Mineral Resources has completely sealed off the shafts, thus accessing the mine is not possible.

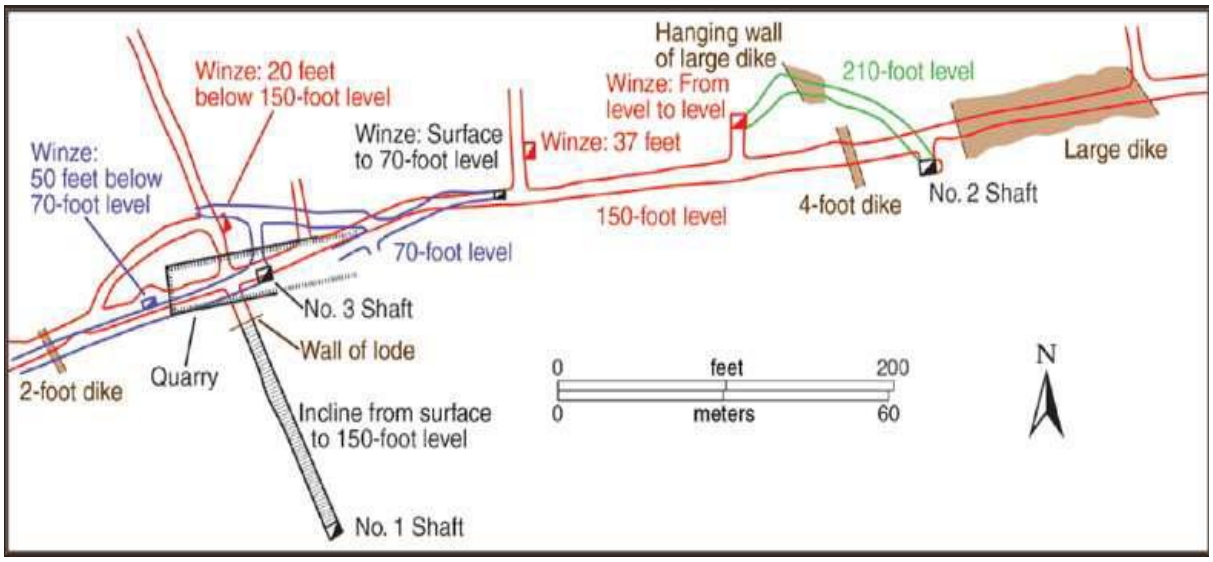

Figure 2.4: Layout plan of the underground workings at the Albert Silver mine (after Van Zijl, 1965; prepared by William Besse).

2.3 Silver Dressing at Albert Silver Mine

Metal dressing was fully documented by Reeks (2012). A documented report on the Albert mine was published in “The Transvaal Mining Argus” in May 1892 and describes the discovery of a rich lode of ore accompanied by reasonable values of pure native copper. This report also mentioned that the argentiferous rock was to be crushed with the aid of a stamp battery that was to arrive at the end of November 1892. “The Transvaal Mining Argus” mentioned that the mounting of the 10-stamp battery was being completed. Conversely, a different report mentioned that a 20-head Sandy croft battery was completely mounted, furthermore it mentioned that an ore dressing plant at the mine included Scoular tables, Frue vanners, continuous bed jig and hydraulic separators. Therefore, this machine was categorised under the concentrating equipment. There were no details about the treatment plant from the sources, so it is imperative to know the metallurgical techniques used in ore separation. The reason of purchasing the equipment at the later stage of the life of the mine is not known. There was no detail information about ore treatment be for

they purchased the ore dressing equipment. The idea of crushing the ore by stamp mill was later and the silver price drop in 1892 was the major aspects that affected both underground and surface developments ideas. During the commissioning of the concentrating plant, the management planned on the routine treating of 50 t of ore per day, which was a very low amount even though it was compared to the standards of the 1890s.

Reeks (2012) further stated that in October 1892, the share value of the mining company had fallen drastically, even though in December of the same year the concentration plant was fully commissioned. In the same month it was mentioned that a smelting plant was to be erected to avoid shipping the concentrate to Europe for smelting.

2.4 Formation of Acid Mine Drainage

Acid Mine Drainage has been a noticeable challenge worldwide. It is the product of pyrite (FeS_2) oxidation in mine waste, bringing about the mobilisation of metals and sulfate (Wolkersdorfer, 2008). Rainfall is one source of oxygenated water responsible for the following reactions (Davis and Ritchie, 1989; Dold, 2014; Jacobs *et al.,* 2014):

$$FeS_2 + 3.5\ O_2 + H_2O \rightarrow Fe^{2+} + 2\ SO_4^{2-} + 2\ H^+ \qquad \text{Equation 2.1}$$

$$Fe^{2+} + 0.25\ O_2 + H^+ \rightarrow Fe^{3+} + 0.5\ H_2O \qquad \text{Equation 2.2}$$

$$FeS_2 + 14\ Fe^{3+} + 8\ H_2O \rightarrow 15\ Fe^{2+} + 2\ SO_4^{2-} + 16\ H^+ \qquad \text{Equation 2.3}$$

Ferric iron can be eliminated from solution at pH values > 3 by hydrolysis due to the following reaction:

$$Fe^{3+} + 3\ H_2O \rightarrow Fe^{3+}(OH) + 3\ H^+ \qquad \text{Equation 2.4}$$

There is a variety of microorganisms, including *Acidithiobacillus ferroxidans*, which play a remarkable part in catalysing the oxidation process of the waste material, such as converting Fe^{2+} to Fe^{3+} (Parker and Robertson, 1999; Dold, 2017). According to Blowes *et al.* (2003), the discharged acidic water is responsible for the mobilisation of trace elements, for example, arsenic, iron, lead, copper, cobalt, manganese, nickel, zinc and uranium. The continuous process of oxidation is also accompanied by the release of these metals and sulfate, minerals that range from

basic sulfate salts to complex multi-component sulfates form along the stream way. Later permeation of water during a different windy season can result in new oxidation reactions and in addition disintegration of these secondary salts, bringing about toxin plumes that can have negative effects on soil and water systems (Jambor *et al.,* 2000).

2.5 Acid Mine Drainage in South Africa

Gold tailings dams are one of the major producers of AMD in South Africa. The effects of AMD have been noticed due to the escalation of AMD at the Blesbokspruit, Springs and the Klip Waterway, in this the contaminants were derived from the southern part of the Witwatersrand slope due to the fact that tailings dams covered a large portion of the upper catchments (Nengovhela *et al.,* 2007; 2009; McCarthy, 2011).

Most gold mines at the Witwatersrand Basin ended operations at different times, and as each mine shuts down and stops pumping water, the groundwater starts to fill the voids and then it is released into neighbouring mines because of the mine workings network. This also occurs as ground water percolation. The neighbouring mines are expected to subsequently pump the resulting water. The resulting water is always of low quality, requiring fundamental treatment. This treatment involved addition of lime to raise the pH and metal extraction whereafter the water is released to the nearby streams. The released water is normally clear with a neutral pH, but with high sulfate concentrations, around 1500 mg/L according to McCarthy (2011).

Coal mining in the Witbank/Middelburg region started in 1894. Numerous mines in the area are abandoned with high rates of acidic water formation. The water is interacting with the neighbouring waterways (tributaries of the Oliphant Stream). However, the acidity of the water is lowered due to dilution. Yet, the water still is highly mineralised and sulfate fixations are increased and with time, the pH of the water in the receiving streams and rivers are lowered (McCarthy, 2011).

A sign of the issue is given by the rising mineralisation and sulfate convergence of the water in the Middelburg and Witbank dams. The sulfate concentrations in the Witbank Dam currently surpass 200 mg/L, which is the prescribed most extreme in water for residential use. The nature of the nearby water is poor to the point that

ESKOM imports water from the eastern ledge for use in the power stations in the Witbank-Middelburg zone (McCarthy, 2011).

Lastly, pyrite is the major mineral in these mining zones that is completely oxidized and it is the major source of acidity. There is no full information on the remediation of the contaminants brought by AMD and also with respect to what extent this will take. However, the issue is probably going to endure for a considerable length of time (Aphane and Vermeulen, 2015).

2.6 Acid Mine Drainage in the Bushveld Igneous Complex

Acid mine drainage researches in South Africa have generally centered around the gold and coal mining ventures, and little past work has been completed to examine or foresee the AMD capability of mined Bushveld deposit with the exception of the work conducted by Lishman (2009). The regular assumption is that mines in the Bushveld Complex do not generate AMD. This observation is upheld by Foose *et al*. (1995) who express that “Platinum-Group elements rich deposits in vast, layered intrusions have low sulfide mineral abundances (1 to 5 wt%) and low total metal plenitudes. Thus, they have a generally limited ability to create huge measures of acidic and (or) metal enriched seepage. A large portion of the other economically extractable magmatic-sulfide deposits contain substantial measures of sulfide minerals (more prominent than 15 weight percentage, many surpassing 40 weight percentage) and precious metal abundances (Lishman, 2009). They have fundamentally more prominent potential for producing acid and (or) metal-enriched drainage.”

Despite the fact that the Platreef deposits are fundamentally low-sulfide deposits, and all things considered do not warrant an immediate comparison with high-sulfide magmatic deposits, for example, Sudbury and Noril’sk, the on-going surge of investigation and mining activity in the Platreef of the Bushveld complex features the requirement for examination of AMD producing capability of these deposits. The study conducted by Lishman (2009) at the Platreef has discovered the potential AMD dangers confronting the future mine that was supposed to be opened at the Platreef and that study advised the mine administration to limit these dangers during the mine configuration stage.

2.7 Acid Mine Drainage Prediction Techniques

2.7.1 Static Test

Acid base accounting (ABA) is a static test procedure that predicts the drainage chemistry where the Net Neutralising Potential (NNP) is determined by subtracting the Acid Generation Potential (AP) from the Neutralising Potential (NP). Static acid base accounting tests are the best AMD predictive methods because they are quick, cheap, use easy analytical procedures requiring user friendly interpretations and correlate with real-life processes (Dold, 2017). The AP is determined by multiplying the percent of total sulfur or sulfide sulfur (depends on the mineral composition of the rock samples) in the sample by a conversional factor (AP = %S × 31.25). The neutralisation potential NP is the amount of the carbonate minerals such as calcite accessible to neutralise acid (Sobek *et al*., 1987). The value of the NP is determined by an experiment whereby an acid is added to a sample and the pH of the liquor is back titrated to a pH of 7 to determine the measure of acid expended (Ferguson and Morin, 1991; Lapakko, 1994).

The NNP is determined by subtracting the AP from the NP using this equation; NNP = NP – AP (Sobek *et al*., 1978; Makiese *et al*., 2015). A ratio of NP to AP is also generally used to appraise the AMD potential and is known as the Net Potential Ratio (NPR). A NNP of 0 is equal to a NP/AP proportion of 1 (Ferguson and Morin, 1991). Units for static test results (AP, NP, and NNP) are expressed in mass (kg, t) of calcium carbonate ($CaCO_3$) per 1000 t of rock: parts per thousand. If the difference between NP and AP is negative, then the potential exists for the waste to produce acid. If the difference between NP and AP is positive, there are fewer chances to form AMD (Lawrence, 1989; Usher, 2003). An expectation of the acid potential, when the NNP is between –20 and 20 is more troublesome (U.S. Environmental Protection Agency, 1994; Price *et al*., 1997; Price, 2009; Ferguson and Morin, 1991; Weber *et al*., 2004).

When the NPR of a sample is more than 3:1, Brodie *et al*. (1991) demonstrated that there is a low risk of acid generation. The ratio between 3:1 and 1:1 alluded that it is a zone of vulnerability, therefore which calls for extra experiments. Those samples with a ratio of 1:1 or less will probably generate acid. Prediction of seepage quality

for a sample in view of these qualities requires assumptions that reaction rates are comparable and that the acid-consuming minerals will disintegrate (Lapakko, 1994). While interpreting data on static tests, the particle size of the sample material and how it is unique in relation to the waste or unit being characterised should be taken into consideration (U.S. Environmental Protection Agency, 1994).

2.7.2 Kinetic Tests

Kinetic tests are conducted after static tests to mirror characteristic oxidation reaction of the field setting. Types of kinetic tests include conventional and modified conventional, humidity cells, Soxhlet extractions, Column leach tests and shake flask extractions. The tests usually use large amounts of sample volume and require a longer time for the experiment than for static tests. These tests give data on the rate of sulfide mineral oxidation and consequently acid generation, and an indication of drainage quality (Smart *et al*., 2002). Of the distinctive kinetic tests utilized, there is no one test that is pronounced as the best. The selection for tests changes with time as experience and understanding increase. In a synopsis article by Ferguson and Erickson (1988), the British Columbia Research Confirmation Test was thought to be the most broadly utilized. A later article by Ferguson and Morin (1991) expressed that the selection of modified humidity cells was more common. From data explored for this report, there seems to be a pattern toward the inclination for modified humidity cell and column type tests.

Kinetic tests can be utilized to evaluate the effect of various factors on the possibility to produce acid. For instance, tests might be immunized with bacteria (a prerequisite for a few tests); temperature of the experiment may also be controlled during the test. Most tests require the sample particle size to be more than the predetermined sieve size; for example, minus 200 mesh (Smart *et al*., 2002).

The kinetic test also include the investigation of particular surface zone and mineralogy available in the sample which may influence the understanding of test information and are critical when making spatial and transient correlations between tests in view of the test data (Sobek *et al*., 1978; British Columbia AMD Task Force, 1989; Price, 2009). Similarly, as with static tests, it is critical to consider the particle

size of the test, especially when comparing test outcomes and field-scale applications (Capriccio *et al*., 1981; Lawrence *et al*., 1990; El Amari and Hibti, 2019).

2.8 Analytical Techniques

Analytical techniques to be used vary in the type of sample that is to be analysed, instrument, detection limit, detection methods, elements measured and susceptibility to interference by other sample components. Elemental analysis by XRF is done on a glass disk and solid, undigested samples (pressed pellets), more commonly elemental analysis is conducted on liquid samples created by digesting and dissolving the sample with strong acids. Mineralogical composition can be successfully determined by XRD and the concentrations of cations in liquid solutions by using of Atomic Absorption Spectroscopy (AAS). These analytical techniques are briefly discussed below.

2.8.1 Atomic Absorption Spectroscopy

In Atomic Absorption Spectroscopy (AAS), liquid or solid samples are converted into the gas phase (vaporised) by the high temperature of a flame, graphite furnace or chemical reaction (Hydride generation). The vaporised atoms are then introduced in a beam of ultraviolet or visible light with the same wavelength as the element of interest (Robinson *et al*., 2005). The vaporised atoms absorb the light and make evolutions to higher electronic energy levels. The concentrations of the elements in the sample are determined by comparing the amount of light absorption with that of standards of known concentration (Skoog *et al*., 2007).

The main advantages of AAS are that it is well established, the equipment is relatively easy to use, inexpensive and the technology is straight forward and well understood. AAS can measure a wide range of concentrations for most metals and metalloids and with relatively low interferences (Skoog *et al*., 2007). The only disadvantage is that AAS measures one element at a time. The technique becomes uneconomical when analysing many elements is required. Although relatively rare, interference by other elements or chemical species can reduce the sensitivity (Robinson *et al*., 2005).

2.8.2. X-ray Diffraction

X-ray Diffraction spectrometry is one of the most cost-effective procedures for the identification of different mineral phases and the semi-qualitative or quantitative estimation of the mineral abundance (Schmitz-Antoniak, 2013). X-ray Diffraction Spectrometers are not limited by grain size and are able to distinguish minerals with similar chemical compositions, such as pyrite and marcasite. XRD may be capable of measuring mineral phases that exist as intergrowth or altered phases that cannot be detected visually or by petrographic analysis (Price, 2009).

XRD is conducted on single crystals or more commonly with rock or ore samples prepared for analysis by crushing and grinding to a powder. The powdered sample is randomly packed into a cavity in a holder. Powdered samples may also be smeared wet into a glass slide for quick analysis (He, 2009). In both cases, a flat surface faces the X-ray beam. Mineral phases are identified by comparison of the locations and intensities of the diffraction peak with those of mineral reference standards in a database such as the International Center for Diffraction Data (ICDD) PDF-4+ database. Detection levels of mineral constituents may be as low as a few tenths of a percentage, using modern high-speed detectors if the peaks of the phase of interest are not overlapped by peaks of other phases (Price, 2009).

2.8.3 X-ray Fluorescence Spectroscopy

In X-ray Fluorescence Spectroscopy (XRF) analysis, a beam of X-rays irradiate the sample. Constituent elements emit fluorescent (secondary) X-rays, when a primary X-ray of sufficient energy strikes the atom in the sample, dislodging an electron from one of the atom's inner orbital shells (lower quantum energy states). The atoms regain stability by filling the vacancy in the inner orbital shell with an electron from one of the higher quantum energy orbital shells. The electron drops to the lower energy states by releasing a fluorescent X-ray. Each element emits a unique fluorescent X-ray energy spectrum (energies and wavelengths) that can be used to identify the elemental source because the quantum state of each electron orbital shell in each atom is different (Potts and Webb, 1992).

Diffraction crystals are used to disperse and sort the emitted fluorescent X-rays by wavelength. The dispersed fluorescent X-rays strike a detector, causing a small

electrical impulse. The elements concentration in the sample is then determined by comparing the electrical impulse of the characteristic wavelengths to that of standard reference materials (Kikkert, 1983). The common use of XRF is to measure the concentrations of major elements for examples Al, Ca, Cr, Fe, K, Mg, Mn, Na, P, Si, Ti in a lithium borate fused disk. XRF can also be used to measure the concentrations of trace elements such as As, Ba, Ce, Cu, La, Nb, Ni, Rb, Sn, Sr, Ta, Th, U, W, Y, Zn, Zr in an undigested pressed pellet. The pellet is created with a bonding agent under high pressure to ensure sample integrity under the vacuum and a consistent surface to receive the X-rays (Price, 2009).

3. CHAPTER THREE: MATERIALS AND METHODS

This chapter discuss the methods and the procedures undertaken in the study (Fig. 3.1).

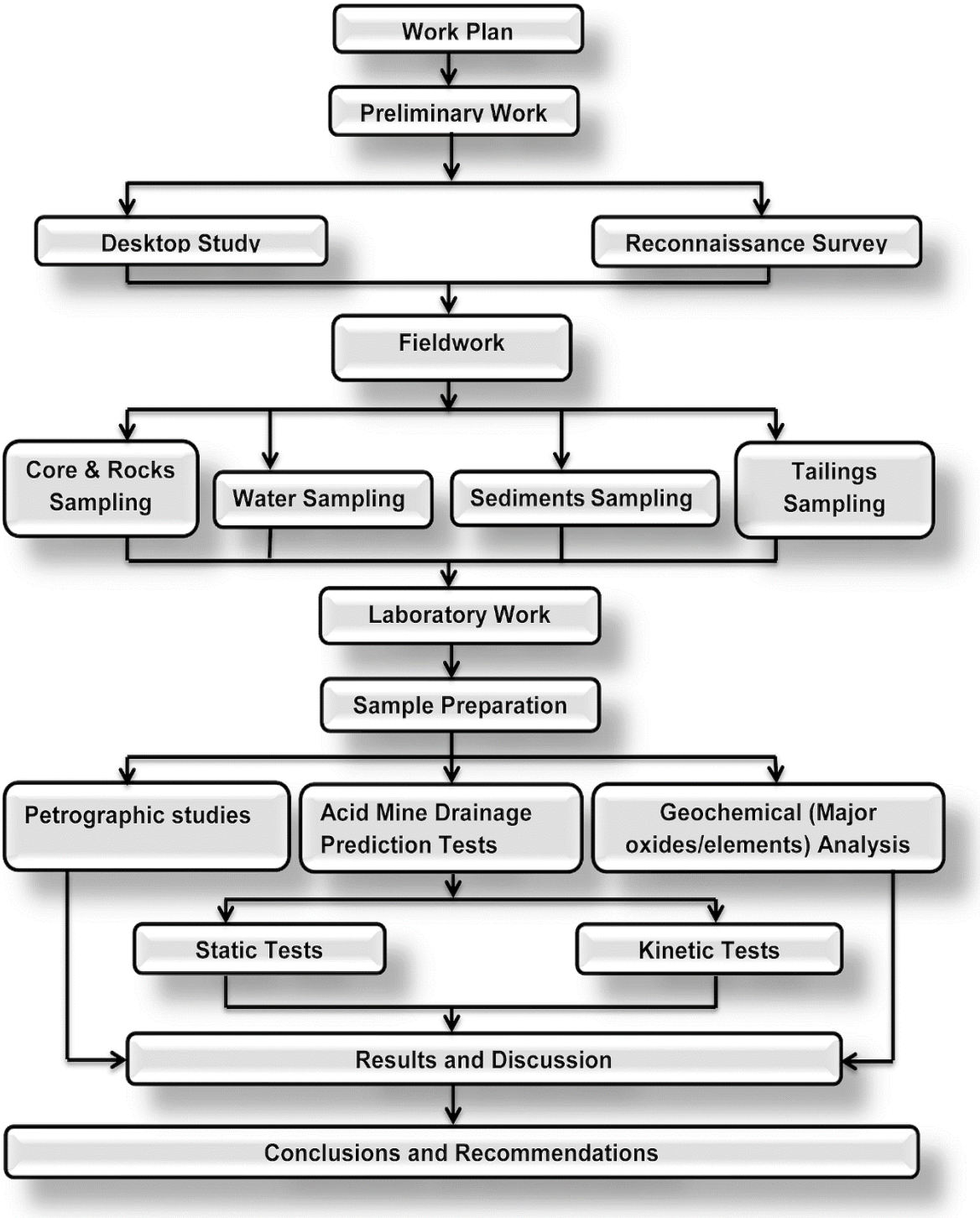

Figure 3.1: Flow-chart showing a summary of the methods and procedures applied in the study.

3.1 Preliminary Work

Preliminary work was conducted about the study before commencement of both field work and laboratory work. This helped in gaining more useful information about the study and the study area in cases of changes occurring in the area which were not presented on topo-sheets and aerial photos; this was done to fully plan and design of fieldwork.

3.1.1 Desktop Study

The work was initiated by a desktop study which involved the collection of secondary information and data from sources such as internet, technical reports, books, journals and geological and topographic maps. Technical reports included historical information.

3.1.2 Reconnaissance Survey

A reconnaissance survey was conducted prior to fieldwork to obtain an overview of the study area and the processes that are occurring within it. This helped in fieldwork logistics preparations and identification of any potential challenges to be encountered during fieldwork.

3.2 Fieldwork

3.2.1 Sampling

Fieldwork involved sampling at the mine site. For fieldwork, the following equipment and materials were used: pick, compass, geological hammer, sledgehammer, magnifying glass, shovel, sample bags, tags, strings, permanent marker, satellite navigation system, tape measure, note book, tape and pen.

3.2.1.1 Rocks Specimens Collection

Rock specimens were collected at the site covering an area of about 1500 × 500 m. Rock specimen collection was guided by the old map found on the Lerama resources website. The equipment and materials used were satellite navigation system, topographic map, tape measure, compass, geological and sledgehammer, note book, sample bags, tags, strings, permanent marker and pen. The following measurements were conducted on the exposed outcrops: general strike (no attitudes

measurements were taken on the granites with the assumption that they are intrusive bodies), coordinates and altitudes using the compass and Garmin eTrex 10 satellite navigation system respectively.

Eleven different rock specimens of about 2 kg mass were collected using the sledgehammer and the geological hammer and marked by using a permanent maker, then put in sampling bags. A maximum of four lithologies were encountered and they were defined by their colour, texture, structures and mineralogy. The observed information was recorded in the field-book. The different boundaries and contacts of the different rock types were represented on the topographic map, using different colour codes, solid and dotted lines, as shown by the modified geological map below (Fig. 3.2).

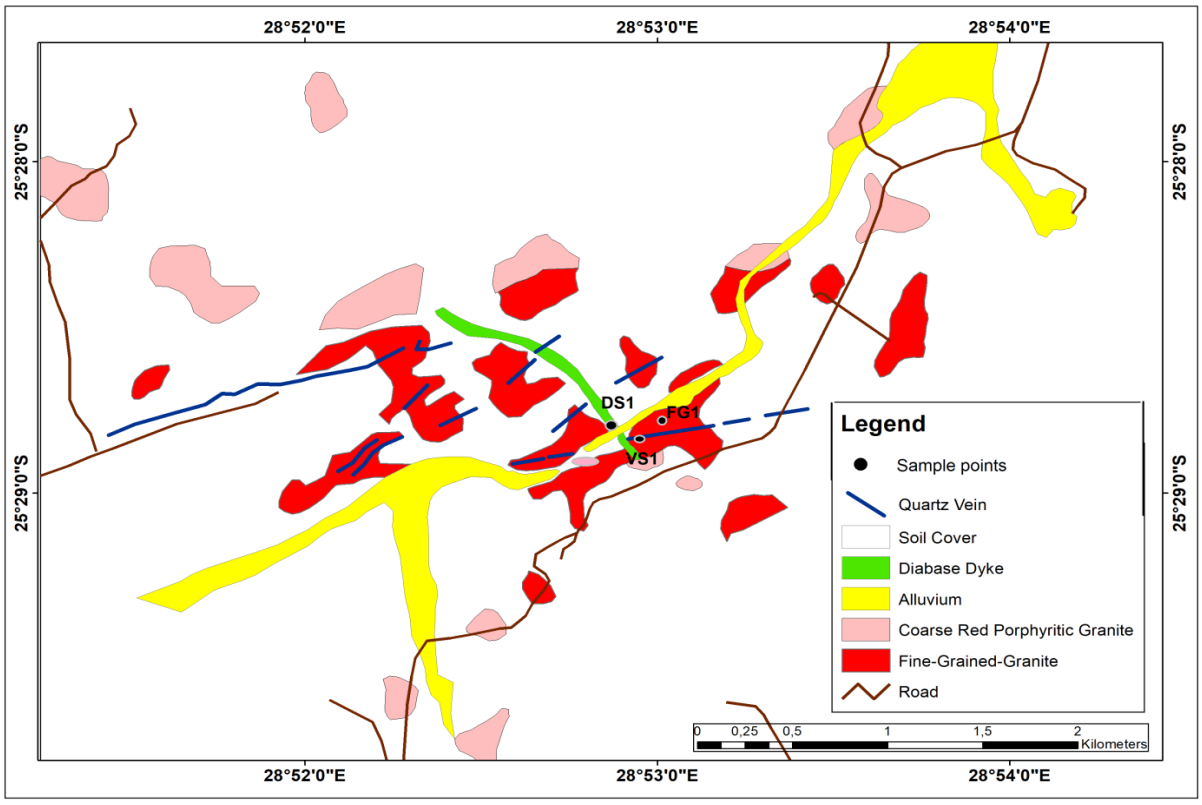

Figure 3.2: Geological map of the study area showing the different lithologies and the sampled points (Modified from a report to Lerama by G. Grantham, Council for Geoscience, 2012).

3.2.1.2 Core Sampling

Broughton and Robertson (1992) and Price (2009) recommended that the initial phases of AMD prediction for either new or existing mines is to survey the local geology, mineralogy, characterise the rocks and collect samples. In this study the core samples were acquired from MINTEK. Core logging was conducted at MINTEK prior to sampling. The core samples were collected for geochemical analysis, petrographic studies and AMD prediction tests, and 17 trays from three boreholes (Fig. 3.3.) were collected. Two core samples were selected per borehole for mineralogical characterisation.

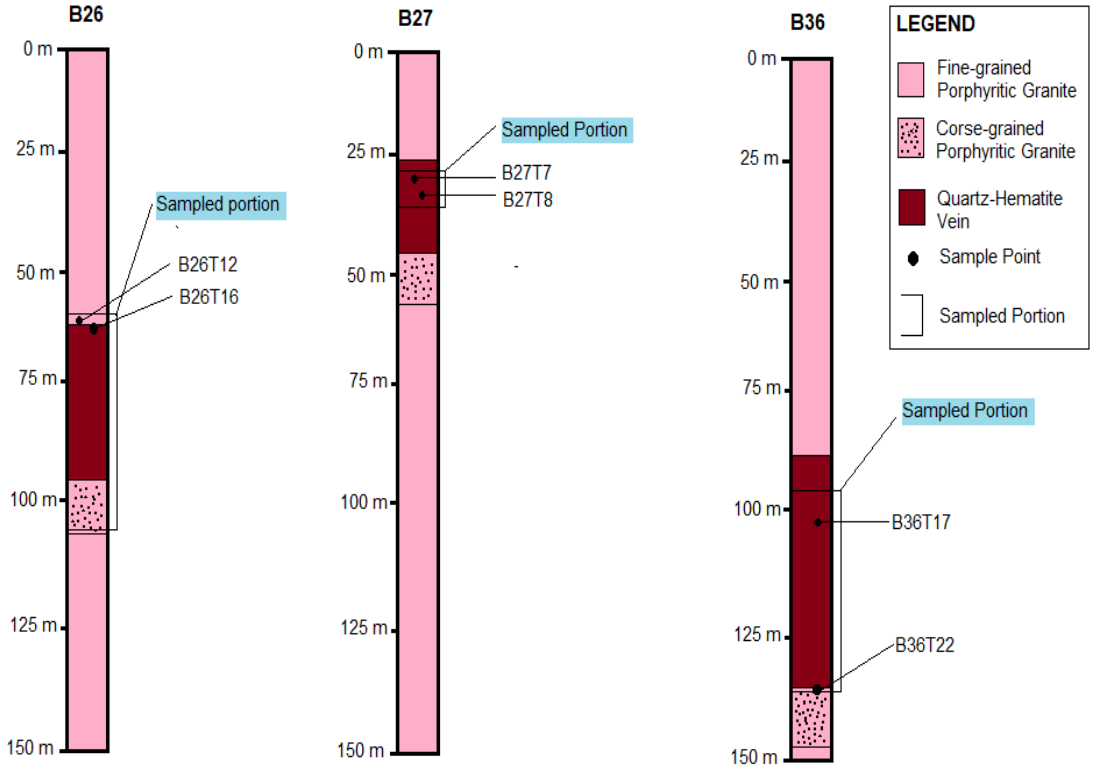

Figure 3.3: Core logs from three boreholes indicating rock sequence and sample points.

3.2.1.3 Water Sampling

Water sampling was done on the 1 – 5 m wide Moses River, to ascertain the current status of water quality in the river, such as the potential threat from AMD. For that investigation, the river was divided into three sections: upstream, mined area and

downstream. Fifteen water samples were collected in 350 mL bottles at an interval of 100 m downstream, with five samples from each section (Fig. 3.4) plus one well. The water bottles and their lids were rinsed twice with the river water prior to actual sampling. A permanent marker was used to label the water bottles. pH, electrical conductivity (EC), temperature, turbidity, salinity and TDS of the samples were measured in the field. The geographical location and the environmental aspects (topography, soil/sediment properties and vegetation cover) of each sample were recorded in the field-book (Table 3.1).

Figure 3.4: Water sampling along Moses River across the Albert Silver Mine (satellite image from GoogleEarth).

3.2.1.4 Sediment Sampling

Sediment sampling was conducted along Moses River, which was divided into three sections: upstream, mined area and downstream. Fifteen sediment samples of about 1 kg mass were collected at an interval of 100 m, with five samples from each section. Higher amounts of metals generally aggregate on smaller sediments on account of the higher surface area (Gibbs, 1973), thus sampling focused on the smaller grains with sieving as support to attain this requirement. High metal loading is found on the riverbank compared to the middle, where the stream water has a higher velocity, thus sampling was done close to the riverbank. A scoop shovel was

used, and the sampling personnel were wearing watertight boots. Sediment sampling was done after water sampling has been conducted. Additional information such as the geographical location of sample points was recorded using a Garmin eTrex 30 navigation system. Environmental aspects were also recorded in the field book (Table 3.1); samples were securely put in a sample bag.

Table 3.1: Water and sediment samples and their location and characteristics

Sample ID	Latitude	Longitude	Altitude, m	Time	Sampling Environment	Water Dynamics
DO1	25°28′28″	28°53′17″	1331	11:22	Tall grass, No trees, Dark sandy Loam soil	Flowing water
DO2	25°28′30″	28°53′15″	1332	11:34	Tall grass, Wetland plants, Clay Loam soil	Slow flowing water
DO3	25°28′32″	28°53′11″	1328	11:45	Tall grass, Tall trees, Clay-loam soil	Huge pool
DO4	25°28′35″	28°53′08″	1330	11:56	Tall grass, light coloured sandy soil	Slow flowing water
DO5	25°28′36″	28°53′06″	1336	12:06	Tall grass, Tall trees, Clay Loam soil	Slow flowing water
MI1	25°28′39″	28°53′2.5″	1331	12:30	Tall grass, Tall trees, Clay soil	Stagnant pool
MI2	25°28′39″	28°52′59″	1329	12:46	Tall grass, Clay Loam soil	Quiet water
MI3	25°28′41″	28°52′56″	1332	13:15	Tall grass, Tall trees, sandy soil	Stagnant water
MI4	25°28′43″	28°52′54″	1333	13:31	Many tall trees, Tall grass, Clay	Fast flow water
MI5	25°28′46″	28°52′57″	1333	13:51	Tall trees and grasses, Clay Loam soil	Fast flowing water
UP1	25°28′48″	28°52′48″	1334	14:40	Tall grass, Dark Clay Loam soil	Stagnant pool
UP2	25°28′49″	28°52′45″	1337	15:08	Tall grass, Dark Clay Loam soil	Stagnant pool
UP3	25°28′50″	28°52′41″	1336	15:39	Tall grass, Clay and Loam portion	Moderatel y flow water
UP4	25°28′50″	28°52′37″	1336	15:50	Tall grass, sandy loam soil	Slow flow water
UP5	25°28′47″	28°52′35″	1338	16:20	Tall grass, Clay Loam dark soil	Stagnant pool
WELL	25°28′41″	28°52′56″	1335	16:32	Tall grass, muddy, rock outcrop	Fast flow water

3.2.1.5 Tailings Sampling

A random sampling method of sample collection was used to collect tailings samples (Fig. 3.). This was due to the fact that the tailings are being eroded to the stream, thus the remainder is in small patches (Fig. 3.5). Fourteen samples of 2 kg were collected at a depth of 30 to 100 cm. This depth was chosen because weathering would have occurred on the surface which would have had a negative effect on the results. A pick and spade were the main tools used to clear the sampling point, collect the sample and to restore the sampled area. A sample bag and a string (cable tie) were used to store and string the sampling bags to minimise cross contamination. Additional information regarding the location of the sampling point such as geographic coordinates, elevation, texture and sample colour were recorded in the field-book (Table 3.2).

Figure 3.5: Tailings sampling plan showing sampling points (image source Google Earth).

Table 3.2: Tailings sample information.

Sample ID	Latitude	Longitude	Elevation, m	Sample properties
T1	25°28′39.7″	28°53′00.6″	1330	Fine texture, whitish to brown and small quartz grains
T2	25°28′40″	28°53′01.0″	1331	Fine texture, yellowish, no visible quartz grains
T3	25°28′40.8″	28°53′00.6″	1333	Fine texture, purplish and visible quartz grains
T4	25°28′40.1″	28°53′01.7″	1332	Fine texture with pebbles, yellowish, no visible quartz grains
T5	25°28′40.2″	28°53′02.6″	1333	Fine texture (clayish), purplish and no visible quartz grains (shinny particles, greasy feel)
T6	25°28′40.3″	28°53′03.6″	1334	Fine texture, purplish to grey and no visible quartz grains
T7	25°28′40.8″	28°53′02.9″	1333	Fine texture, yellowish, no visible quartz grains
T8	25°28′42.4″	28°53′02.2″	1335	Fine texture, yellowish, no visible quartz grains
T9	25°28′42.8″	28°53′01.3″	1336	Fine texture, brownish to yellowish, no visible quartz grains
T10	25°28′41.5″	28°53′00.9″	1334	Fine texture, brownish to yellowish, no visible quartz grains
T11	25°28′45.3″	28°52′58.8″	1337	Fine texture, blackish, no visible quartz grains
T12	25°28′46.5″	28°52′59.3″	1339	Fine texture, yellowish, no visible quartz grains
T13	25°28′46.2″	28°53′00.2″	1339	Fine texture, brownish, no visible quartz grains
T14	25°28′45.4″	28°53′005″	1339	Fine texture, brownish, small to no visible quartz grains

3.3 Laboratory Work

3.3.1 Sample Preparations

Thin Section Preparation

Three boreholes were drilled at the Albert silver mine by the MINTEK drilling team, and 17 trays were couriered to the University of Venda. Amongst the three boreholes, two representative core samples were selected per borehole and three surface rocks samples were also selected adding up to nine rock specimens. This involved the determination of any sulfide and carbonate minerals available in the samples since they are responsible for AMD generation and neutralisation. The following sample preparation procedure was followed:

- Step 1: Cutting a slab, a suitable size slab for mounting on a slide was cut from a piece of rock or drill core with a diamond saw,
- Step 2: Initial Lapping of the slab, the slab was labelled on one side and the other side was lapped flat and smooth first on a cast iron lap with 400 grit carborundum, then finished on a glass plate with 600 grit carborundum,
- Step 3: Glass slide was added after drying on a hot plate, a glass slide was glued to the lapped face of the slab with epoxy,
- Step 4: Slab was sectioned using a thin section saw, the slab was cut-off close to the slide. The thickness was further reduced on a thin section grinder,
- Step 5: Final Lapping, a finished thickness of 30 microns was achieved by lapping the section by hand on a glass plate with 600 grit carborundum, a fine grinding with 1000 grit prior to polishing was optional,
- Step 6: Polishing, the section was placed in a holder and spun on a polishing machine using nylon cloth and diamond paste until a suitable polish was achieved for microscope or SEM studies,
- Step 7: Final inspection

Preparations of the Water Samples

The preparation of water samples was undertaken at the Department of Mining and Environmental Geology Laboratory at the University of Venda (Fig. 3.6). The process was undertaken to remove solid particles from the water samples through filtering by a 0.45 µm membrane filter; getting the sample ready for analysis and thus prevent disturbance during analysis. Atomic Absorption Spectrometer (AAS) was used for water sample metal and metalloid analysis.

Preparation of Samples for Geochemical Analysis

At the laboratory, 3 rock specimens, 14 tailing samples and 15 stream sediment samples were prepared for geochemical analysis. Preparations incorporated drying overnight at 85 °C using the Vacutec drying machine to eliminate any available moisture. This was followed by crushing and sieving to smaller particle size (1 to 4 mm) (Gibbs, 1973) and to remove plant fragments that were incorporated in the samples during sampling. These samples were then milled to 75 µm using the Retsch RS 200 milling machine and a 2 g sample was used to produce pressed pellets for XRF analysis.

Scheme 1

Take measured volume (50 ml) of well mixed, acid preserved sample into a beaker

⇩

Add 5 ml conc. HNO_3 + few glass beads

⇩

Slow boil and evaporate on a hot plate upto 10-20 ml

⇩

Add conc. HNO_3 (few ml) until the completion of digestion (Do not let the sample dry)

⇩

Wash down the beaker with deionized water (3 times)

⇩

Filter and pour the sample in 100 ml volumetric flask and makeup it 100 ml, mix thoroughly

Scheme 2

Select atleast three concentrations of standard solution of a particular metal to be analysed

⇩

Aspirate blank solution and adjust zero

⇩

Aspirate each standard solution into flame

⇩

Prepare a calibration curve for absorbance versus concentration of standard solution
(This step is unuseful for the instruments equipped with direct concentration readout)

⇩

Take the reading of the prepared sample solution directly from the instrument

⇩

Use the appropriate dilution factor for the samples having higher concentration of metal ions

Figure 3.6: Flow chart showing all the steps involved in the preparation of water samples for geochemical analysis (Bhavtosh and Shweta, 2013).

3.3.2 Sample Analysis

3.3.2.1 Petrographic Study

The important mineralogical characteristics of the sulfide and carbonate minerals were studied under the microscope using cross polarised light (XPL) and plane polarised light (PPL) for the prediction of the generation and neutralisation of AMD. These include grain characteristics or morphology (euhedral and framboidal), grain surface area and mineral dissemination (Maiyana, 2003). The surface area was calculated from the grain size measured by the computer software IMAGEJ. This software analyses the rock specimen photograph, therefore there is no input data. These results are outlined in Chapter 4.

3.3.2.2 Geochemical Sample Analysis

Water Samples Analysis

Elemental analysis was conducted through ASS on 15 water samples. This technique was selected due to the advantages listed in section 2.8.1 above, even though other techniques possess all those traits, but the shortcoming is the high cost of using them. Water sample analysis was done to obtain the concentrations of Pb, Zn, Cu, As and Fe with the assumption that their source is the quartz-hematite veins and the tailings dam that was disturbed and introduced by mining activities.

Whole Rock Geochemical Analysis

X-ray Fluorescence spectrometry was used to analyse the rocks specimens, tailings and sediment samples to establish the metal concentration in these samples. Three rock specimens, 14 tailings and 15 sediment samples were analysed. The major oxides analysed were SiO_2, Al_2O_3, Fe_2O_3 and K_2O while the trace metals analysed were Pb, Zn, Cu and As (Chapter 4). Pressed pellet XRF analysis was selected over Lithium borate fusion due to the fact that the samples consist of more than 5% of sulfide minerals which minimise the optimum detection limit from being achieved if the sample was fused under lithium borate fusion process (Price, 2009).

For the purpose of AMD prediction, geochemical analysis was conducted on the rock specimen to estimate the elements of concern that will be leached at low pH weathering conditions and to verify the lithological and mineralogical composition

that were identified by the use of X-ray diffraction spectroscopy. This technique was selected due to its ability to conduct simultaneous measurements of concentrations from a large number of samples, thus making it a cost-effective technique.

The total sulfur (%S) and the total carbon (%C) concentration of 20 samples were analysed by a LECO S632 analyser at the ALS Chemex lab in Edenville, Gauteng province. This technique uses high-temperature combustion and infrared spectrophotometry with a specific end goal to quantify the total sulfur and total carbon content of the specific sample. The sulfur (%S) content analysis was conducted on the core samples and surface rock samples, the findings were utilised to compute the Acid Potential (AP). The total carbon (%C, Table 4.9) was utilised to calculate the CO_3-NP by multiplying the %C with the convention factor 83.3 (equation 3.1).

$$CO_3\text{-NP} = \%C \times 83.3 \qquad \text{Equation 3.1}$$

3.3.3 Static Tests

Two static tests were conducted; this includes the Acid base accounting and the net acid generating tests. Acid Base Accounting (ABA) was adopted to determine the Acid Generating Potential and Acid Neutralising Potential of the geological materials. Twenty samples (one representative sample per tray) were selected for the static test. The Acid Potential (AP) was determined through the method that was developed in 1974 and was modified by Sobek *et al*. (1978). Equation 3.2 was used to calculate the AP. The sulfide sulfur was multiplied by the conversion factor 31.25 to get the AP as shown by equation 3.2 (Ferguson and Morin, 1991; Lapakko, 1994). The units for the AP are commonly kg $CaCO_3$ per tonne of material.

$$AP = \%\text{Sulfide Sulfur} \times 31.25 \qquad \text{Equation 3.2}$$

The Neutralising Potential (NP) was determined using the standard Sobek method, where the basic fizz test was conducted to choose the acid normality and volume (Table 3.3). Considering this data, hydrochloric acid (HCI) was added to the sample and then boiled to the point of no reaction. The subsequent solution was then back titrated to pH 7 with sodium hydroxide (NaOH) to determine the amount of acid consumed by the sample (Equation 3.3) (Ferguson and Morin, 1991; Lapakko, 1994).

The full procedure followed during the determination of the neutralising potential (NP) was as follows: weigh samples of 2.00 g (finer than 60 mesh) into 250 mL Erlenmeyer flasks, add a fizz rating (Table 3.3) designated amount of HCl and add 125 mL with distilled/de-ionised water; boil the mixture for 5 min until the reaction is complete (note, the reaction is termed complete when there is no gas evolution) and allow it to cool to room temperature, filter the mixture using a 0.45 µm membrane filter, back titrate the filtrate liquor using 0.1N Sodium Hydroxide (NaOH) to pH 7.0 using a pH meter; the concentration of NaOH should be equivalent to that of HCl added and measure the volume of NaOH added. If less than 3 mL of NaOH is needed to titrate to pH 7.0, the test should be rerun with a higher volume or concentration of HCI because there was not enough HCI added. Use the HCI normality, HCI volume, NaOH normality, NaOH volume and weight of the sample to calculate the NP using equation 3.3.

Table 3.3: Fizz rating and acid additions parameters

Reaction	Fizz Rating	Acid normality, N	Acid Volume, mL
None	0	0.1	20
Slight	1	0.1	40
Moderate	2	0.5	40
Strong	3	0.5	80

$$\mathrm{NP} = \frac{(\text{Acid normality} \times V) - (\text{Base normality} \times V) \times 50}{\text{Mass of Sample}} \qquad \text{Equation 3.3}$$

The Net Neutralising Potential (NNP) is obtained by subtracting AP from NP and it is a measure of the contrast between the neutralising and acid potential as shown in equation 3.4 (Sobek *et al*., 1978; Makiese *et al*., 2015; Skousen *et al.,* 2002; Smart *et al*., 2002). The NNP might be either positive or negative. Tests directed by Ferguson and detailed by Lapakko (1994) showed that NNP values under –20 (kg $CaCO_3$/t) are probably going to produce acid and those with NNP values more than 20 were not likely to produce acid. For NNP values between –20 and 20 (kg $CaCO_3$/t), it is hard to determine the acid potential (uncertain). The Neutralising Potential Ratio (NPR) is calculated by dividing the NP through the AP (Equation 3.5).

For NPR less than 1, the material is acid producing and if NPR is above 1, it is acid neutralising (Ferguson and Morin, 1991).

The single addition Net Acid Generation (NAG) test procedure was as follows: place 2.5 g of weighed pulverised sample into a 250 mL conical flask, add 125 mL of 15% H_2O_2, cover the flask with a watch glass and allow the mixture to react overnight in a well-ventilated area, measure pH before boiling the mixture (pre-boil pH), heat solution until bubbling stops or for a minimum of 2 h, give it time to cool to room temperature, add an amount of de-ionised water to sustain the 125 mL volume, measure the pH after boiling the mixture (post-boil pH). This pH is also known as the NAG_{pH} (Smart *et al*., 2002). Thereafter filter the mixture using a 0.45 µm membrane filter; keep the filtered sample solids residue and liquor, back titrate the filtrate liquor with 0.1 M NaOH to pH 4.5 and 7.0 while recording the volume added at pH 4.5 and pH 7, and then calculate the NAG (equation 3.6). The sequential NAG test included that the filtered solid sample residue is returned to the flask, then the single addition procedure will be repeated in a sequential form until the NAG_{pH} is > 4.5 and no more reaction taking place, then the NAG can be calculated (Skousen *et al.,* 2002; Smart *et al*., 2002).

$$NNP = NP - AP \qquad \text{Equation 3.4}$$

$$NPR = \frac{NP}{AP} \qquad \text{Equation 3.5}$$

$$NAG = \frac{50 \times V_{NaOH} \times M_b}{m} \qquad \text{Equation 3.6}$$

Where: V_{NaOH} Volume of NaOH, L

50 Stoichiometric conversation factor

M_b Molarity of the base (NaOH)

m Mass of the sample, g

3.3.4 Kinetic Test

Kinetic tests were conducted to mimic the field conditions. The column leach test was adopted for this study due to the fact that it fits the small scale site conditions, it is less complicated to conduct and it is less costly compared to the other kinetic

tests, while producing similar results. The column leach test was conducted by stacking the approximately 6 mm crushed samples in a cylindrical column. It was carried out in the form of cycles, namely; wetting and drying cycles, in this, a measured amount of de-ionised water was introduced into the column and drained out then enabling the column to dry. Each cycle was for a period of a few days to possibly more than seven days, however, for this study each cycle was ran for 3.5 days each as suggested by the U.S. Environmental Protection Agency (1994).

A small amount of the input water was sampled and taken for analysis as control sample. The leachate was collected, and its volume was measured. A 50 mL of the leachate was filtered and acidified to prepare them for elemental analysis. The following water quality parameters were measured on the unfiltered and unacidified water sample: dissolved oxygen (DO), temperature, pH, redox potential, EC, sulfate, total iron, ferrous iron, acidity and alkalinity.

4. CHAPTER FOUR: RESULTS AND DISCUSSION

4.1 Results and Interpretation

This section presents the results obtained during the study. The results were presented according to the expected outcome of the study which includes the determination of the current AMD status and the prediction of the AMD potential.

4.1.1 Mineralogical Characterisation

The mineral characterisation included the use of optical properties of minerals under the microscope for the purpose of mineral identification to identify different rock types. This was done in order to determine the potential for acid mine drainage. The mineralogical properties that were studied for the prediction of AMD include morphology (framboidal and euhedral), surface area and mineral dissemination. The XRD results were also used to quantify different minerals present in each sample to confirm the AMD potential.

Mineralogical characterisation is an essential component of drainage chemistry predictions. This is so because the mineralogical properties determine the physical, geochemical stability and relative weathering rates of geological materials under different weathering conditions. This was highly important in the interpretation of the kinetic test (column leach test) and static tests (acid base accounting and net acid generation) results. Therefore, petrographic and XRD analysis were adopted for the study as stated above.

4.1.1.1 Petrographic Results

The petrographic results describe in detail the nine selected samples of the Albert silver mine, which include both physical and optical properties of the minerals of the core and rock specimen. The samples were initially studied visually to fully describe the physical properties of the minerals and also using petrographic microscopy to ascertain the optical properties of the minerals. The scale of the photomicrographs is 200 µm. The XRD results confirmed the occurrence of such minerals and further confirmation was conducted by a literature review.

B26T12-2: Chloritised fine grained porphyritic granite

Sample B26T12-2 was obtained from borehole number 26, tray 12 and sample number 2 within the tray. The cross-sectional view of borehole 26 shows the sample's location (Fig. 4.3). This specimen was located on the contact between the quartz-hematite vein and the fine-grained porphyritic granite on the high alteration zone. The rock specimen has a dark greenish colour resulting from rock alteration (Fig. 4.1). The rock alteration was found to be chloritisation and was also found by Bailie and Robb (2004), Maulenbeld *et al*. (2014) and Champion (1970). Occurrence of a greenish phenocryst was observed scattered within the sample (Fig. 4.1).

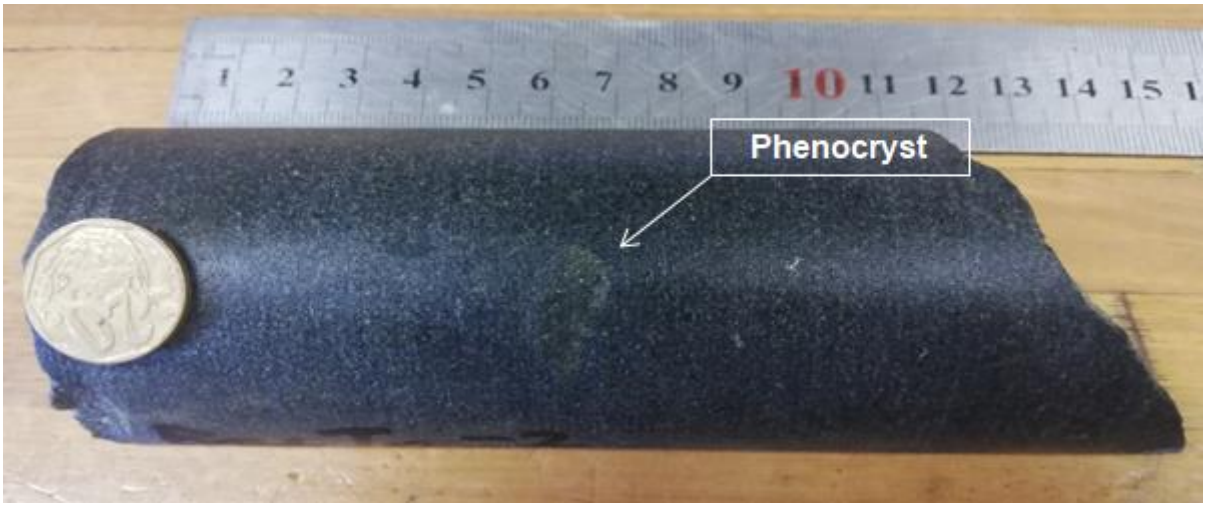

Figure 4.1: Dark coloured core sample (B26T12-2) with greenish phenocryst.

Microscopically, the specimen revealed abundance of quartz that showed brownish colour under PPL while occurrence of chlorites were found to be greenish and dark green in colour under XPL and PPL (Fig. 4.2). The third most prominent mineral was muscovite, which was identified by its cleavage and dark grey colour under XPL.

Summarized, specimen B26T12-2 is fine textured with the major minerals quartz and muscovite. Chlorites occurred as product of a chloritization process which was confirmed by the sample location point. The presence of those minerals has also been shown by Bailie and Robb (2004), Maulenbeld *et al.* (2014) and Champion (1970). Consequently, specimen B26T12-2 is an altered fine-grained porphyritic granite.

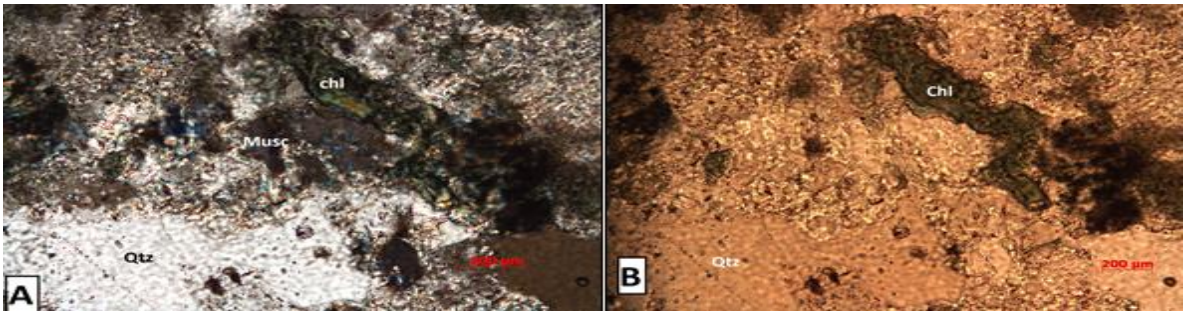

Figure 4.2: Photomicrographs of sample B26T12-2.
A XPL and **B** PPL: whitish grey quartz (Qtz) under XPL and brownish under PPL, greenish chlorite (Chl) under XPL and darker green under PPL and dark grey muscovite (Mus) under XPL and light brown under PPL.

B26T16-1: Mineralised quartz vein and fine-grained porphyritic granite

Sample B26T16 is from borehole number 26, tray number 16 and sample number 1 within the tray (Fig. 4.3). This specimen was located at the contact between the mineralised quartz vein and fine-grained porphyritic granite, evidenced by both rock types being present in the same sample. Macroscopically, the specimen contained pyrite, which was evident by the metallic golden brassy coloured grains, while the other part of the specimen shows alteration. Chloritization was confirmed by the greenish mineralisation. The mineralogy of the specimen revealed that this sample is a mixture of the fine-grained porphyritic granite and the mineralised quartz vein (Fig. 4.3).

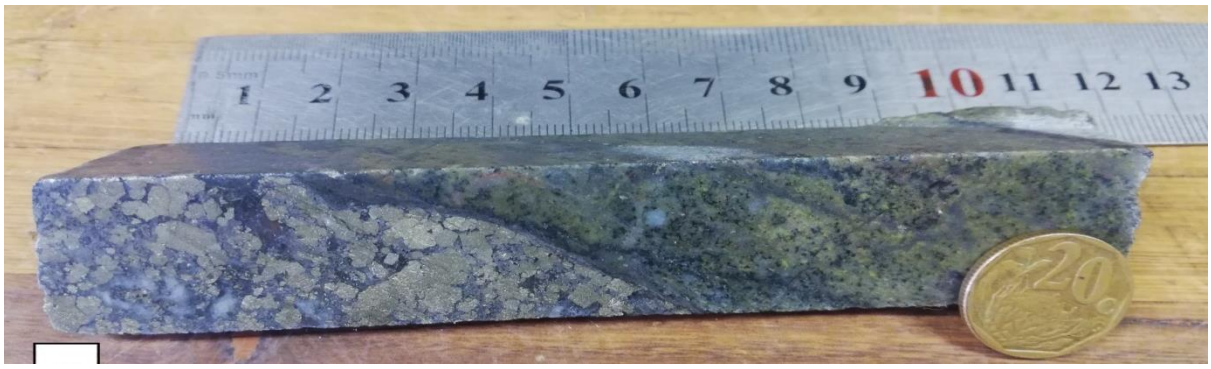

Figure 4.3: Greenish core sample (B26T16) with metallic brassy coloured pyrite grains, the greenish colour is from the chlorite.

The microscopic analysis showed that the light grey to light brownish mineral is quartz, recognized by its hexagonal crystal system, and being found in abundance in

the samples (Fig. 4.4). The dark minerals appear to be pyrite which was confirmed by the cubic crystal system and the isotropic property that makes it appear opaque under XPL and when the stage is rotated (Fig 4.4 A). Thirdly, the specimen contains a dark brown reddish mineral which appeared to be arsenopyrite, which was confirmed by its weak, white with bluish tint to faint reddish yellow pleochroism and its strong, red-violet anisotropy (Fig. 4.4).

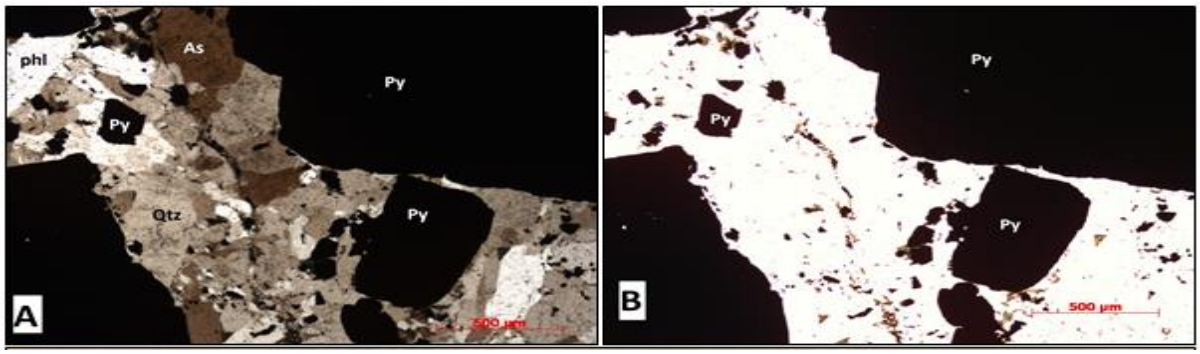

Figure 4.4: Photomicrographs of sample B26T16-1.

A XPL and **B** PPL: whitish brown quartz (Qtz) under XPL and whitish under PPL, opaque, cubic (dark) pyrite (Py) under XPL and also under PPL and brownish red pleochroic arsenopyrite (As) under XPL and whitish under PPL, elongated whitish phlogopite (Phl) under XPL and also under PPL.

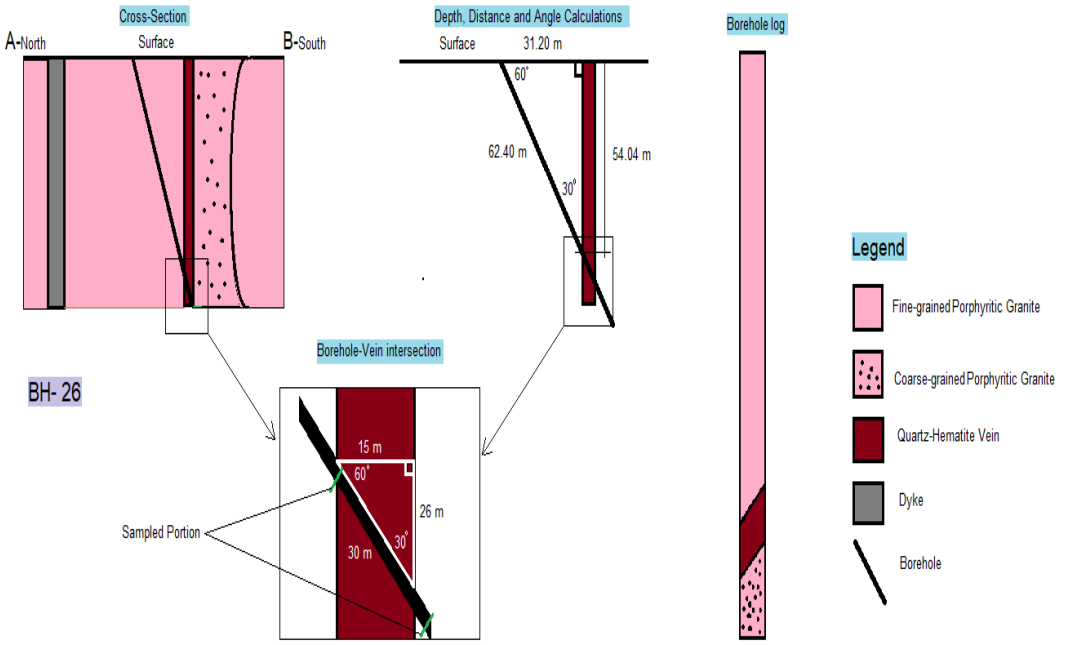

Figure 4.5: Cross-sectional view of borehole 26 showing the sampled portion of the core.

B27T7-2: Mineralised quartz vein

Sample B27T7-2 is from borehole number 27, tray number 7, and sample number 2 within the tray (Fig. 4.6). The mineralogical composition revealed that this specimen is from the mineralized quartz vein, which is evident by the whitish grey minerals in the specimen being quartz and the metallic brassy coloured minerals being disseminated pyrite grains.

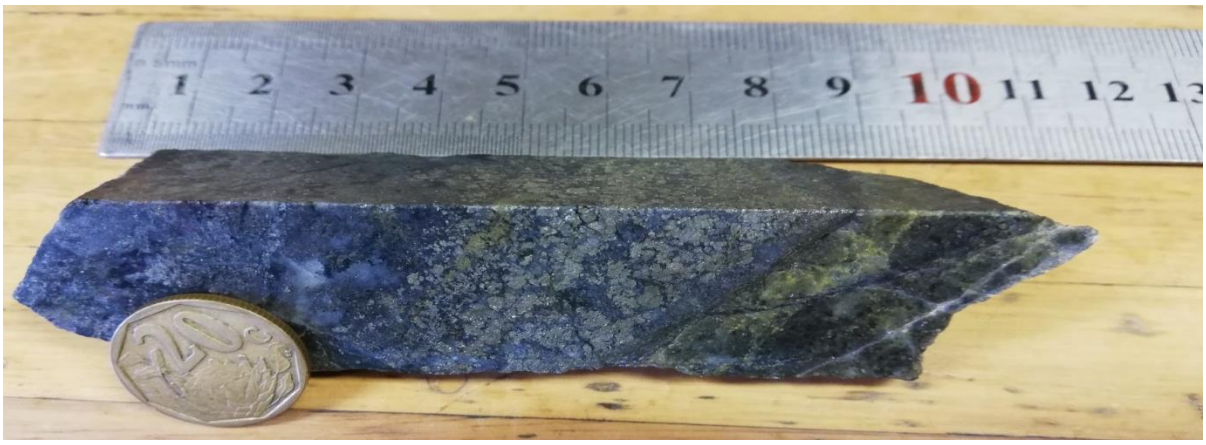

Figure 4.6: Dark core sample (B27T7-2) with metallic brassy coloured pyrite grains (in the centre of the image).

The petrographic analysis showed that the specimen is dominated by a whitish grey mineral which is quartz (Fig. 4.7). According to the description above, the arsenopyrite was identified by its weak, white bluish tint to faint reddish yellow pleochroism and strong red-violet anisotropy. In this specimen the arsenopyrite appears yellowish red due to its pleochroism. The dark opaque mineral in the specimen appears to be pyrite (Fig. 4.7). The specimen shows minor dark greyish mineralisation which is muscovite with a distinct cleavage in PPL (Fig. 4.7). In summary, this specimen is a mineralised quartz vein from the Albert load (quartz-hematite vein).

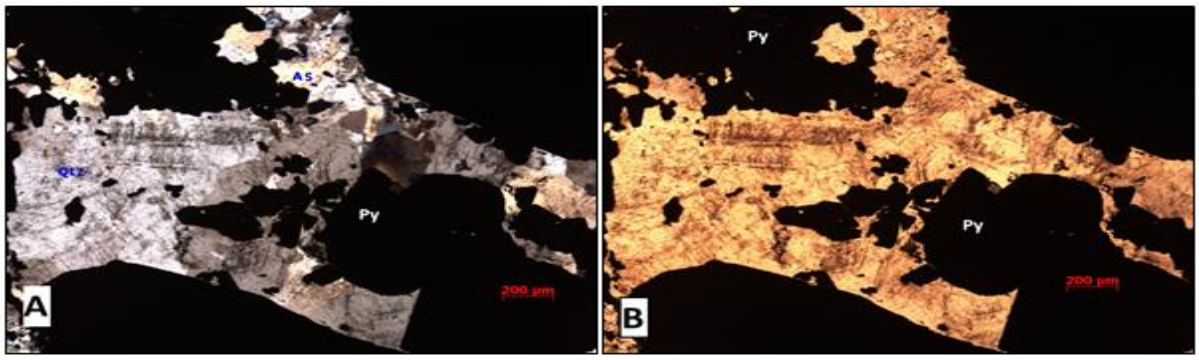

Figure 4.7: Photomicrographs of sample B27T7-2,
A XPL and **B** PPL whitish grey quartz (Qtz), under XPL and brownish under PPL, opaque, cubic (dark) pyrite (Py) under XPL and also under PPL and brownish yellow pleochroic arsenopyrite (As) under XPL and brownish under PPL.

B27T8: Mineralised quartz vein

The rock specimen B27T8 was obtained from borehole 27 at the Albert silver mine and it was sample number 1 within tray 8 (Fig. 3.2 and Fig. 3.3). This sample of the mineralised quartz vein shows that the specimen is dominated by whitish quartz and metallic brassy coloured pyrite in minor grains and metallic silver samples of arsenopyrite (Fig. 4.8).

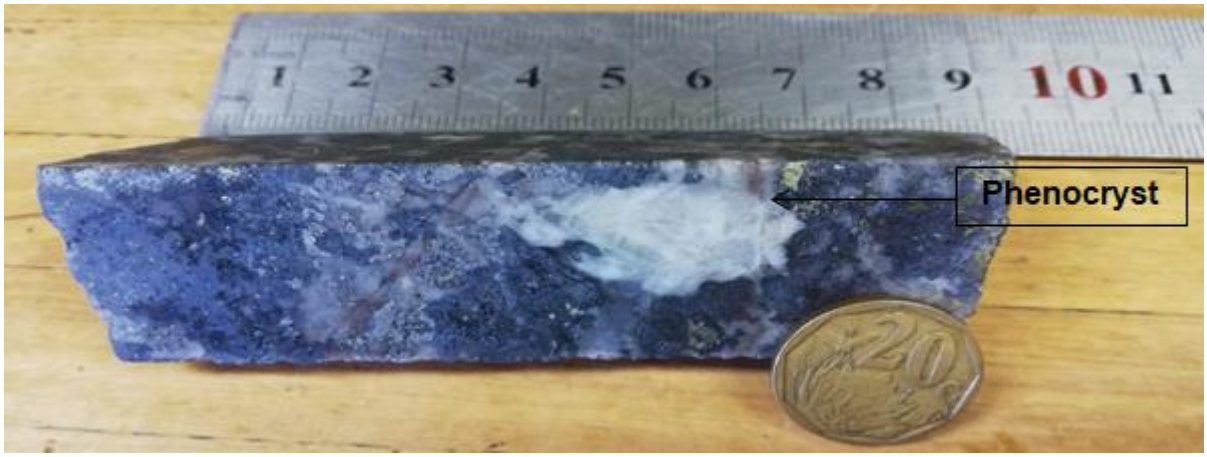

Figure 4.8: Dark core sample (B27T8) with metallic coloured, silvery disseminated arsenopyrite, brassy coloured pyrite grains and a large quartz phenocryst.

Microscopically, the specimen is dominated by whitish grey quartz (Fig. 4.9). The reddish-brown mineral is hematite and possesses brownish grey anisotropism, and under PPL this mineral appears light brownish (Fig. 4.9). The specimen contains a bluish pleochroic mineral, which is arsenopyrite. In summary, specimen B27T8 is medium to fine textured, with the major mineral quartz; pyrite and arsenopyrite occur as a product of mineralisation.

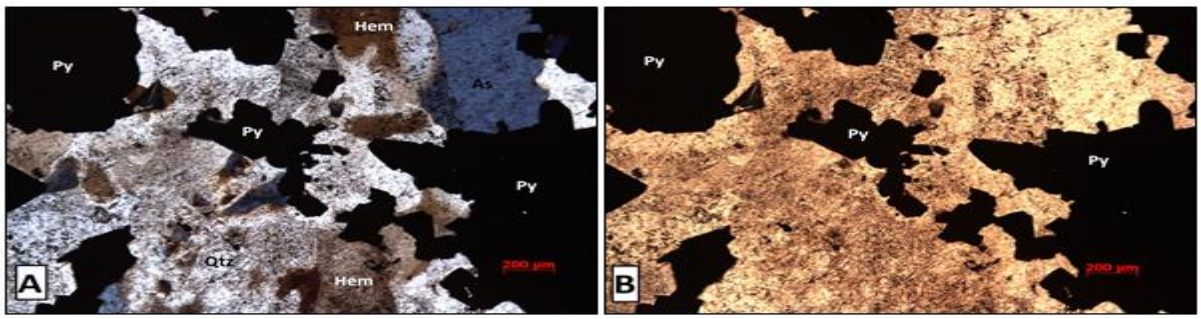

Figure 4.9: Photomicrographs of sample B27T8,
A XPL and **B** PPL whitish grey quartz (Qtz) under XPL and brownish under PPL, opaque, cubic (dark) pyrite (Py) under XPL and also under PPL and bluish pleochroic arsenopyrite (As) under XPL and brownish under PPL and brownish hematite under XPL and light brownish under PPL (Hem).

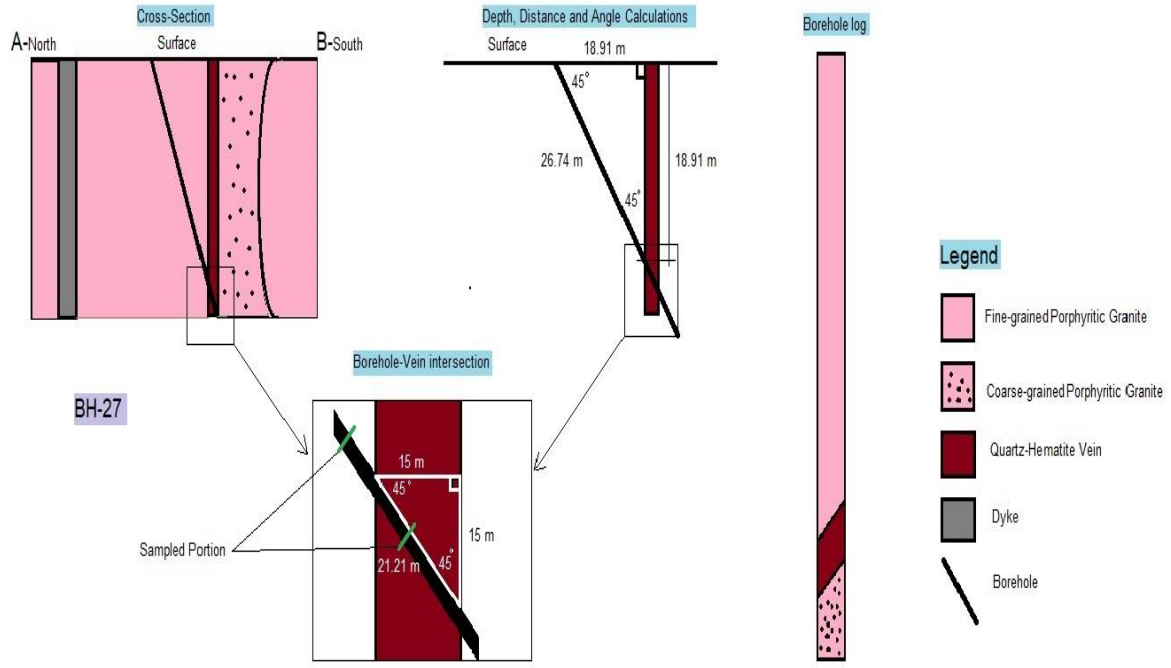

Figure 4.10: Cross-sectional view of borehole 2 showing the sampled portion of the core.

B36T17: Hematitised fine grained porphyritic granite

Sample B36T17 was obtained from borehole number 27 at the Albert silver mine in tray number 17 and it was sample number 2 in the tray. Mineralogically, this specimen was dominated by quartz and maroonish minerals (Fig. 4.11). Macroscopically, the specimen appeared maroonish in colour; the maroon colour was the result of rock alteration. The process was found to be hematitisation mineralogy. The intensive alteration (hematitisation) suggests that this sample was along the contact between the quartz-hematite vein and the fine-grained porphyritic granite (Fig. 4.11). According to Bailie and Robb (2004), the northern part of the quartz-hematite vein possesses high hematitisation rock alteration. White quartz phenocrysts were found scattered on the specimen, some appeared to be minor veins.

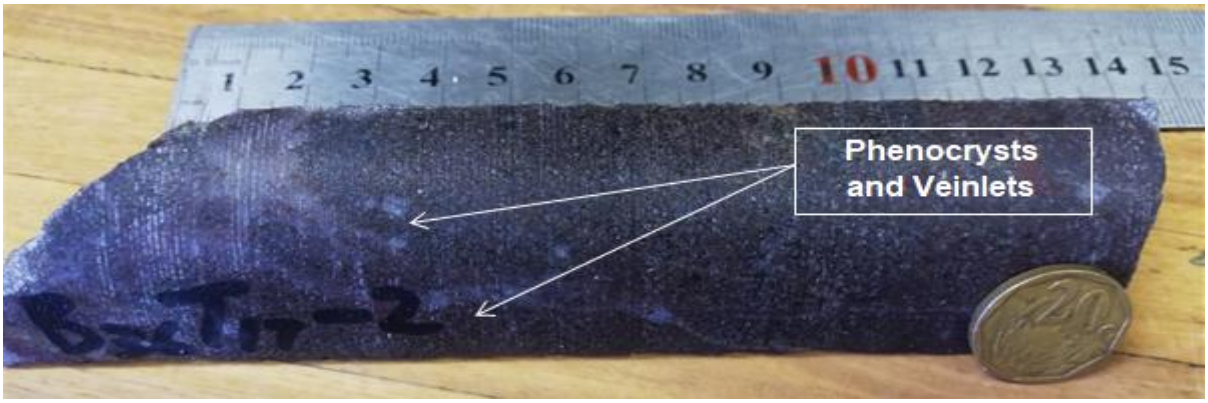

Figure 4.11: Dark maroonish core sample (B36T17) with elongated quartz phenocrysts, the maroon colour is due to the hematite.

The petrographic analysis showed that the specimen was dominated by a grey mineral which was quartz and this mineral appears brownish under PPL. Muscovite was also identified in this specimen; this was by its cleavage and dark grey colour under XPL. Hematite was identified by its brownish grey anisotropism under the PPL; this mineral appears light brownish (Fig. 4.12). In summary, it was concluded that this sample was a hematitised fine grained porphyritic granite, therefore it was confirmed that this sample was from the host rock. The literature review, visual observation and XRD were used to confirm the mineralogy.

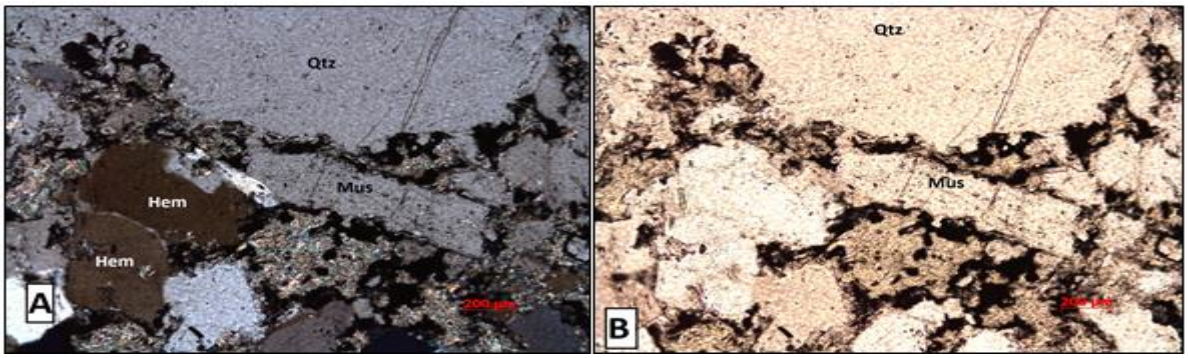

Figure 4.12: Photomicrographs of sample B36T17-2.
A XPL and **B** PPL greyish quartz (Qtz) under XPL and brownish under PPL, greyish elongated muscovite (Mus), under XPL and brownish under PPL and dark to brownish hematite (Hem), under XPL and light brownish to white under PPL

B36T22: Fine grained porphyritic granite

Sample B36T22-1 was obtained from borehole number 36 at the Albert silver mine in tray number 22 and it was sample number 1 within the tray. The cross-section shows the location of the specimen sampling point which is the unaltered portion of the host rock (Fig. 3.3 and Fig. 4.15). Macroscopically, the specimen shows a pinkish colour, and large plagioclase feldspar phenocrysts are also clearly visible. In the pinkish minerals are feldspars whereas the white and dark minerals are quartz and the ferromagnesian minerals that occur as minor minerals. This includes the likes of biotite respectively. The mineralogical composition aided in the confirmation that this specimen was obtained from the fine-grained porphyritic granite which formed the host rocks (Fig.4.13).

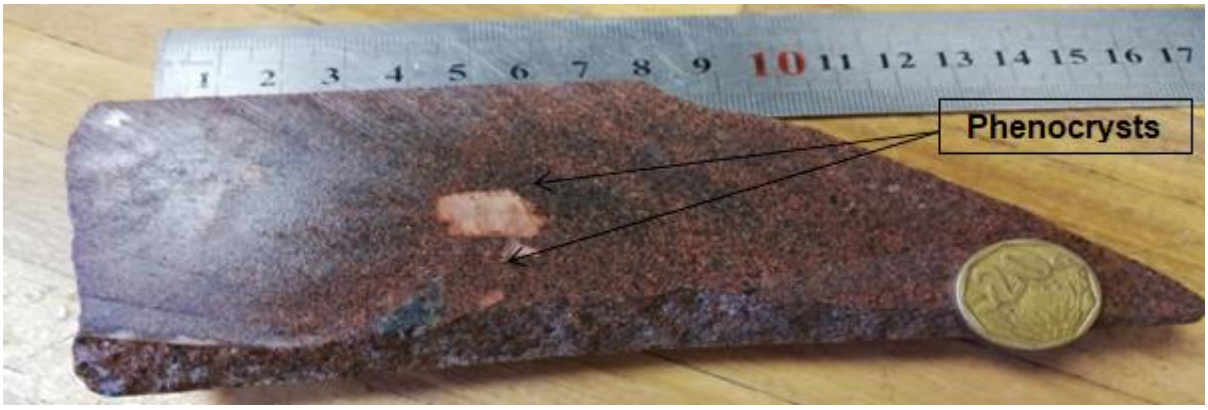

Figure 4.13: Pinkish core sample (B36T22) with a large plagioclase feldspar phenocryst.

Microscopically, it was evident that the specimen was dominated by light and dark greyish minerals; the light grey most abundant mineral was quartz, which was clearly identified by their hexagonal crystal system as part of its optical property (Fig. 4.14). The plagioclase feldspar which was the dominant feldspar mineral in the specimen was seen by their elongated dark brown property under both XPL and PPL (Fig. 4.14). The striated dark grey minerals are muscovite and microcline under XPL; these minerals are brownish under PPL (Fig. 4.14). Mineralogically, it was classified as the fine grained porphyritic granite.

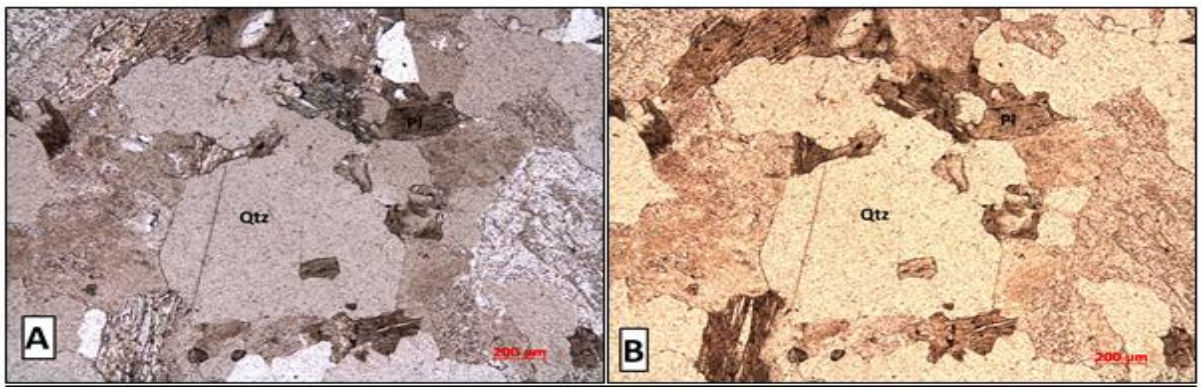

Figure 4.14: Photomicrographs and photograph of sample B36T22,
A XPL and **B** PPL greyish quartz under XPL, brownish under PPL (Qtz), elongated dark brown plagioclase under XPL and also under PPL (Pl) and striated brownish muscovite (Mus) and microcline (Mic) under XPL and also brownish under PPL.

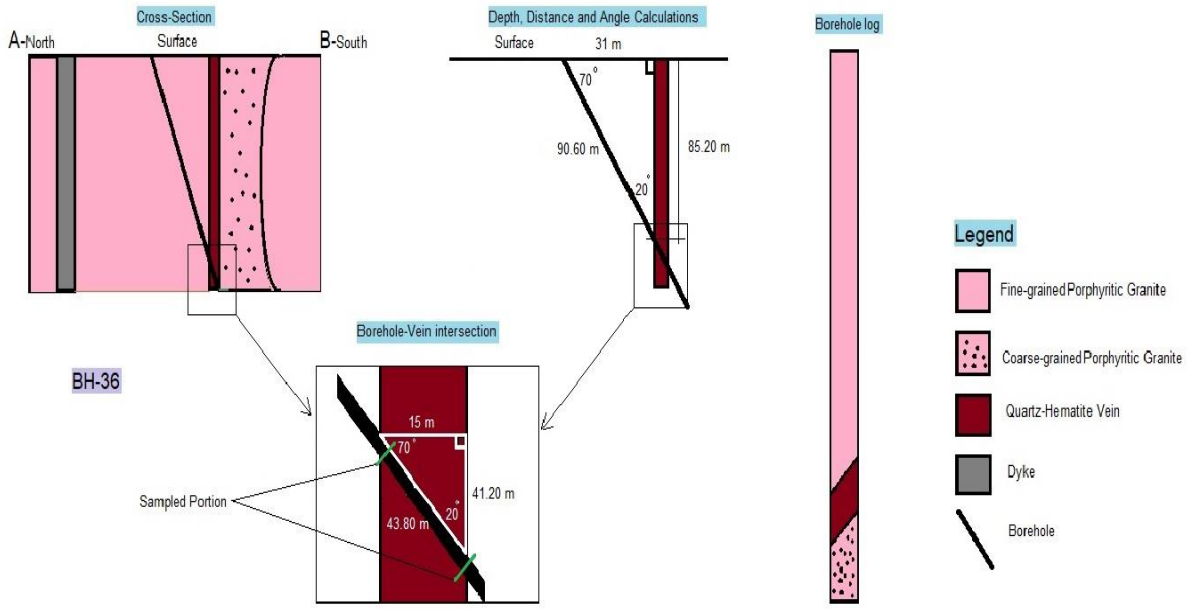

Figure 4.15: Cross-sectional view of borehole 36 showing the sampled portion of the core.

FG1: Fine grained porphyritic granite

Specimen FG1 was obtained on the outcrop at the Albert silver mine. This is a surface sample from the host rock within the vicinity of the mine. The geological map (Fig. 3.3) shows the sample location. The macroscopic and microscopic analysis showed that the mineralogy of this sample is similar to that of B36T22. Fig. 4.16 also

shows the comparative pinkish surface sample with large plagioclase feldspar phenocryst as discussed above. The accessory minerals in this specimen include whitish quartz and dark biotite minerals. The fine texture of the specimen also confirmed the source rock of the specimen, which is the felsic intrusive igneous rock.

Microscopically, it was confirmed that this specimen was obtained from the fine grained porphyritic granite which forms the host rocks. In this, the whitish grey most abundant mineral is quartz, which was confirmed by the deformed hexagonal crystal system. The elongated dark brown minerals are plagioclase under both XPL and PPL (Fig. 4.17). The optical mineralogy showed an evidence of striated dark grey minerals which appear to be muscovite and microcline under XPL; these minerals are also brownish under PPL (Fig. 4.17). In summary, the mineralogy confirmed that this is unaltered fine-grained granite.

Figure 4.16: Pinkish surface sample (FG1) with quartz and plagioclase feldspar phenocrysts.

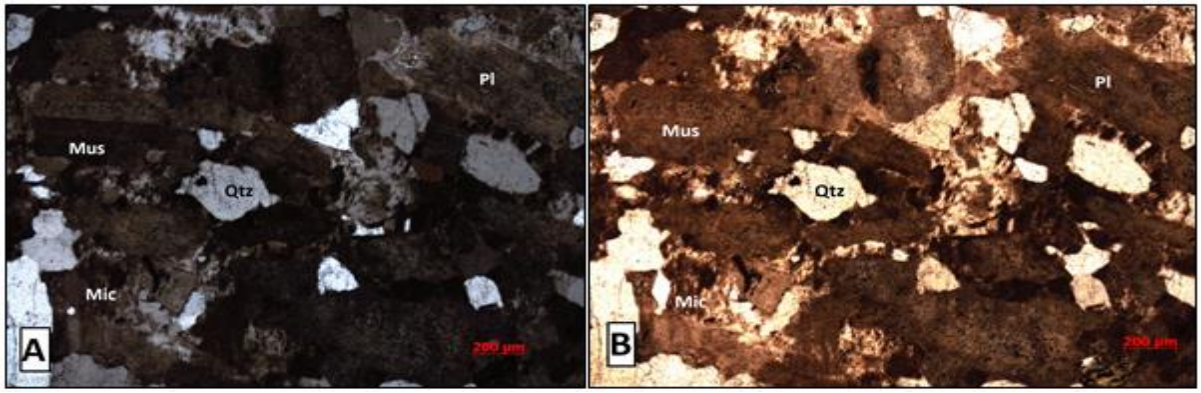

Figure 4.17: Photomicrographs of sample FG1.

A XPL and **B** PPL greyish quartz (Qtz) under XPL, light brownish under PPL, elongated dark brown plagioclase (Pl) under XPL and also under PPL and striated brownish microcline (Mic) and muscovite (Mus) under XPL and also brownish under PPL.

VS1: Quartz-hematite vein

Sample VS1 was obtained from the outcrop at the vicinity of the Albert silver mine. The geological map shows the lithologies and the specimen sampled location (Fig. 3.3). The specimen is from the quartz-hematite outcrops which formed part of the Albert load gossans. Macroscopically, the specimen contained a combination of whitish and maroonish minerals, which are quartz and hematite respectively (Fig. 4.18).

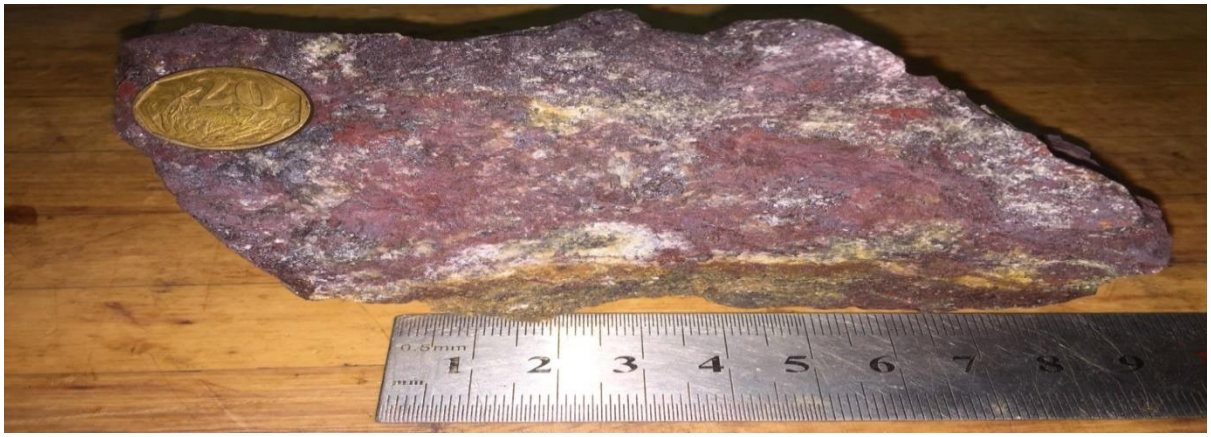

Figure 4.18: Maroonish surface sample (VS1), the maroon colour is due to the hematite and the white colour on the sample is due to the quartz.

The petrographic analysis showed that the specimen is dominated by a whitish to grey mineral, which was confirmed to be quartz and this was also due to their brownish colour under PPL. The hematite in the specimen was identified by its brownish grey anisotropism under XPL and under PPL this mineral appeared light brownish (Fig. 4.19). The mineralogy confirmed that the specimen was a quartz vein; this was further confirmed by literature review and XRD.

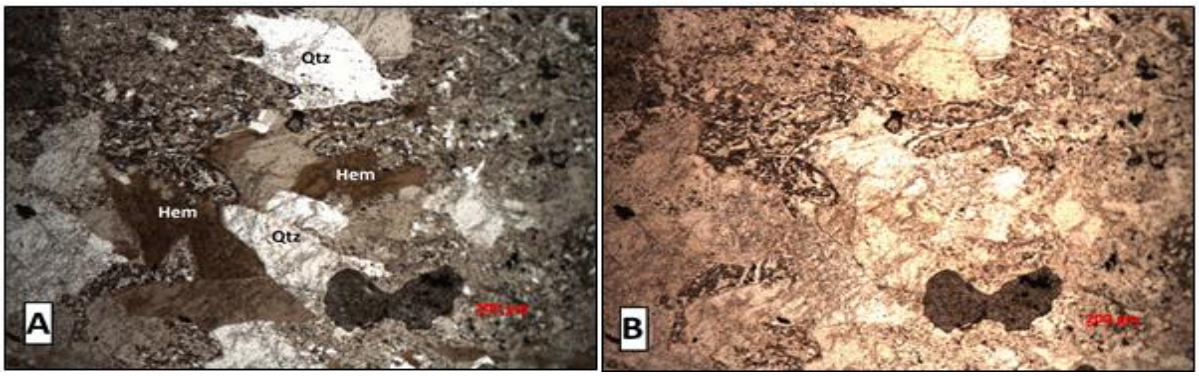

Figure 4.19: Photomicrographs of sample VS1.
A XPL and **B** PPL white to greyish quartz (Qtz), under XPL and brownish under PPL, dark brownish hematite (Hem) under XPL and light brownish to white under PPL.

DS1: Diabase dyke

Specimen DS1 was obtained from the outcrop within the vicinity of the Albert silver mine, with the geological map showing the specimen sampled location (Fig. 3.3). The rock specimen has a greyish surface (Fig 4.20); according to the mineralogy, this sample is from a diabase dyke. This is proven by the whitish, felsic minerals which include Plagioclase, chlorite, sepiolite, and quartz, whereas Augite, muscovite, hornblende, ilmenite, sepiolite and magnetite are the dark minerals which led to the specimen having an intermediate colour.

Figure 4.20: Greyish surface sample (DS1); the colour is due to the equal amount of mafic and felsic minerals.

The mineralogical composition successfully showed that the elongated brownish minerals are plagioclase under XPL and light brownish under PPL (Fig. 4.21). The yellowish distinct shaped mineral is augite under XPL and brownish under PPL, the brown elongated minerals with a distinct cleavage is muscovite under XPL and this minerals is light brownish under PPL, the other brownish mineral with cleavage is hornblende under XPL and it is light brownish under PPL and the greenish mineral is chlorite under XPL and this mineral is brownish under PPL.

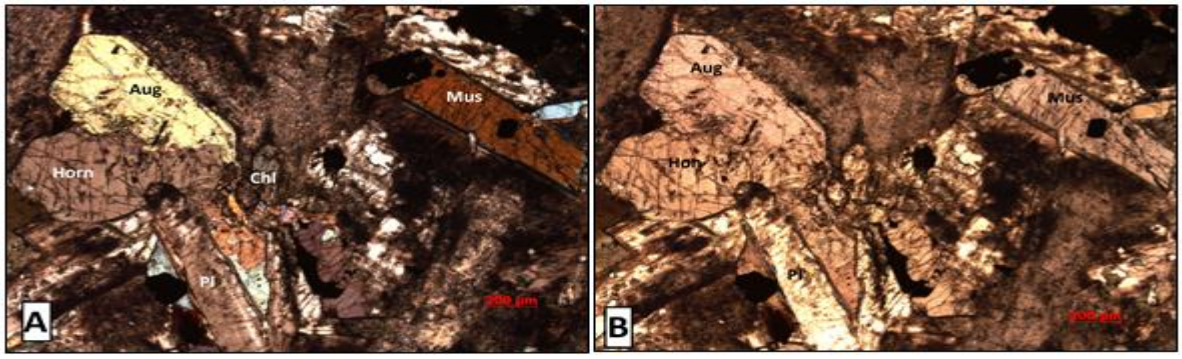

Figure 4.21: Photomicrographs of sample DS1.
A XPL and **B** PPL elongated brownish plagioclase (Pl) under XPL and light brownish under PPL, yellowish distinct shaped Augite (Aug) under XPL and brownish under PPL brown elongated cleavage muscovite (Mus) under XPL and light brownish under PPL and brownish cleavage hornblende (Horn) under XPL and light brownish under PPL and greenish chlorite (Chl) under XPL and brownish under PPL.

4.1.1.2 XRD Results of Rocks

The XRD results (Table 4.1) revealed different types of minerals within each rock type and their weight percentage (wt%). The results were further confirmed by comparing them with the XRF results and the petrographic studies.

B26T12: Chloritized fine-grained granite

The minerals within the chloritized fine-grained granite are quartz, muscovite and chlorite with a high weight wt% of quartz (71.31 wt%) followed by muscovite with 20.71 wt% and less content of chlorites (7.98 wt%) (Table 4.1). Other minerals were identified by petrographic studies.

B26T16: Quartz vein and chloritized fine grained porphyritic granite

Specimen B26T16 is composed of quartz (61.66 wt%), pyrite (16.85 wt%), arsenopyrite (9.14 wt%), phlogopite (7.66 wt%), chlorite (3.27 wt%) and galena (1.42 wt%) (Table 4.1). It was confirmed that the quartz vein and chloritized fine-grained porphyritic granite were located on the contact between the mineralised quartz vein and the altered host rock. It is a chloritized fine-grained porphyritic granite, which was confirmed by minerals of the quartz vein and the host rock. The visual observations also confirmed the location of this rock.

B27T7: Mineralised quartz vein

Specimen B27T7 was confirmed to be the mineralised quartz vein due to its composition of quartz (50.97 wt%), arsenopyrite (18.59 wt%), pyrite (16.39 wt%), muscovite (8.17 wt%), chalcopyrite (4.09 wt%) and pyrope, a member of the garnet family (1.8 wt%) (Table 4.1). The high content of quartz and sulfide minerals led to the confirmation of the rock name, this was also supported by the lack of in feldspars and other granitic minerals.

B27T8: Mineralised quartz-hematite vein

The minerals within the mineralised quartz-hematite vein are quartz (52.5 wt%), hematite (24.72 wt%), arsenopyrite (6.69 wt%), pyrite (6.12 wt%), calcite 5.6 wt%), magnetite (2.25 wt%) and tennantite (2.12 wt%) (Table 4.1). The classification of the specimen was confirmed by the high quartz content followed by hematite and sulfide

minerals. The specimen contains a certain percentage of the acid neutralising mineral calcite. Tennantite is a member of the sulfosalts, and it is a source of copper, having been confirmed by the sample's XRF results (Table 4.3). The mineralogy of B27T7 and B27T8 is similar to B27T7 except that the latter has less hematite and tennantite.

B36T17: Quartz hematite vein

The XRD results revealed that specimen B36T17 has a quartz (78.01 wt%) content followed by muscovite (14.81 wt%) and minor hematite (7.18 wt%). This mineralogy was utilised in the confirmation of the specimen name. Furthermore, the minerals were identified through petrographic studies, confirming its composition.

B36T22: Fine grained porphyritic granite

The specimen B36T22 is a fine grained porphyritic granite proven by its composition having plagioclase (43.95 wt%), quartz (39.58 wt%), muscovite (6.75 wt%), microcline (6.53 wt%) and chlorite (3.19 wt%) (Table 4.1). The high content of plagioclase feldspar and the deficiency of sulfide minerals was the main confirmation of the specimen name.

FG1: Fine grained porphyritic granite

The specimen FG1 is a fine-grained porphyritic granite due to its composition of quartz (36.66 wt%), plagioclase (34.65 wt%), microcline (19.14 wt%), chlorite (4.9 wt%) and muscovite (4.65 wt%) (Table 4.1). The high content of microcline was the main confirmation of the specimen name, since quartz is slightly higher than plagioclase feldspar. Both specimens B36T22 and FG1 were confirmed to be the fine-grained granite with B36T22 being a core sample from depth and FG1 being a surface rock specimen obtained from the granitic outcrop.

VS1: Quartz hematite vein

The minerals within the quartz hematite vein are quartz and hematite with a high weight %wt of quartz (73.61 wt%) followed by hematite with 26.39 wt% (Table 4.1). This was a surface specimen with no sulfide minerals, this was also confirmed by the petrographic studies.

DS1: Diabase dyke

The specimen DS1 was confirmed to be a diabase dyke due to its composition of plagioclase (49.29 wt%), augite (15.5 wt%), muscovite (10.85 wt%), hornblende (7.72 wt%), chlorite (6.12 wt%), ilmenite (3.12 wt%), sepiolite (2.55), magnetite (2.51 wt%) and quartz (2.34 wt%) (Table 4.1). The high content of plagioclase feldspar and the deficiency of quartz minerals was used in the confirmation of the specimen name.

Based on the results of the rock description, mineral phases and experiments, it was possible to classify the specimen in terms of its potential to produce AMD (Table 4.2). The chloritized fine grained porphyritic granite, fine grained porphyritic granite and the diabase dyke have a low potential to produce AMD. The mineralised quartz vein with deficit sulfide minerals also had a low potential to produce AMD which includes samples such as B36T17 and VS1. The mineralised quartz vein has a high potential to produce AMD and includes specimen B26T16, B27T7 and B27T8. In summary, the sulfide bearing specimens have a high potential to produce AMD.

Table 4.1: XRD mineralogical composition results in wt%

Mineral	B26T12	B26T16	B27T7	B27T8	B36T17	B36T22	DS1	FG1	VS1
Quartz	71.31	61.66	50.97	52.5	78.01	39.58	2.34	36.66	73.61
Muscovite	20.71		8.17		14.81	6.75	10.85	4.65	
Chlorite	7.98	3.27				3.19	6.12	4.9	
Arsenopyrite		9.14	18.59	6.69					
Hematite				24.72	7.18				26.39
Plagioclase						43.95	49.29	34.65	
Pyrite		16.85	16.39	6.12					
Magnetite				2.25			2.51		
Microcline						6.53		19.14	
Augite							15.5		
Calcite				5.6					
Chalcopyrite			4.09						
Galena		1.42							
Hornblende							7.72		
Ilmenite							3.12		
Phlogopite		7.66							
Pyrope			1.8						
Sepiolite							2.55		
Tennantite				2.12					

The XRD data analysis showed that 33.33% of the selected samples contained sulfide minerals (Fig. 4.22). These samples are B26T16 (27.41 wt% sulfide minerals), B27T7 (39.07 wt% sulfide minerals) and B27T8 (12.81 wt% sulfide minerals). The available sulfide minerals and their total percentage in all the samples (Table 4.1) included pyrite (39.36 wt%), arsenopyrite (34.42 wt%), chalcopyrite (4.09 wt%) and galena (1.42 wt%). Carbonate minerals (calcite) were found in sample B27T8 with 5.6 wt%. According to the XRD results, borehole 36 and the surface rocks have a low potential to produce AMD while borehole 26 and 27 have a high potential to produce AMD (Table 4.1 and Fig. 4.22).

Table 4.2: Description of the samples subjected to AMD prediction tests from the Albert Silver Mine; mineral content in table. 4.1

Sample ID	Description/Specimen Name	AMD Potential
B26T12	Chloritized fine-grained porphyritic granite	Low AMD potential
B26T16	Mineralised quartz vein and altered (chloritized) fine-grained porphyritic granite	High AMD potential
B27T7	Mineralised quartz vein	High AMD potential
B27T8	Mineralised quartz hematite vein	High AMD potential
B36T17	Quartz hematite vein	Low AMD potential
B36T22	Fine-grained porphyritic granite	Low AMD potential
VS1	Quartz hematite vein	Low AMD potential
FG1	Fine-grained porphyritic granite	Low AMD potential
DS1	Diabase dyke	Low AMD potential

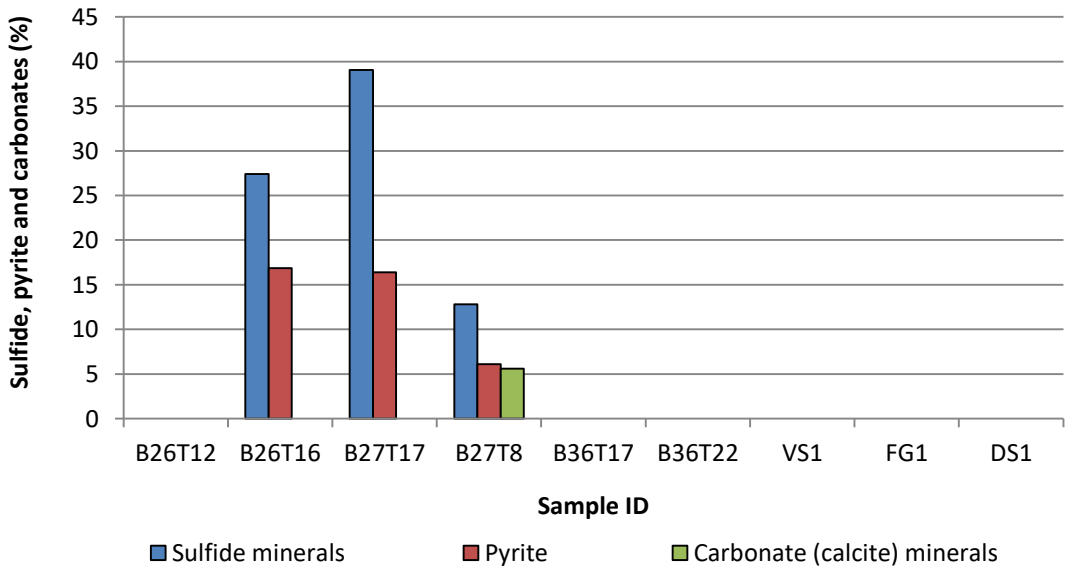

Figure 4.22: Samples containing sulfides, carbonates and pyrite.

4.1.1.3 Factors Influencing Acid Mine Drainage

The rate of AMD formation is influenced by the proportion of sulfide and carbonate minerals, their morphology (framboidal and euhedral), surface area and mineral dissemination. The petrographic results showed no evidence of carbonate minerals; therefore this section focuses on the study of pyrite which is the major di-sulfide

mineral for AMD formation. The study investigates the critical features of pyrite that are responsible for AMD generation, namely: morphology, surface area and mineral dissemination.

Morphology

The morphological properties of the studied minerals are euhedral and framboidal. Euhedral crystal structure (cubic for pyrite) is a mineral morphological property where the crystals are fully formed or undeformed from the original structure. This property of the pyrite grains has a direct influence in the AMD formation as euhedral crystals are less vulnerable to weathering, which is mostly observed by the undeformed cubic edges of the pyrite. This could mean otherwise for other cases such as providing a weak zone for the grain. It is believed that euhedral grains are fully formed with less instability (Maiyana, 2003).

The framboidal pyrite grain morphology is an opposite of the euhedral pyrite grain morphology. In this case, the rock consists of mineral grains that are either deformed or with not well-formed crystal faces. Framboidal grains can be due to weathering of grains or incomplete grain formation during crystallisation. Practically, it is evident that the framboidal grains are more vulnerable to weathering (Weber, 2004). The study revealed both morphologies i.e. euhedral and framboidal crystal shapes. According to the petrographic studies and visual observations, pyrite was identified in only three samples (B26T16, B27T7 and B27T8). Euhedral pyrite crystals were identified in B26T16. Framboidal pyrite crystals were identified in specimen B27T7 and a mixture of both morphologies were identified in specimen B27T8.

In this investigation, there was an equivalent outcome in terms of the euhedral and framboidal pyrite grains implying that the rate of acid formation will be at a normal rate (Fig. 4.23). Yet, the outcome of this morphological analysis in terms of the potential to produce acid is uncertain.

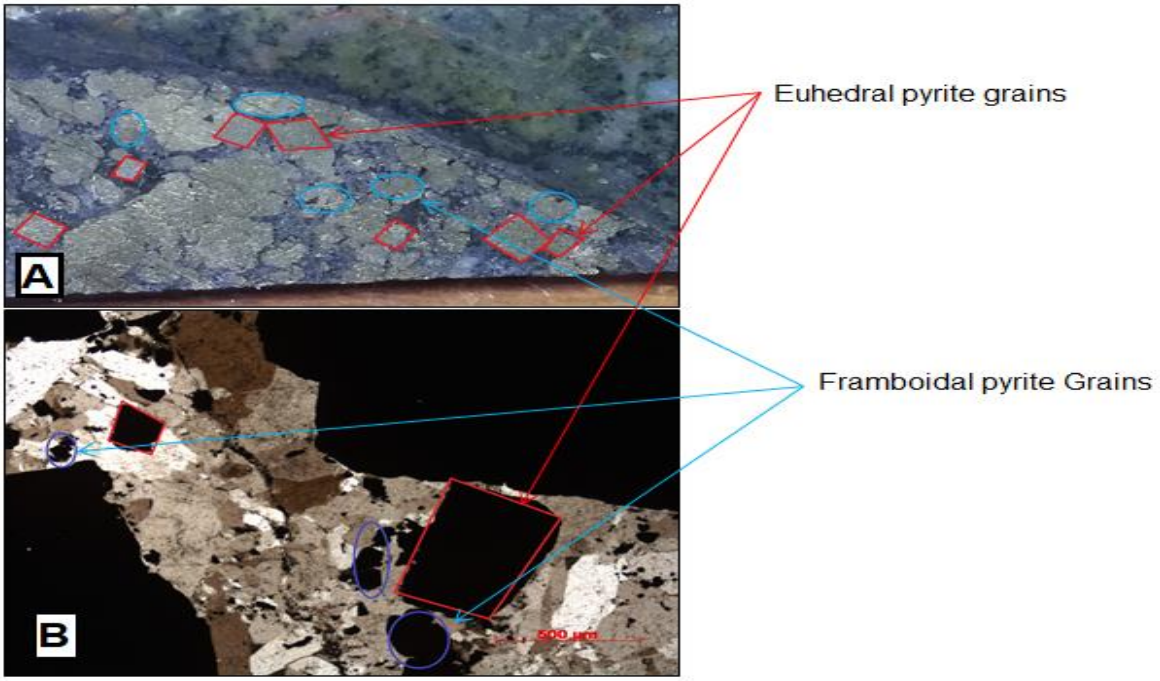

Figure 4.23: **A**: core sample and **B**: Thin section under XPL photomicrography; illustration of the pyrite grain morphology; euhedral (red cubic shapes) and framboidal pyrite grains (blue oval shapes).

Surface Area

The cross sectional surface area of the minerals was measured with the IMAGEJ software. This was initiated by calibrating the software (setting a scale) with a 20-cent coin on the samples photo as a scale. The diameter of the coin with 1.9 cm was used as a known distance. Therefore, the photo was magnified to view each grain clearly and the freehand tool was utilised to draw the borders of each grain. The software then measured the area of the drawn polygon (Fig. 4.24).

Seven pyrite grains from the mineralised quartz vein and altered (chloritized) fine-grained porphyritic granite (B26T16) with well identified euhedral morphology were selected, numbered and their surface areas measured (red cubic shapes) (Fig. 4.24). The mean of their surface area was 0.054 cm^2. Five pyrite grains from the mineralised quartz vein and altered (chloritized) fine-grained porphyritic granite (B26T16) which had perfect framboidal morphology were selected and had a mean surface area of 0.0596 cm^2. The selected framboidal pyrite grains had a larger surface area when compare to the euhedral grains. This is because they contained numerous framboidal grains and this consequently increases the ability to produce

acid. Furthermore, the number of framboidal pyrite grains is higher compare to the number of euhedral grains (Fig. 4.24). This has also been documented by Pugh *et al*. (1981) about the characteristics of pyrite and other associated sulfide minerals in the acid formation.

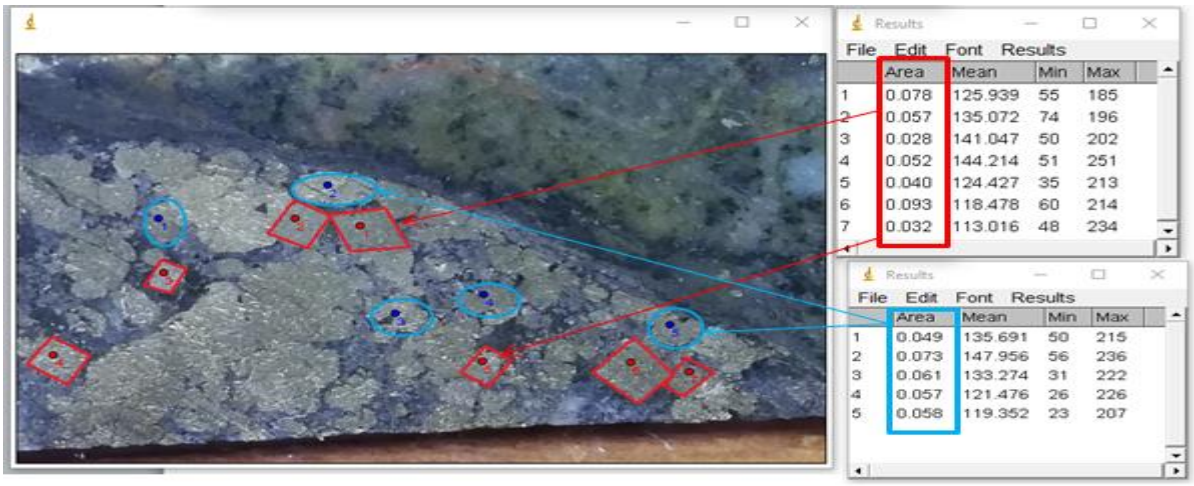

Figure 4.24: Calculation of the cross sectional pyrite grain surface area on the representative hand specimen using the IMAGEJ software; the red rectangle is the surface area for the euhedral pyrite grains and the blue rectangle is the surface area for the framboidal pyrite grains.

Mineral Dissemination

Disseminated minerals are identified by their scattering properties; this particular property provides instabilities in terms of physical and chemical resistance to weathering which renders disseminated pyrite grains vulnerable to weathering (Weisener and Weber, 2010) (Fig. 4.25). Disseminated pyrite grains are rarely found in large amounts in proximity which might have affected the intensity of AMD formation due to the fact that the pyrite quantity is relevant for the intensity of AMD formation.

According to the literature, disseminated pyrite is found along the weak zones of the fractured host rock. These areas of most host rocks show a characteristic hydraulic permeability, which is a direct influence of weathering if water accesses that zone since it will interact with the disseminated pyrite grains. The clustered large pyrite grains are known to be massive. Massive pyrite grains (Fig. 4.25) are less vulnerable

to weathering because its reaction time will be longer compared to the reaction time of disseminated pyrite grains (Schippers, 2004).

The study showed that the disseminated pyrite grains mostly contain a mixture of euhedral and framboidal grains and the massive pyrite grains are mostly dominated by framboidal grains. The disseminated pyrite grains show great potential to acid formation due to its vulnerability to weathering.

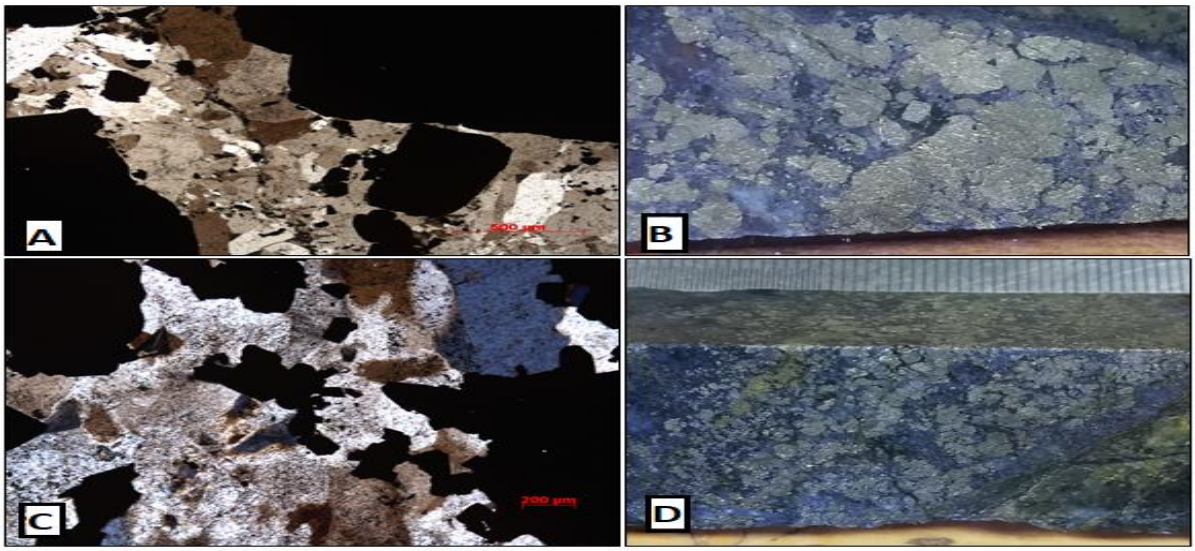

Figure 4.25: Massive and disseminated pyrite grains.

A massive pyrite grains photomicrograph under XPL, **B** massive pyrite grains core sample, **C** disseminated pyrite grain photomicrograph under XPL and **D** disseminated pyrite grains core sample.

4.1.2 Whole Rock Geochemistry

This section outlines the X-Ray Fluorescence Spectrometry results of the rock specimens and core samples and their interpretation. This was conducted for numerous purposes such as determining the source of sediment loading and metal concentration for the prediction of AMD.

Rock Specimen Geochemistry

A minimum of two representative samples were obtained from each borehole intersection and three surface rock specimens namely B26T12, B26T16, B27T7, B27T8, B36T17, B36T22, FG1, VS1 and DS1. These samples were carefully

prepared for major oxide and elemental analysis using XRF spectrometry (Table 4.3).

According to Bailie and Robb (2004), the Albert Silver mine is a type III Sulfide-Carbonate ore body (base and precious metal rich) type of mineralisation (see Chapter 2). This mineralisation type is rich in Cu, Pb, Zn and Ag (Bailie and Robb, 2004) which was also observed in this study with copper concentrations ranging from 110.9 to 28420.6 ppm, Pb concentrations ranging from 54 to 95684 ppm and Zn concentrations ranging from 89 to 17269 ppm (Table 4.3, Fig. 4.26).

Table 4.3: Whole rock geochemistry of selected samples from the Albert Silver Mine, oxides in %; trace metals ppm

Mineral	B26T12	B26T16	B27T7	B27T8	B36T17	B36T22	DS1	FG1	VS1
SiO_2	72.78	88.32	57.44	53.97	86.08	73.73	48.82	74.37	89.53
Al_2O_3	16.69	9.58	2.05	–	12.29	13.15	11.85	13.36	–
Fe_2O_3	6.99	3.89	19.04	39.5	5.33	3.32	12.53	3.13	23.27
CaO	0.3	0.19	0.03	0.04	0.25	0.69	6.74	0.74	0.09
K_2O	4.35	2.67	0.12	0.05	3.63	1.61	2.44	6.33	0.05
Cu	43.6	2643.1	8400.8	28420.6	86.5	55.6	125.8	10.9	882.1
Zn	256.2	1382	17268.9	5689.9	103.4	505.8	172.8	89.2	368.1
As	18.4	3332.8	10270	1679.8	144.3	19.9	5.8	12.1	134.6
Pb	171.2	31051.3	95683.6	15650.3	1344.1	185	54.1	112.6	1253.6
S	108.9	921.3	19681.2	13018.7	118.1	43	129.7	–	102.8

The Albert Silver mine is hosted in a quartz hematite vein (Champion, 1970). This is also evident from the high abundance of SiO_2 (89.53 %) and Fe_2O_3 (23.27%) in VS1 (surface vein sample, Table 4.3, Fig. 4.26), these values were found to be the highest amongst all the samples. The Albert lode is hosted within a fine-grained porphyritic granite that was intruded by a dolerite/diabase dyke (Champion, 1970 and Maulenbeld *et al*., 2014); these lithologies are enriched in Al_2O_3, CaO, and K_2O and they are depleted in SiO_2 (Table 4.3, Fig. 4.26).

The lowest concentration of SiO_2 (wt%) is encountered in sample DS1, which is because this sample is from a SiO_2 deficit diabase dyke. The highest concentration

of SiO_2 was observed in sample VS1, which is a quartz-hematite vein enriched in SiO_2. The Al_2O_3 concentrations are due to microcline and muscovite (Table 4.3). The highest values were observed in samples B26T12, FG1, B36T17 and DS1, with lowest values in samples VS1 (quartz-hematite vein) and sample B27T8. Sample B27T8 and VS1 show the highest concentration of Fe_2O_3 (Fig. 4.26) because VS1 is a quartz-hematite vein and the composition of B27T8 is dominated by the iron oxide and iron sulfide minerals hematite, magnetite, pyrite, arsenopyrite and tennantite (Table 4.1). High concentrations of CaO were found in calcium rich plagioclase feldspar in DS1, and K_2O was found in FG1. These values result from muscovite.

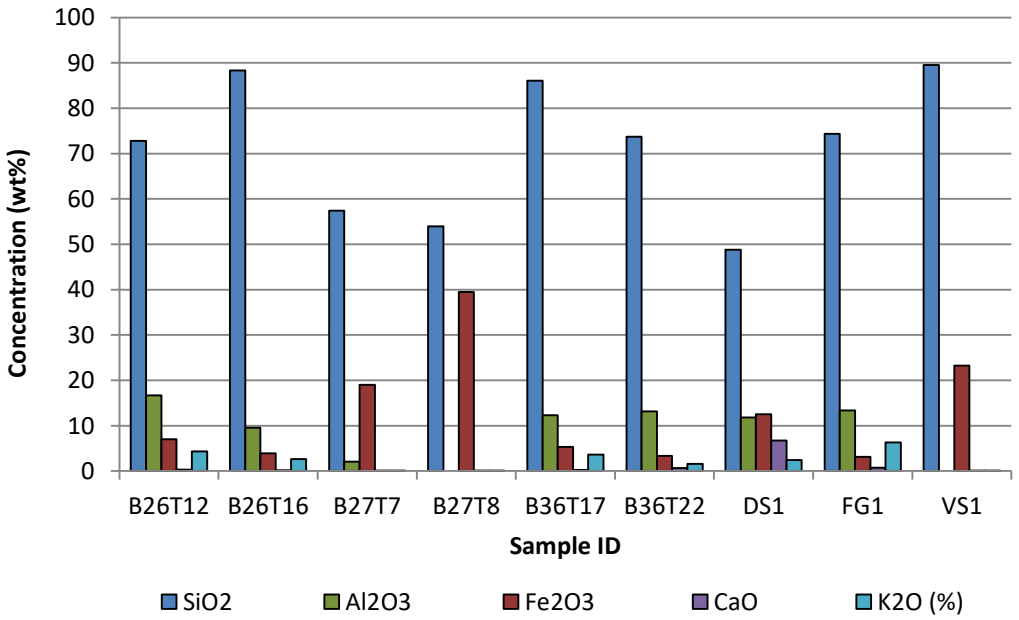

Figure 4.26: Concentration (wt%) of the major oxides in the rocks samples from the Albert Silver mine.

The elements that have a high potential to contribute to the drainage chemistry include Cu, Pb, Zn and As, because they are mobile at low pH and occur in high quantities in the rock. Pb is the major element of concern with concentrations up to 95684 ppm. These values were observed in sample B27T7, other samples with higher values of Pb include B26T16 and B27T8 with values of 31051 ppm and 15650 ppm respectively.

According to the XRD data (Section 4.1.1.2) Cu is found in chalcopyrite and tennantite. This is shown by the whole rock geochemistry data with higher Cu concentrations in samples B27T8 and B27T7 with values of 28421 ppm and 8401 ppm respectively. These samples were the only ones that contain tennantite and chalcopyrite (Fig. 4.27). The highest concentrations of Zn are 17269 ppm, 5690 ppm and 1382 ppm in samples B27T7, B27T7 and B26T16 respectively (Fig. 4.27). The lowest values were obtained from B36T17, DS1, B26T12, VS1 and B36T22 (Table 4.3).

Arsenopyrite and tennantite are the major source of As in the study area. Concentrations of As range from 6 to 10270 ppm. The highest concentrations of the measured sulfur were found in samples B27T7, B27T18 and B26T16 (Fig. 4.27). These were the only ones that contain sulfide minerals (Section 4.1.1.2), which confirms that the sulfur is from sulfide minerals.

The boreholes of concern included borehole 26 and Borehole 27, as they contain high concentrations of all the listed potentially polluting elements. This is confirmed by the XRD data and the concentration of the sulfur. Borehole 36 and the surface rocks are of less concern relating to leachable elements. According to the data, the western part of the vein from the Moses river-Vein intersection contains high concentrations of Cu, Pb, Zn and As since borehole 26 and borehole 27 are located at the western part of the vein from the Moses river.

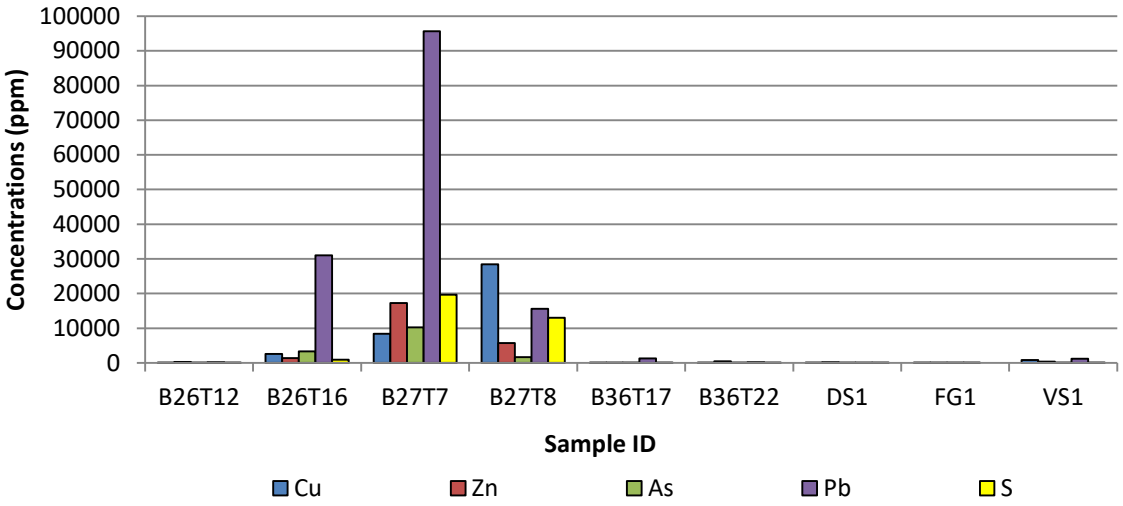

Figure 4.27: Graphical representation of the elemental concentrations in the core samples obtained from the Albert Silver mine.

4.1.3 Current Status of Acid Mine Drainage in the Moses River

4.1.3.1 Water Quality Results

Physicochemical Parameters

The water samples were collected from downstream to upstream at the Moses River and the on-site parameters (pH, EC, TDS and Salinity) oppose the potential effects of the AMD on the river (Fig. 4.28, 4.29). The pH (both field and laboratory) ranged around 7, indicating a circum neutral environment. The mine is located on the middle stream (MI1–5). Thus, it was expected that from the middle stream, the pH drops to acid levels. The highest discovered field pH values were on the first sample of the downstream DO1 with a value of 7.3 and the lowest value was at the upstream in samples number 3 with a value of 7.0, the lab pH also had values ranging above 7 (Table 4.4, Fig. 4.29).

The same outcomes were expected with the electrical conductivity (EC). The field measurement of the EC showed high values at sample number 3 of the middle stream (MI3) which was potentially from the mine remnants. The EC values peaked at DO4 and stayed high until UP3, which might be due to the mining activities. According to Behar (1997), the water from the Moses river is not polluted since the EC ranges below 500 µS/cm and partially peaked to 512 µS/cm. The highest field

EC value measured was 500 µS/cm and the lowest one 247 µS/cm (Table 4.4, 4.5 and Fig. 4.28).

Total Dissolved Solids (TDS), is a measure of the mass of dissolved solids within a liquid. There is a conversion factor used to derive the TDS from EC. Salinity is similar to TDS because it is a measure of the dissolved salt concentrations in the solution and designated conversion factor is used to derive the salinity from EC and it is expressed in g/L. It is meant to express the salinity of ocean water and not fresh water but is reported here as the instrument recorded salinity (Fig. 4.28 and 4.29).

Table 4.4: Physicochemical parameters of water samples measured in the field; sampling times in tab. 3.1

Sample ID	Temp, °C	pH	EC, µS/cm	TDS, mg/L	Salinity, mg/L	Turbidity, NTU
DO1	9.8	7.78	281	216	152	3.17
DO2	11.3	7.30	252	182	113	3.10
DO3	9.5	7.24	240	154	115	3.59
DO4	11.2	7.41	451	308	221	3.67
DO5	10.8	7.34	473	326	213	3.37
MI1	11.3	7.17	465	333	225	3.27
MI2	11.5	7.62	469	375	253	7.35
MI3	11.8	7.52	520	346	273	4.17
MI4	11.9	7.45	470	329	227	3.54
MI5	11.0	7.45	448	317	216	3.55
UP1	10.5	7.22	490	351	251	3.74
UP2	11.5	7.16	495	350	260	3.54
UP3	12.0	7.00	460	345	225	3.98
UP4	11.9	7.01	285	262	170	3.90
UP5	11.5	7.11	275	212	138	3.97
WELL	22.2	8.72	310	216	151	0.61

Table 4.5: Physicochemical parameter of water samples measured in the laboratory

Sample ID	Temp, °C	pH	EC, µS/cm	TDS, mg/L	Salinity, mg/L	Turbidity, NTU
DO1	21.6	7.25	230	176	119	2.92
DO2	21.4	7.22	306	210	140	3.20
DO3	21.9	7.10	247	151	102	3.09
DO4	21.7	7.23	241	149	106	2.90
DO5	21.9	7.19	217	148	105	2.91

MI1	22.0	7.19	211	197	101	3.50
MI2	22.1	7.16	314	212	149	5.91
MI3	22.2	7.28	304	203	145	3.84
MI4	22.1	7.26	330	220	176	3.46
MI5	22.2	7.19	281	221	133	3.63
UP1	22.3	7.05	220	220	152	3.94
UP2	22.3	7.02	326	228	157	4.00
UP3	22.1	7.09	335	214	168	4.22
UP4	22.2	7.14	382	284	192	5.12
UP5	22.1	7.08	315	220	148	4.93
WELL	21.8	8.61	364	255	172	0.35

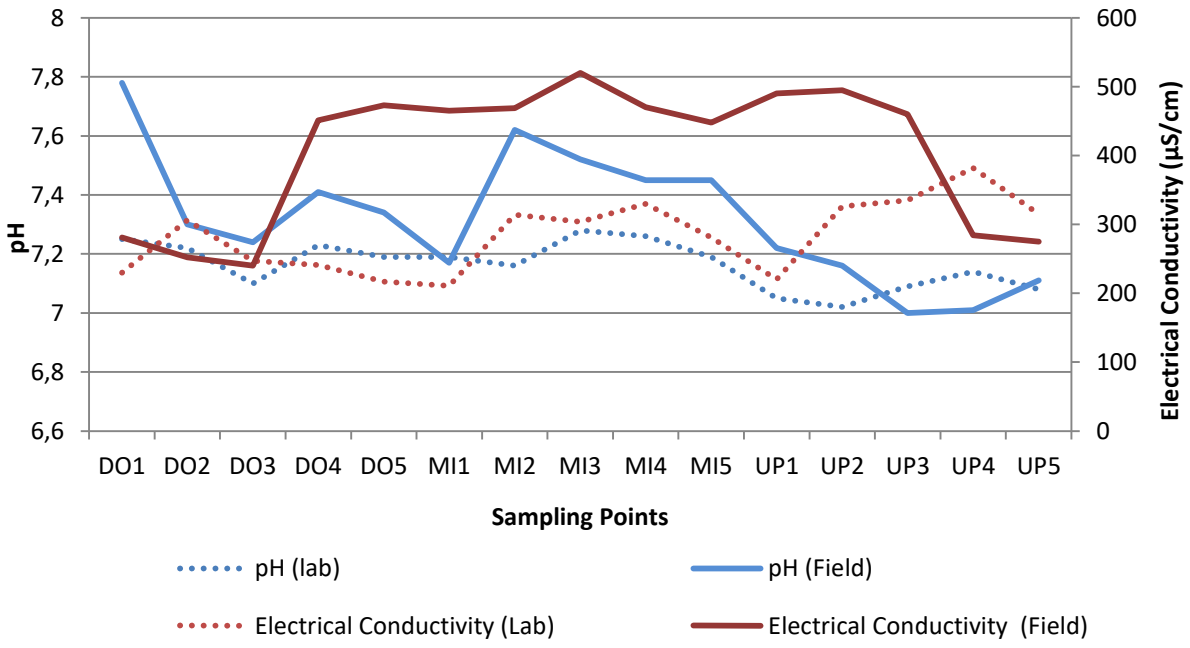

Figure 4.28: Comparison of laboratory and field physicochemical parameters (pH and electrical conductivity) of the Moses River from downstream to the upstream.

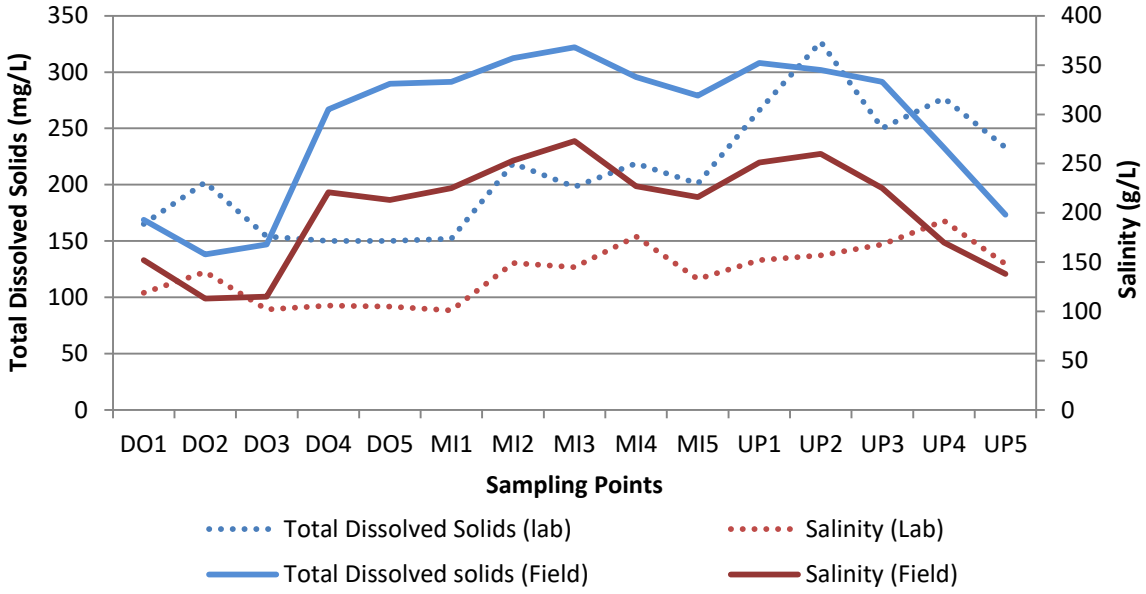

Figure 4.29: Comparison of laboratory and field physicochemical parameters (TDS and Salinity) of the water in the Moses River from downstream to the upstream.

Metal Concentration Results

The elements of interest that were analysed by ASS were Zn, Pb, As and Cu. The results show changes in elementary concentrations in different sampling areas (downstream to upstream) to decipher the effect of the Albert Silver mine on the Moses river (Tab. 4.6, Fig. 4.30).

Based on the results obtained, Cu concentrations are below the detection limit for all the samples, which suggests that Cu has completely been washed away or it is immobile due to the high pH-values. The Zn concentrations ranged between below the detection limit for sample number DO1 to UP1 and then also in sample UP3, with the highest Zn concentration of 0.009 mg/L in sample UP5. The lowest As concentration was 2.172 mg/L and the highest one 14.24 mg/L, in sample numbers DO1 and MI2 respectively. The Pb concentrations ranged from below 0 mg/L to 0.079 mg/L, with the highest and lowest concentrations in samples DO1 and UP3 respectively. These results mirror the varying metal mobility as a function of the pH values.

Table 4.6: Concentrations of elements in the water samples in mg/L; Cu below the detection limits; bdl: below detection limit

Sample ID	Zn	As	Pb
DO1	bdl	2,172	bdl
DO2	bdl	6,790	0,014
DO3	bdl	6,792	0,016
DO4	bdl	6,703	0,005
DO5	bdl	11,090	0,038
MI1	bdl	13,680	0,020
MI2	bdl	14,240	0,018
MI3	bdl	7,174	0,064
MI4	bdl	6,616	0,066
MI5	bdl	8,449	0,053
UP1	bdl	6,360	0,063
UP2	0,005	2,748	0,060
UP3	bdl	7,341	0,079
UP4	0,005	5,380	0,068
UP5	0,009	3,741	0,047

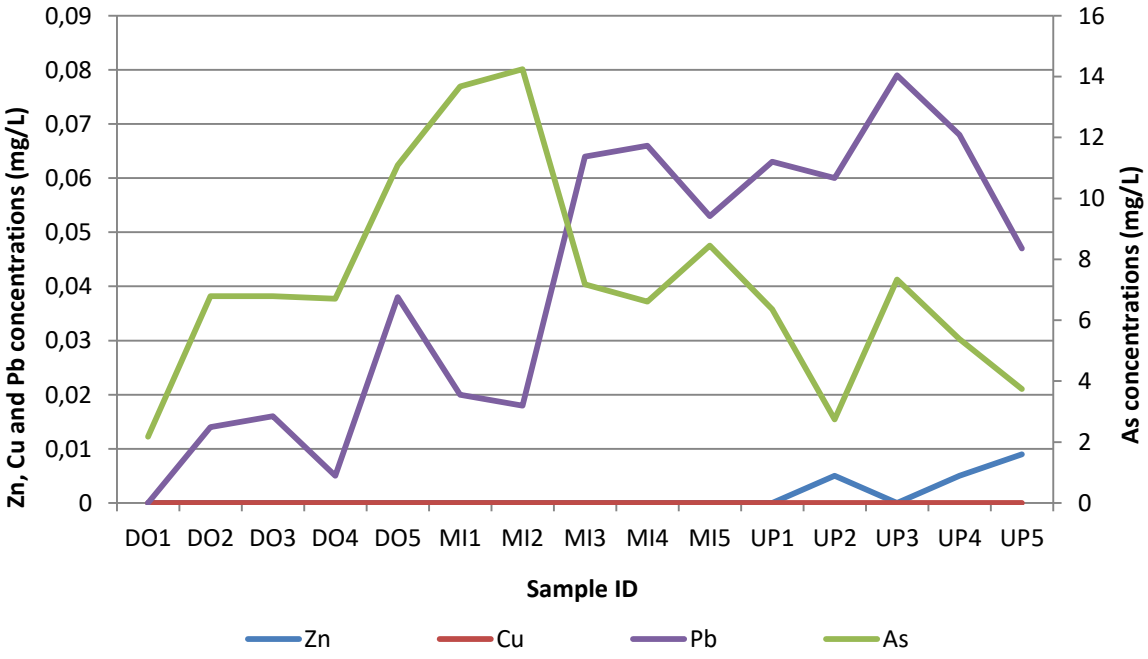

Figure 4.30: Element concentrations in the water samples from the Moses River.

4.1.3.2 Geochemical Analysis of Tailings and Sediments

Tailings Geochemistry

The maximum concentration of the major oxides had SiO_2 (94.28%) with the lowest concentrations for Al_2O_3 (0%) and K_2O (0.05%) (Table 4.7). The mean values showed the concentrations which were high and low as a factor of average abundance. The concentration of Pb and Cu were the highest, Zn and As were the lowest abundance, which was also supported by the mean values.

SiO_2 has the highest concentrations of all the oxides with the highest one being 94.28% for sample T1 (Fig. 4.31, Table 4.7). This is because the SiO_2 in that sample is from the mineral quartz and it is resistant to weathering. The Al_2O_3 has the lowest concentrations followed by K_2O. These lowest concentrations are from the same sample VS1 and this is a rock sample obtained from the surface outcrop of the quartz-hematite vein that is depleted in Al_2O_3 and K_2O for its composition obtained through XRD analysis. According to the detailed geological description of Champion (1970), Bailie and Robb (2004) and Robb *et al.* (1994), Al_2O_3 and K_2O were dominantly from muscovite that is found as a minor mineral in the granitic host rock. This is also supported by the XRD data (Section 4.1.1.2). Thus, these major oxides have low mean values (Table 4.7 and Fig. 4.31). According to the literature and the XRF analysis, the source of Fe_2O_3 in the tailings is the quartz hematite vein of the mined Albert lode (Fig. 4.31).

Table 4.7: Tailings samples geochemistry result; oxides in %; trace metals in ppm

Sample ID	SiO_2	$Al2O_3$	Fe_2O_3	K_2O	Cu	Zn	As	Pb
T1	94.28	6.68	1.34	2.97	214.4	25.7	13.6	126.5
T2	83.72	8.56	1.98	3.19	369.0	31.5	24.6	228.9
T3	88.46	7.25	5.50	2.66	2602.3	106.5	259.2	2414.7
T4	88.89	7.62	2.08	3.02	267.5	21.9	29.5	274.7
T5	77.90	5.24	14.41	2.18	4452.3	301.2	566.0	5273.2
T6	78.66	8.93	8.19	3.17	2192.8	168.4	693.9	6464.9
T7	80.65	12.2	2.92	2.74	343.9	43.6	66.8	622.6
T8	81.46	10.79	2.62	1.90	98.6	41.8	55.2	513.9
T9	92.39	7.97	1.71	2.51	166.0	33.7	28.8	268.0
T10	87.98	9.34	2.19	3.08	167.7	31.9	32.9	306.7
T11	94.26	5.47	2.08	2.06	373.2	26.1	31.7	295.4
T12	91.88	7.91	2.38	2.17	231.9	33.4	10.3	96.4
T13	88.54	8.42	2.50	2.70	625.3	28.9	29.5	274.6
T14	91.08	6.52	2.01	2.35	259.6	43.8	13.6	126.3

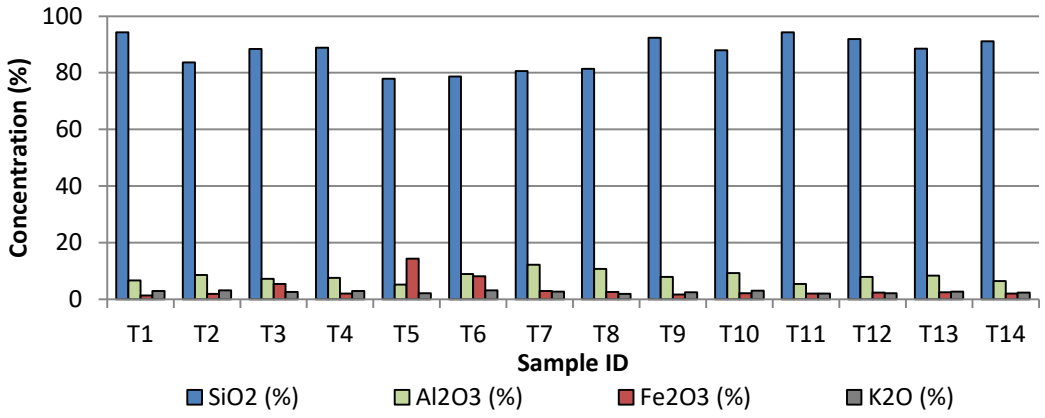

Figure 4.31: Concentration of major oxides from tailings and rock specimens obtained from the abandoned tailings dam and surface outcrops at the Albert Silver mine.

The Albert Silver mine ended operations at around 1914. Since then, the abandoned tailings dam has undergone intensive erosion, as it was poorly engineered. The highest elemental concentrations from the tailings were found in sample numbers 3, 5 and 6. These findings are in line with the idea behind the intensive erosion. These results are from samples obtained along the tailings dam wall where the eroded

material was deposited (Fig. 3.4). The samples after the wall (sample number 1, 2 and 4) and those that are far away from the wall (upwards toward the former crusher location, sample number 11 to 14) revealed the lowest concentrations as they were subjected to intensive water erosion.

The concentration of Pb was found to be the highest amongst the selected elements reaching up to 6464.9 ppm. This element is a major element in the sulfide mineral galena (PbS). The fact that Pb is very little detected in water samples means that it is tightly bound to the ore material. Cu has the second highest concentrations after Pb, reaching up to 4452.3 ppm. According to Maulenbeld *et al*. (2014), this element has numerous sources, but the XRD data showed that chalcopyrite and tennantite are the major sources of copper in the study area (Table 4.1). The element with the third highest concentration is As with values reaching up to 693.9 ppm. The major source of this element is arsenopyrite and tennantite. All the minerals mentioned as sources of the selected elements are found dominant in the Albert lode (quartz-hematite vein). Therefore, the Albert lode, as expected, is the source of the selected elements in the tailings dam. The XRF data supports the findings about the sources of these elements. In addition, amongst the 3 rock samples DS1, FG1 and VS1, only the quartz-hematite vein (Albert lode, VS1) had high values of the selected elements (Fig. 4.32). Studies on the soil geochemistry of the farm by Robb *et al.* (1994) showed high values of Pb, Cu, As and Zn along the quartz-hematite veins as proof that the veins are the major source of these elements.

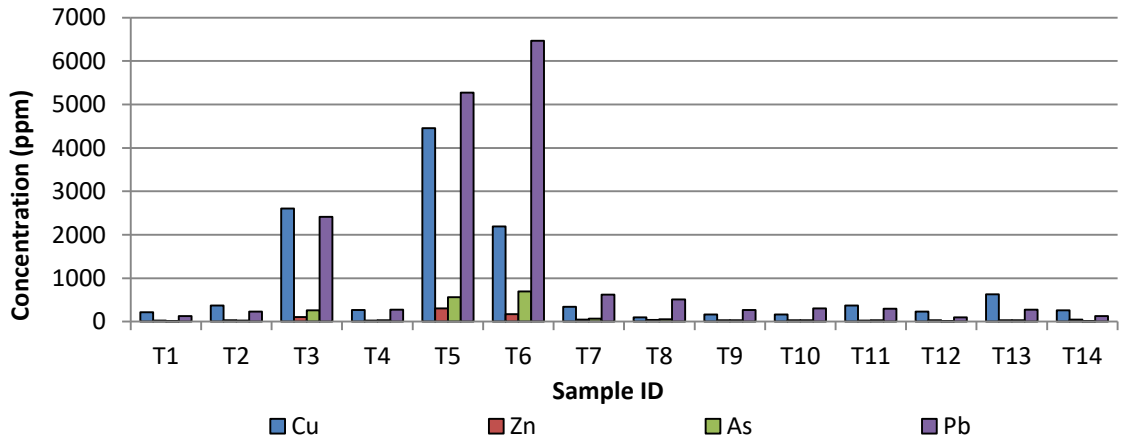

Figure 4.32: Concentrations in samples of tailings collected from the tailings dam at the Albert Silver mine. Stream Sediments Geochemistry.

The stream sediments in the Moses River are the result of weathering and erosion of the nearby rocks and soils. The tailings, quartz-hematite vein and the host rock granite are being eroded to the river causing sediment and metal loading. The quartz hematite vein is the major source of Fe_2O_3, Pb, Cu, As and Zn. According to the literature documented by Baillie and Robb (2004), numerous major oxides within the study area are from the granitic host rock except Fe_2O_3. This information will be utilised to determine the environmental effect on the river derived from mining activities and natural processes such as weathering of the quartz-hematite vein.

The iron oxide (%) concentration decreases upstream, shown by the exponential dotted trend line, with peaks at critical areas where the river interacts with the gullies caused by water erosion from the tailings dam and the quartz-hematite vein (Fig. 3.4, Fig. 4.33). The highest concentration of 5.13% is at sample number 2 located downstream (S-2-D). This was found to be high because the sample is at the river corner where much of the sediments get deposited. The second highest peak with 3.26% is at sample number 1 in the middle stream section (S-1-M). This was due to the erosion discharge from the tailings dam. The third highest peak with 4.79% was at sample number 4 of the middle stream section (S-1-M). This is the point where the river interacts with the quartz-hematite vein. Therefore, these values suggest that natural weathering processes are the major source of iron oxide in the river (Fig. 4.33).

According to the concentrations of Fe_2O_3 (Fig. 4.33), the quartz-hematite vein and the tailings are the sources of the stream sediments. This was proven by the low values found upstream, which is after the interaction zone of the quartz-hematite vein and the river with values of 1.94% at sample number 3 (S-3-U) from upstream section were registered and this is where a small outcrop of the quartz-hematite vein interacts with the river (Fig. 4.33).

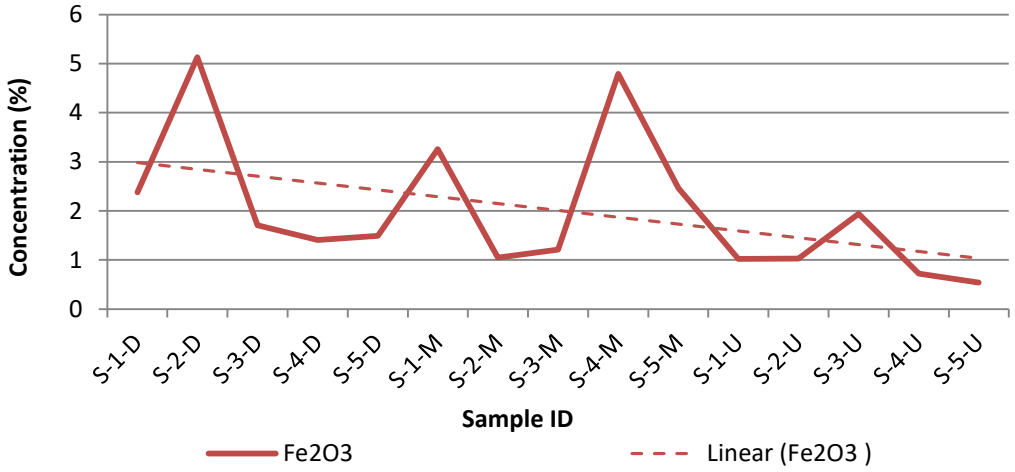

Figure 4.33: Graphical depiction of the concentrations of iron oxide (%) in the sediment samples from downstream to upstream obtained from the Moses River. Expon.: exponential fitting of the Fe_2O_3 concentrations.

The trace metal concentrations (Fig. 4.34) were used to determine the natural and man-made sources of stream sediments and to decipher the natural and man-made environmental effects on the Moses River. The four elements Pb, Cu, As and Zn were selected because they are dominant within the quartz-hematite veins. Consequently, they are good indicators to prove that their sources are the quartz-hematite vein and the abandoned tailings.

The exponential trend lines were included on the charts to show the gradual change in metal concentrations from downstream to upstream. The peaks from the graphs were also the main focus to decipher the sources of these elements. The exponential trend lines showed a decrease in elemental concentration from downstream to upstream. This simply means that there is high concentration of Pb, Cu, As and Zn downstream as compared to upstream which is after the quartz-hematite vein.

According to Bailie and Robb (2004), the Albert lode is enriched in Pb, Cu, As and Zn. Therefore, high concentrations of these elements at critical points of the river confirmed the sources and these high values were at the same points as the peak values for the above explained iron oxide as shown in Section 4.3. The peak values of almost all the elements were at S-2-D, S-1-M, S-4-M and S-3-U with Pb values being 672.8, 769.7, 706.7 and 113.8 ppm respectively. The peaks for Cu were at S-1-M and S-4-M with values of 330.4 and 675.8 ppm respectively. The As peak was

found at S-2-D, S-1-M and S-4-M with values of 72.2, 82.6 and 75.9 ppm respectively. Zn is more or less decreasing linearly upstream. The highest value of Pb from downstream to upstream was at S-1-m, at the point where the river receive sediments from the eroded tailings which confirms that the Pb in the sediments is from the tailings rather than from the vein suggesting that Pb is from a man-made source and this is the same case with As. The highest peak for Cu is at S-4-M, which is where the quartz-hematite vein interacts with the river suggesting that Cu values are from a natural source.

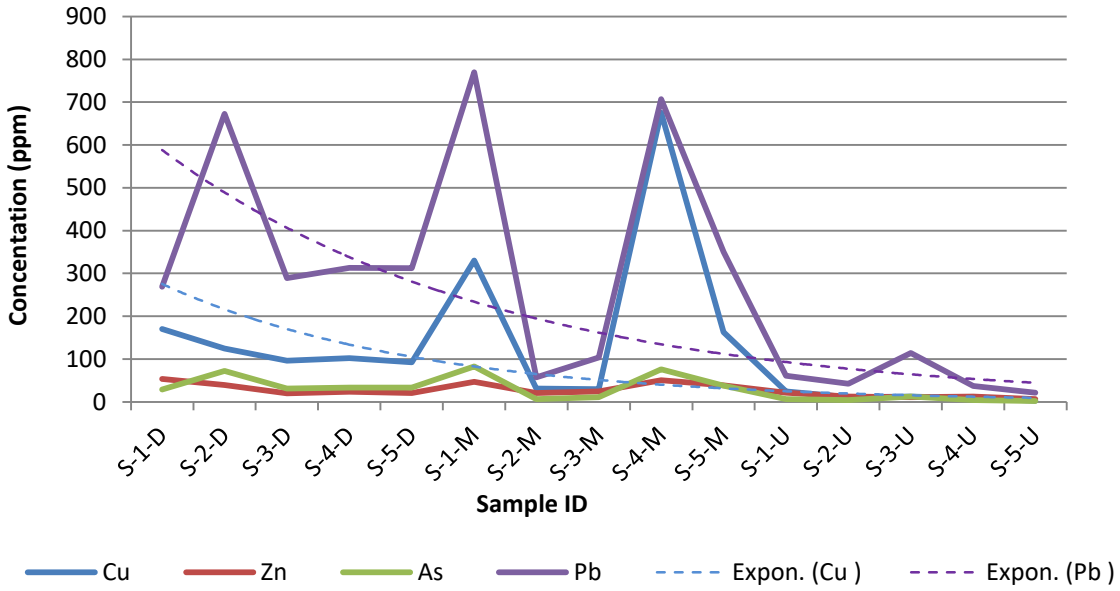

Figure 4.34: Concentrations of metals in sediment samples from the Moses River.

4.1.4 Acid Mine Drainage Prediction

The static and kinetic tests were conducted as a requirement for the prediction of the AMD potential. The adopted static tests were the widely used ABA and NAG tests. The column leach test was selected as the kinetic test method to mimic the environmental condition of weathering to produce the AMD. This section contains results that complement the mineralogical results discussed above.

4.1.4.1 Static Tests

The static tests were conducted to fully classify the samples in terms of their potential to produce or neutralise acid. These two tests were conducted: acid base

accounting and net acid generation. The results of these tests were used to quantify the acid formation and neutralisation potential.

Acid Base Accounting

Classification of the samples into acid generating and non-acid generating involved the determination of the total sulfur (%), AP and NP (Table 4.8 and Fig 4.35). The calculated NNP were plotted in graphical form (Fig. 4.35). The samples were classified into “acid generating”, “uncertain” and “non-acid generating”. Based on the classification guide developed by Price *et al*. (1997), Price (2009), Ferguson and Morin (1991) and Weber *et al*. (2004), three samples were located within the uncertain zone (Fig. 4.35). According to this classification, samples with NNP above 20 kg $CaCO_3$/t were non-acid generating, while those with NNP values below –20 kg $CaCO_3$/t were acid generating. In this case, only one sample (B27T8) was found to be acid generating. NNP values between 20 and –20 kg $CaCO_3$/t represent uncertain samples.

Table 4.8: ABA sample classification results, AP, NP and NNP in kg $CaCO_3$/t; total S in %; ↓: non-acid generating, ↔: unclear; ▲: acid generating.

Sample ID	Total S	AP	NP	NNP	NPR	Classification
B26T12	0,10	3,1250	36,1650	33,0400	11,5728	↓
B26T13	0,06	18,7500	36,2223	17,4723	1,9319	↔
B26T14	0,35	10,9375	35,7997	24,8622	3,2731	↓
B26T15	0,35	10,9375	35,8860	24,9485	3,2810	↓
B26T16	0,49	15,3125	36,0670	20,7545	2,3554	↓
B26T17	0,23	7,1875	35,8911	28,7036	4,9935	↓
B26T18	0,22	6,8750	87,5211	80,6461	12,7300	↓
B27T7	0,26	8,1250	36,0634	27,9384	4,4386	↓
B27T8	3,05	95,3125	36,0770	-59,2355	0,3785	▲
B27T9	0,92	28,7500	75,7800	47,0300	2,6358	↓
B36T16	0,01	0,3125	35,1555	34,8430	112,498	↓
B36T17	0,07	2,1875	35,9494	33,7619	16,4340	↓
B36T18	0,75	23,4375	36,9428	13,5053	1,5762	↔
B36T19	1,54	48,1250	36,0855	-12,0395	0,7498	↔
B36T20	0,43	13,4375	35,9881	22,5506	2,6782	↓
B36T21	0,27	8,4375	35,9341	27,4966	4,2589	↓
B36T22	0,03	0,9375	36,7224	35,7849	39,1706	↓
VS1	0,05	1,5625	35,4306	33,8681	22,6756	↓
FG1	0,01	0,3125	36,2221	35,9096	115,911	↓
DS1	0,09	2,8125	39,3653	36,5528	13,9966	↓

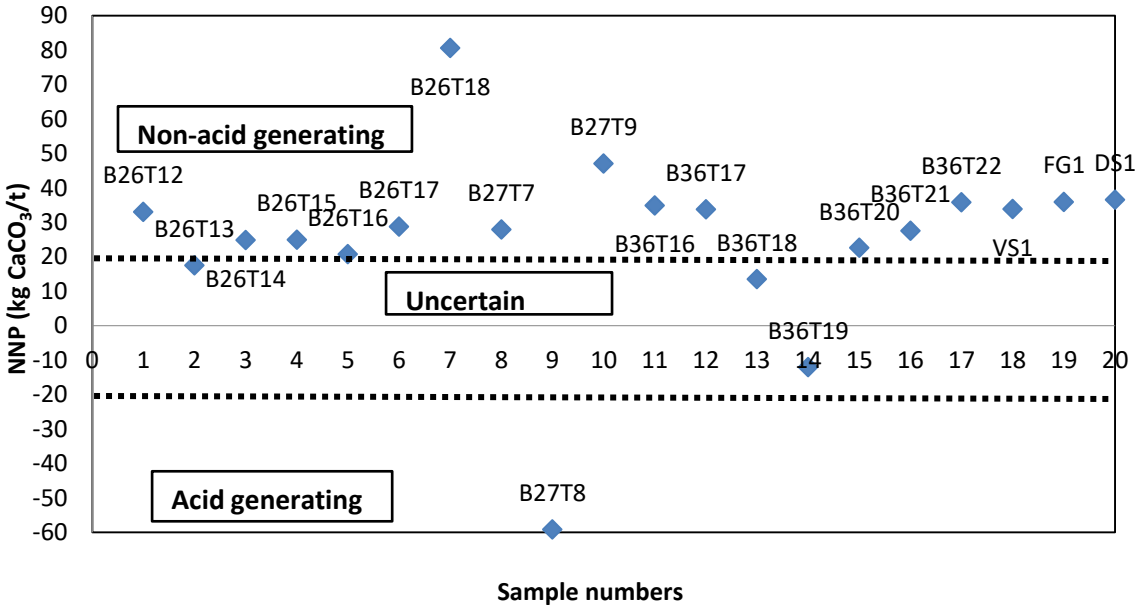

Figure 4.35: Acid mine Drainage potential sample classification plot based on NPR.

The ratio of the NP and AP (NPR) plot classifies the samples into acid generating and non-acid generating (Fig. 4.36). The dotted line was the major component of the classification as it separates the samples with an NPR above 1 and those with an NPR below 1 (Price *et al.,* 1997). Out of the 20 selected samples, only two samples were classified as acid generating which represented 10% of the samples. Consequently, 80% of the total number of samples was non-acid generating which influenced the supposition that according to the NPR the samples are non-acid generating. The analysis of the NNP and NPR plots revealed that the majority of the samples are non-acid producing (80%).

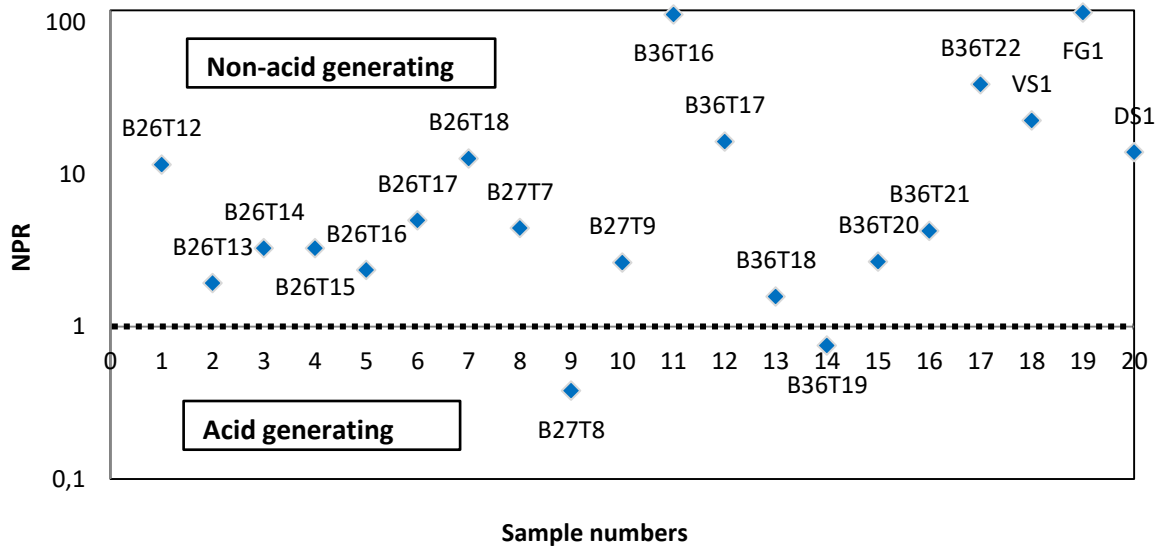

Figure 4.36: Acid mine Drainage potential sample classification plot based on NPR.

The experimentally determined Sobek NP and the calculated CO_3-NP were compared to deduce any correlation of the two (Fig. 4.37). The Sobek NP was determined through laboratory acid digestion and titration (Section 3.3.3), whereas the CO_3-NP was computed from the carbon % obtained through analytical procedure. According to the results (Table 4.9, Fig. 4.37), the Sobek NP values showed more exaggerated NP because the CO_3-NP shows an NP specifically from the carbonate minerals such as calcite or dolomite. In this the Sobek NP represents the experimental NP whereas the CO_3-NP represents the elemental NP.

Based on the results, either method can be used to determine the neutralisation potential of the geologic material (Fig. 4.37). Yet, the Sobek NP is higher for samples B26T18 and B27T9, this was also observed on the CO_3-NP. The XRD results (Section 4.1.1.3) showed calcite in sample B27T8 which is close to sample B27T9 (with high NP values). The NP values correlate with the NNP and NPR classification, as the samples B26T18 and B27T9 have high NP values and are classified as non-acid generating.

Table 4.9: Results of the experimentally determined Sobek NP and the CO_3-NP calculated from the C; NP in kg $CaCO_3$/t

Sample ID	C, %	Sobek NP	CO_3-NP
B26T12	0.03	36.1650	2.499
B26T13	0.02	36.2223	1.666
B26T14	0.14	35.7997	11.662
B26T15	0.11	35.8860	9.163
B26T16	0.05	36.0670	4.165
B26T17	0.01	35.8911	0.833
B26T18	0.66	87.5211	54.978
B27T7	0.02	36.0634	1.66
B27T8	0.08	36.0770	6.664
B27T9	0.11	75.7800	9.163
B36T16	<0.01	35.1555	0.000
B36T17	0.02	35.9494	1.666
B36T18	<0.01	36.9428	0.000
B36T19	0.02	36.0855	1.666
B36T20	0.02	35.9881	1.666
B36T21	0.03	35.9341	2.499
B36T22	0.02	36.7224	1.666
VS1	0.08	35.4306	6.664
FG1	0.04	36.2221	3.332
DS1	0.04	39.3653	3.332

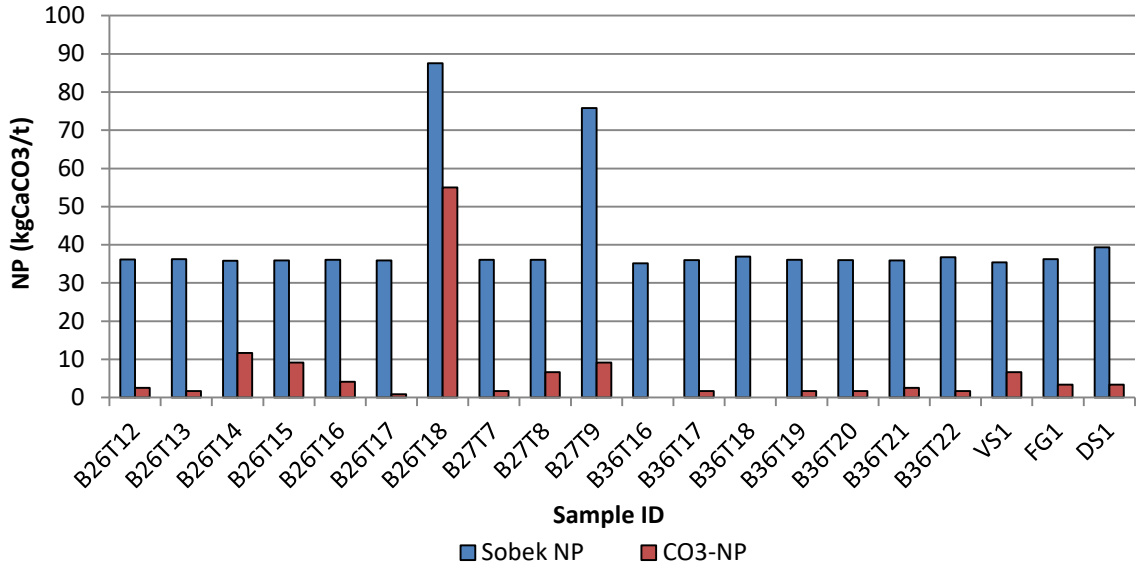

Figure 4.37: The comparison between the experimentally determined Sobek NP and the calculated CO_3-NP.

Net Acid Generation

The NAG test (Table 4.10) was conducted to evaluate the potential to produce or neutralise acid generated by the sample through the oxidation of the available sulfide minerals by a strong oxidising agent (H_2O_2). The experiment was also conducted to improve the ABA results which are a requirement for the AMD prediction. The single addition NAG test was adopted since the XRD and petrographic studies showed that the sample contains fewer amounts of sulfide minerals (in terms of weight %) that will be oxidised by the oxidising agent during the experiment.

According to the results for the 20 samples (Table 4.10), only 3 samples can be classified as potentially acid forming (PAF), with NAG values above 5 (B26-T17, B27-T8 and B36-T19). The classification of the sample was such that samples with NAG_{pH} less than 4.5 are acid generating; these samples are also expected to have an $NAG_{pH4.5}$ and $NAG_{pH7.0}$ below 5. In this, the NAG_{pH} is the pH of the liquor prior to titration whereas the $NAG_{pH4.5}$ and $NAG_{pH7.0}$ are post titration. The potentially acid forming samples contain a noticeable amount of pyrite. The other 17 samples had NAG value less than 5 and were therefore classified as non-acid forming (NAF). Generally, in all the samples, the $NAG_{pH4.5}$ was lower than that of the $NAG_{pH7.0}$.

According to the $NAG_{pH,}$ most of the samples were potentially acid forming (NAG_{pH} < 4.5) except for a few samples with NAG_{pH} > 4.5 (Table 4.10). The samples that had NAG_{pH} > 4.5 had less or no sulfide minerals and were samples B26-T18, B36-T22, VS1 and DS1. The curves in the appendix are the titration curves plotted against the volume of the base (NaOH) introduced during the titration. The blue curve is the actual Ep titration curve (pH) and the red curve is the equivalence points curve (dpH/dmL).

The NNP and NAG were used together to improve the prediction confidence, identify uncertain samples and better define cut-off criteria for material classification. The samples were plotted in four quadrants in terms of their potential to generate acid. The NNP was compared with NAG_{pH} to further classify the samples. The samples in the first quadrant were labelled as non-acid generating since they contained NNP values higher than 20 kg $CaCO_3$/t and NAG_{pH} higher than 4.5. This quadrant had three samples which makes 15% of the total number of samples (Fig. 4.38, Table 4.11). The second quadrant had no samples meaning there were no samples with NNP values below -20 kg $CaCO_3$/t and NAG_{pH} higher than 4.5. The third quadrant was labelled as potentially acid generating with only one sample in this quadrant which makes 5% of the total number of samples. The fourth quadrant was labelled as uncertain and had 12 samples which comprises of 60% of the samples.

This type of classification possesses an extra portion in the middle of the upper and lower quadrants, which is another source of uncertainty and it had three samples which made 15% of all samples. Therefore, the overall classification of the samples according to the NAG against the NNP shows that most samples have an uncertain potential to produce AMD.

Furthermore, the ABA (NPR) and NAG (NAG_{pH}) were used to further classify the samples according to its potential to produce acid. The NPR is the ratio of the NP and AP as discussed above and the NAG_{pH} is the post boil pH in the NAG test. The samples were classified into four quadrants like the above classification with the difference being the fact that the classification is in terms of the NPR values being either above or below 1 (Fig. 4.39, Table 4.12).

Table 4.10: Net acid generating results; ↓: potentially non-acid generating; ▲: potentially acid generating.

Sample ID	NAG_{pH}	$NAG_{pH4.5}$	$NAG_{pH7.0}$	Classification
B26-T12	3,59	0,3756	1,0842	↓
B26-T13	3,75	0,3756	1,2983	↓
B26-T14	2,83	1,4083	2,3496	↓
B26-T15	2,90	1,2207	3,9280	↓
B26-T16	2,52	3,1924	4,2935	↓
B26-T17	2,39	4,3196	5,2364	▲
B26-T18	5,62	–	0,0960	↓
B27-T7	4,21	0,0960	0,7350	↓
B27-T8	2,37	5,1836	12,378	▲
B27-T9	2,69	1,8238	2,8307	↓
B36-T16	3,67	0,3936	1,6179	↓
B36-T17	3,62	0,2952	1,0873	↓
B36-T18	3,22	0,7872	2,5133	↓
B36-T19	2,36	5,1955	7,1059	▲
B36-T20	2,96	1,0828	2,8908	↓
B36-T21	3,46	0,3792	1,3974	↓
B36-T22	4,88	–	0,7135	↓
FG1	3,98	0,3720	1,4518	↓
VS1	5,37	–	0,1976	↓
DS1	5,36	–	0,1987	↓

Table 4.11: Results used to plot the Acid mine Drainage potential sample classification on NNP and the NAG-pH

Sample ID	NAG-pH	NNP
B26T12	3,59	33,04
B26T13	3,75	17,4723
B26T14	2,83	24,8622
B26T15	2,9	24,9485
B26T16	2,52	20,7545
B26T17	2,39	28,7036
B26T18	5,62	80,6461
B27T7	4,21	27,9384
B27T8	2,37	-59,2355
B27T9	2,69	47,03
B36T16	3,67	34,843
B36T17	3,62	33,7619
B36T18	3,22	13,5053
B36T19	2,36	-12,0395
B36T20	2,96	22,5506
B36T21	3,46	27,4966
B36T22	4,88	35,7849
VS1	3,98	33,8681
FG1	5,37	35,9096
DS1	5,36	36,5528

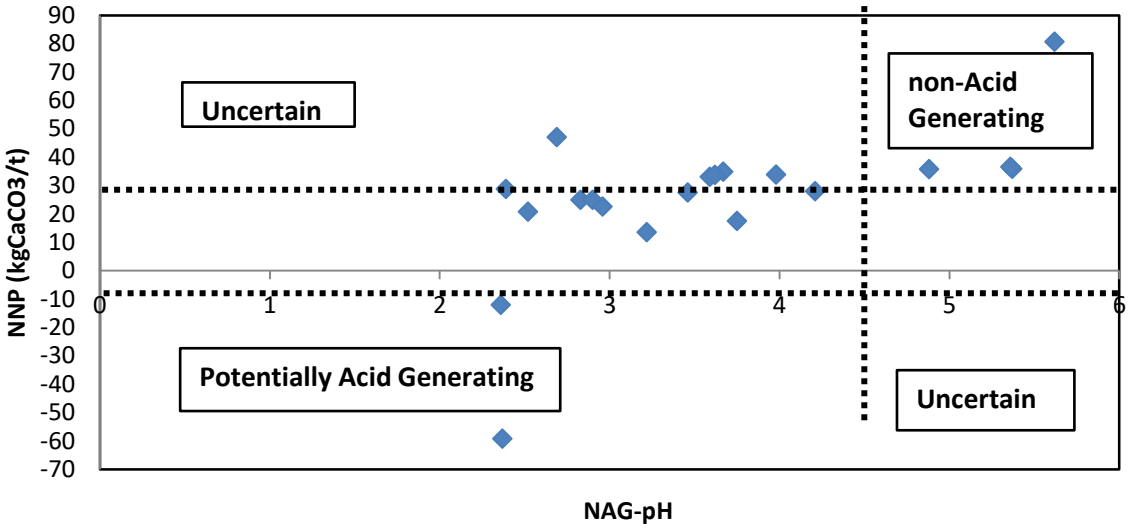

Figure 4.38: Acid mine Drainage potential sample classification plot based on (NNP) and the NAG_{pH}.

Table 4.12: Results used to plot the Acid mine Drainage potential sample classification on NPR and the NAG-pH.

Sample ID	NAG-pH	NPR
B26T12	3,59	11,5728
B26T13	3,75	1,9319
B26T14	2,83	3,2731
B26T15	2,9	3,281
B26T16	2,52	2,3554
B26T17	2,39	4,9935
B26T18	5,62	12,73
B27T7	4,21	4,4386
B27T8	2,37	0,3785
B27T9	2,69	2,6358
B36T16	3,67	112,498
B36T17	3,62	16,434
B36T18	3,22	1,5762
B36T19	2,36	0,7498
B36T20	2,96	2,6782

B36T21	3,46	4,2589
B36T22	4,88	39,1706
VS1	3,98	22,6756
FG1	5,37	115,911
DS1	5,36	13,9966

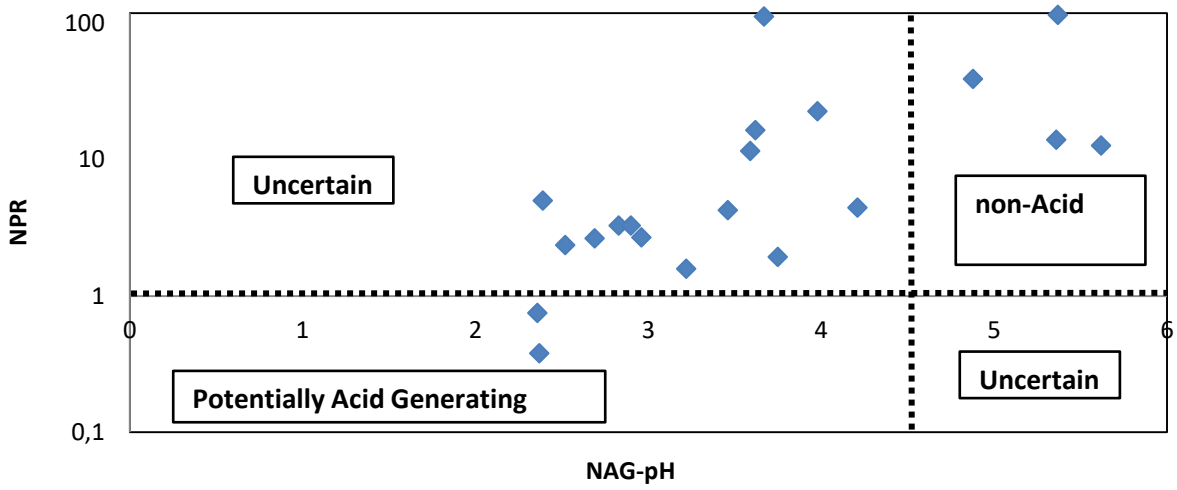

Figure 4.39: Acid mine Drainage potential sample classification plot based on NPR and the NAG_{pH}.

The figure fully portrays the classification of the samples; the dotted lines being the major chart dividers to provide a clearer classification. The vertical dotted line separated the samples having NAG_{pH} lower than 4.5 to those of NAG_{pH} higher than 4.5 while the horizontal dotted line separates the samples having NPR values higher than 1 from those with NPR values lower than 1. The samples containing acid generating NPR values and non-acid generating NAG_{pH} were classified as uncertain this applied to samples with acid generating NAG_{pH} and non-acid NPR values. There were four samples in the first quadrant (non-acid generating). The second quadrant (uncertain) had no samples at all. The third quadrant (potentially acid generating) had two samples and the fourth quadrant (Uncertain) had 14 samples which made 70% of the samples. This led to the conclusion that the acid generating potential of the samples is uncertain.

4.1.4.2 Kinetic Test

The main aim of conducting kinetic column leach AMD prediction tests was to improve the prediction of AMD by investigating the long-term weathering effects that are linked to acid formation or neutralisation rates. The samples containing acid generating and acid neutralising minerals were subjected to 20 weekly cycles of wetting and drying as discussed in section 3.4.7. This section addresses the outcomes of these weekly cycles.

Column Leachate Physicochemical Parameters

The column leach test experiment was run for 20 weeks and there were no controlled aspects in this experiment with the purpose to determine the influence of the rock composition on the leachate over the set period. There were four columns running simultaneously where each column contained rock samples from one borehole; column A: B26, column B: B27, column C: B36 and column D: SRO.

The experiments were run in weekly cycles (Section 3.4.7), where weekly analysis of the leachate physicochemical parameters dissolved oxygen (DO), pH, redox potential, EC, ions (sulfate, total iron and ferrous iron), alkalinity and acidity were conducted (Table 4.13–117, Fig. 4.40–44).

The initial pH and EC of the distilled water was measured at the beginning of each cycle and the leachate pH was measured at the end of the cycle. The leachate pH remained neutral around pH 7.0 for the entire 20 weeks with only B26 reaching as low as pH 5.98 at cycle number 14 then picks up. This means that the leachate did not reach the acidic condition, therefore it was considered as non-acid producing (Fig. 4.40). The experiment showed higher EC readings at cycle number 1 for all the boreholes including the surface rocks which was due to the reactive duct particles since there was no initial flushing conducted. The highest EC reading was on B36 (147.5 µS/cm) and the lowest reading was at cycle number 6 on the SRO reaching as low as 13.85 µS/cm. The EC readings complement the pH value as they are also constant throughout the experiment showing less or no leaching of anions and cations.

Table 4.13: pH and electrical conductivity (EC) results.

	pH, –				EC, µS/cm			
Weekly Cycle	**B26**	**B27**	**B36**	**SRO**	**B26**	**B27**	**B36**	**SRO**
1	8.43	7.78	7.84	7.59	105.8	108.9	147.5	49.80
2	8.03	7.98	7.94	7.8	53.40	51.60	42.60	20.50
3	7.97	7.79	7.92	7.74	51.80	51.30	33.60	17.75
4	7.52	7.65	7.79	7.64	55.70	53.10	31.80	17.21
5	7.42	7.70	7.76	7.68	56.60	54.80	30.70	15.36
6	7.02	7.04	7.11	7.11	58.70	54.80	26.80	13.85
7	7.18	7.54	7.91	7.64	58.60	55.20	27.40	18.16
8	6.39	6.66	6.91	6.85	79.90	77.00	36.50	27.50
9	6.85	6.90	7.06	6.98	76.40	74.30	34.00	25.50
10	6.66	6.82	6.92	6.85	84.40	82.90	46.80	27.90
11	7.35	7.31	7.35	7.26	85.40	72.70	40.00	25.80
12	7.50	7.37	7.49	7.36	76.30	70.70	36.70	23.60
13	6.10	6.49	6.60	6.63	86.90	80.80	45.30	26.00
14	5.98	6.40	6.53	6.69	83.00	76.90	43.90	25.10
15	6.90	7.07	7.06	6.99	84.70	85.40	46.50	27.60
16	7.14	7.18	7.26	7.10	71.90	77.20	40.10	22.20
17	6.32	6.50	6.64	6.78	76.60	72.70	37.40	20.25
18	7.32	7.12	7.26	7.28	77.00	75.30	34.80	26.40
19	7.51	7.32	7.47	7.54	77.20	84.00	38.40	23.10
20	7.62	7.37	7.49	7.55	81.60	82.70	37.50	21.70

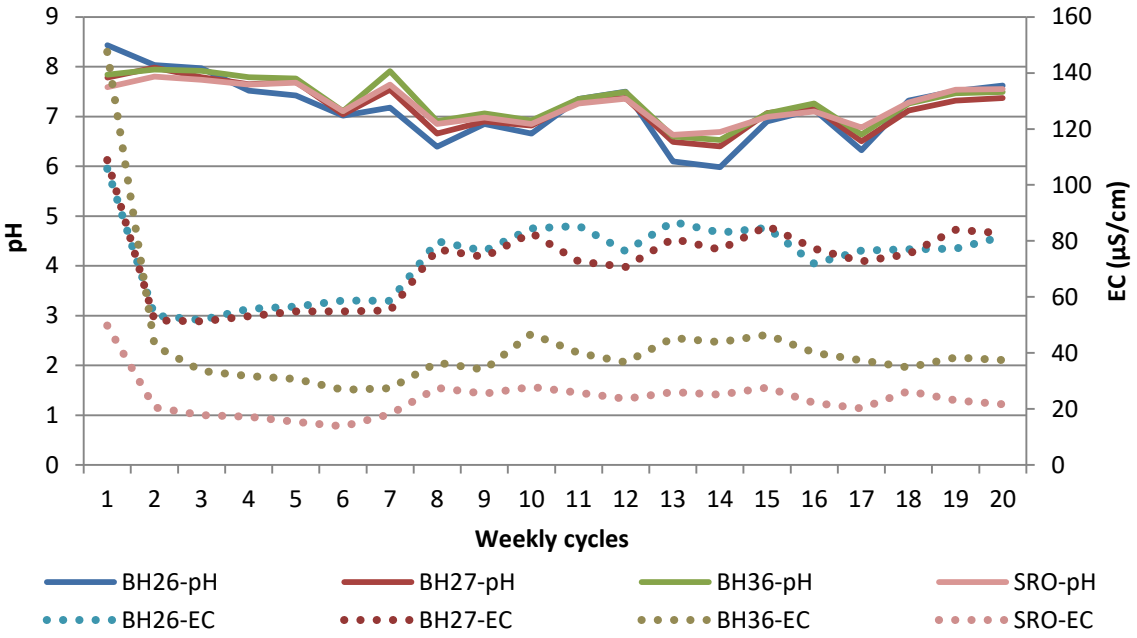

Figure 4.40: pH and EC readings for all the boreholes and surface rocks specimen for 20 weeks of leaching.

The redox potential is the ability of a chemical species to gain or lose electrons. This means that a positive redox reading indicates that the chemical species has potential to gain electrons and the negative redox that it has potential to lose electrons when it is reacted with another chemical species. The experiment showed that the redox potential ranged between 420 mV and 305 mV (Table 4.14 and Fig. 4.41). There was no increase or decrease in the redox potential over the 20 weeks duration of the experiment; which means that the samples did not induce redox reactions.

Table 4.14: Redox potential results in mV, values converted to the standard hydrogen electrode (SHE).

Weekly cycle	B26	B27	B36	SRO
1	412	412	413	413
2	420	419	418	418
3	413	412	412	412
4	309	305	327	343
5	342	320	337	351
6	336	332	340	349
7	343	311	359	362
8	405	384	382	402
9	335	328	365	370
10	335	317	367	351
11	338	334	371	363
12	328	323	372	365
13	403	354	394	370
14	397	351	402	373
15	337	333	383	362
16	331	311	370	382
17	380	350	358	383
18	345	306	362	371
19	368	330	376	386
20	355	350	383	400

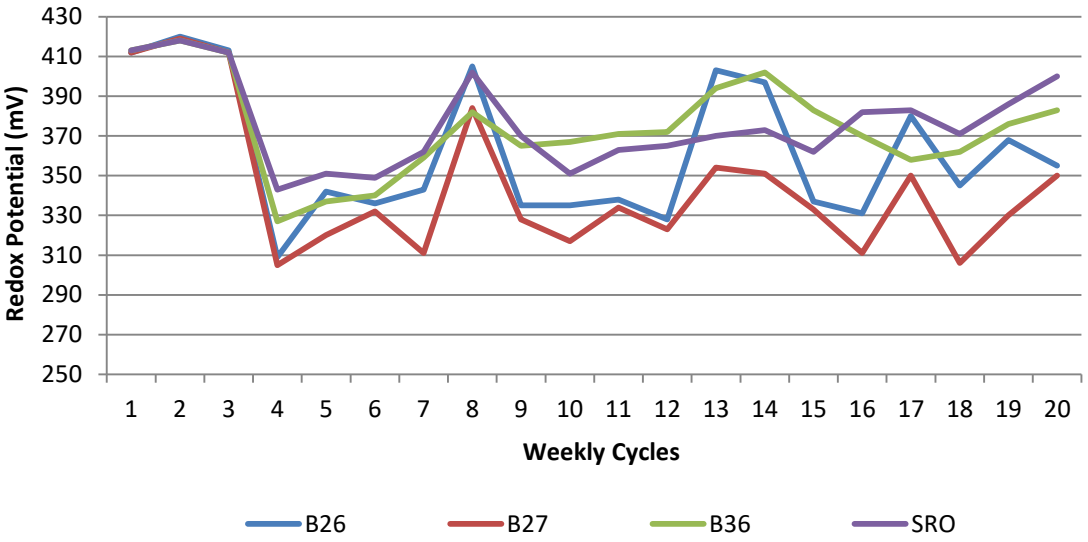

Figure 4.41: Redox Potential for the borehole samples and surface rocks specimen for the entire 20 weeks, results converted to the standard hydrogen electrode.

The dissolved oxygen (DO) is the non-bonded oxygen in the water samples. It is a key parameter in determining the water quality, since extremely high and low values of the DO might have adverse effects on the water quality. During the experiment, the O_2 was introduced with the water at the beginning of the cycle since this was a closed system experiment. The iron sulfides in the samples are expected to react with the dissolved oxygen and the water to produce sulfuric acid. The DO values were recorded to decipher the possibility of acid formation. The DO concentration (mg/L) and saturation (%) ranged about 7 mg/L and 80% respectively (Fig. 4.42). The DO (mg/L) concentrations reach the highest value of 8.02 mg/L in cycle number 2 of B27 with the lowest value at cycle number 15 of the SRO (4.04 mg/L). The DO (%) reached the highest value of 99% in cycle number 5 and this was on B36 and it reached the lowest value of 58.9% on cycle number 15 of the SRO (Table 4.15 and Fig. 4.42).

Table 4.15: Dissolved oxygen (DO) results in mg/L (1st 4 columns) and % (last 4 columns).

Weekly Cycle	B26	B27	B36	SRO	B26	B27	B36	SRO
1	7.91	7.79	7.70	7.77	97.3	96.2	95.1	96.1
2	8.07	8.07	8.02	7.98	98.0	97.8	95.3	96.6
3	7.77	7.67	7.65	7.64	97.8	96.8	96.6	94.9
4	7.39	7.36	7.37	7.37	97.4	97.4	97.1	97.1
5	7.53	7.49	7.60	7.45	98.4	97.7	99.0	97.4
6	6.23	6.17	7.42	7.43	81.6	81.2	97.0	96.9
7	5.35	5.48	7.20	5.82	72.2	74.2	97.0	78.6
8	5.71	5.78	7.35	5.69	75.5	76.5	96.1	76.9
9	6.01	5.29	7.31	5.68	80.3	70.9	95.7	75.4
10	6.11	5.18	5.71	4.86	84.8	72.6	80.3	68.1
11	5.58	6.20	6.28	4.95	72.6	80.0	81.4	64.2
12	5.09	5.64	6.34	5.03	67.4	74.7	84.0	66.3
13	5.06	5.48	5.51	4.22	72.0	78.1	78.6	60.0
14	5.12	5.59	5.58	4.69	72.0	78.8	78.7	66.1
15	4.32	4.93	5.10	4.04	63.2	72.0	74.4	58.9
16	6.82	5.04	6.81	6.70	96.4	71.7	96.2	94.6
17	6.57	5.35	6.69	6.63	93.9	77.1	96.7	95.6
18	6.89	5.27	6.91	6.83	97.2	74.7	97.1	96.0
19	6.92	5.47	6.89	6.87	97.5	77.1	97.1	96.2
20	6.83	5.39	6.84	6.79	98.8	77.8	98.6	97.6

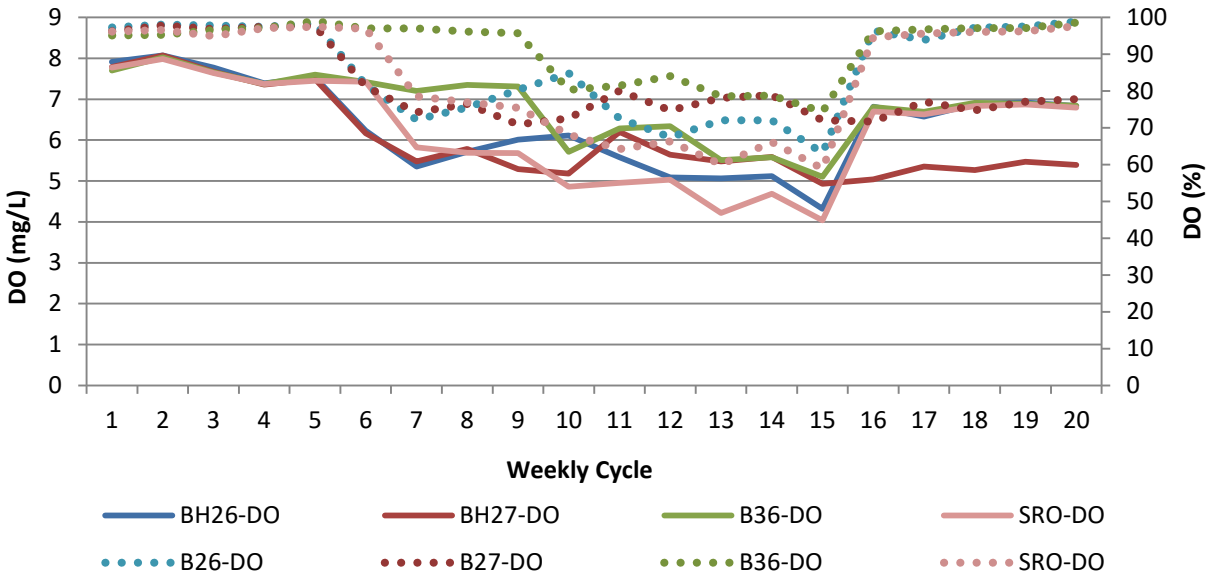

Figure 4.42: The Dissolved Oxygen (DO) for all the Borehole and surface rocks specimen for all the 20 weekly cycles.

Alkalinity and Acidity

Alkalinity is the buffering capacity of the solution to resists changes in pH, due to the available carbonate minerals such as $CaCO_3$. The acidity is the capacity of a solution to neutralise bases, due to the availability of acid producing minerals such as sulfide minerals. The alkalinity and acidity were determined by acid-base titrations. There were no changes in the acidity reading over the course of 20 weeks (Table 4.16; Fig. 4.43); as supported by the circumneutral pH values. There was a gradual increase in alkalinity in B26 and B27 for the entire 20 weeks experiment, this was due to the calcite in B27 (Table 4.1). However, the cause of the gradual increase in B26 is unknown.

Table 4.16: The alkalinity and acidity results.

Weekly Cycles	Acidity, mmol/L				Alkalinity, mmol/L			
	B26	B27	B36	SRO	B26	B27	B36	SRO
1	0.096	0.076	0.096	0.104	0.040	0.072	0.064	0.160
2	0.096	0.060	0.080	0.216	0.236	0.356	0.292	0.016
3	0.064	0.136	0.096	0.176	0.292	0.392	0.224	0.120
4	0.096	0.040	0.052	0.088	0.404	0.440	0.088	0.020
5	0.040	0.028	0.064	0.096	0.360	0.484	0.144	0.056
6	0.056	0.036	0.048	0.120	0.420	0.460	0.160	0.032
7	0.032	0.040	0.044	0.092	0.280	0.256	0.100	0.108
8	0.068	0.052	0.068	0.144	0.580	0.592	0.260	0.060
9	0.060	0.140	0.056	0.088	0.440	0.644	0.212	0.172
10	0.072	0.056	0.096	0.160	0.636	0.640	0.292	0.168
11	0.108	0.096	0.076	0.176	0.656	0.612	0.220	0.196
12	0.080	0.052	0.100	0.212	0.600	0.520	0.200	0.120
13	0.072	0.064	0.076	0.140	0.560	0.600	0.240	0.280
14	0.100	0.052	0.112	0.132	0.700	0.680	0.232	0.180
15	0.080	0.052	0.092	0.180	0.704	0.740	0.252	0.196
16	0.064	0.062	0.100	0.080	0.580	0.692	0.180	0.120
17	0.072	0.048	0.096	0.060	0.700	0.660	0.160	0.120
18	0.096	0.056	0.056	0.068	0.640	0.700	0.180	0.176
19	0.100	0.064	0.116	0.136	0.692	0.760	0.196	0.208
20	0.112	0.068	0.092	0.248	0.632	0.760	0.180	0.128

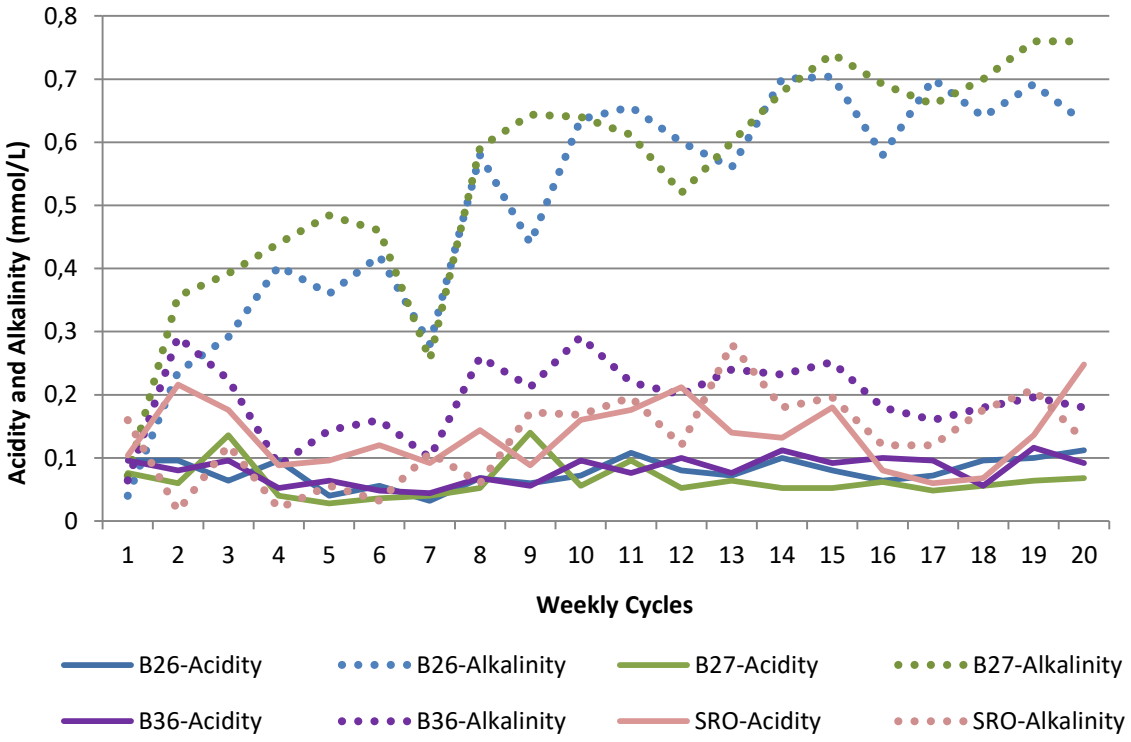

Figure 4.43: Alkalinity and Acidity of borehole samples and rock specimens during the 20 weekly cycles. Some samples displayed an increasing alkalinity trend, while acidity was more or less constant.

Sulfate and Ferrous Iron

Sulfate (SO_4^{2-}) is an anion and it is produced by the reaction of pyrite or marcasite, water and the dissolved oxygen. The higher the rate of reaction, the higher the SO_4^{2-} concentrations in the leachate. The sulfate in this study was determined by using spectrophotometry during the 20 weekly cycles (Table 4.15). The experiment showed high values of SO_4^{2-} in the first 5 cycles, which might be due to the reactive dust particles as the SO_4^{2-} concentrations decreased gradually to values between 0 and 1 mg/L (Fig. 4.44, Table 4.15). These results show that there was no AMD reaction due to the constantly low values of SO_4^{2-} and this is in line with the pH values that suggested acid neutralising conditions instead of acid generating conditions. The highest concentrations are found in cycle number 1 for all borehole samples and surface rocks.

Table 4.17: Sulfate and ferrous iron results, concentrations in mg/L; –: below detection limit

Weekly cycle	Fe^{2+}				SO_4^{2-}			
	B26	B27	B36	SRO	B26	B27	B36	SRO
1	0.02	0.10	0.31	0.07	5	8	6	8
2	0.01	–	–	0.05	–	–	1	–
3	0.02	0.06	0.19	0.07	–	1	2	2
4	0.05	0.05	0.04	0.09	2	1	–	1
5	0.15	–	0.18	0.01	1	–	1	1
6	0.02	0.01	0.06	0.01	–	–	1	1
7	–	–	0.13	0.01	–	–	1	–
8	–	–	0.03	0.01	–	–	–	–
9	–	–	0.02	0.01	–	–	–	–
10	0.01	–	0.06	0.01	–	–	1	–
11	0.01	–	0.01	–	–	–	1	–
12	–	–	0.01	0.01	–	–	–	–
13	–	–	0.01	–	–	–	1	–
14	–	–	0.01	0.01	–	–	–	–
15	–	–	–	–	–	–	1	–
16	–	–	0.01	0.01	–	–	1	–
17	–	–	0.01	0.01	–	–	1	–
18	0.02	–	–	–	–	–	–	–
19	–	–	0.01	–	–	–	–	–
20	–	–	0.01	0.01	–	–	–	–

Ferrous iron (Fe^{2+}) is a cation, and like SO_4^{2-}, Fe^{2+} is produced during AMD formation. In this study, only Fe^{2+} was investigated. According to the acid neutralising conditions, the concentrations of Fe^{2+} in the beginning of the experiment values reaching up to 0.31 mg/L on the first cycle of B36 was apparently caused by the available soluble dust particles (Fig. 4.44). Depletion (very likely resulting from precipitation) of Fe^{2+} started in cycle number 5 for B27 and SRO, at cycle number 6 for B26 and at cycle number 11 for B36 (Table 4.17 and Fig. 4.44).

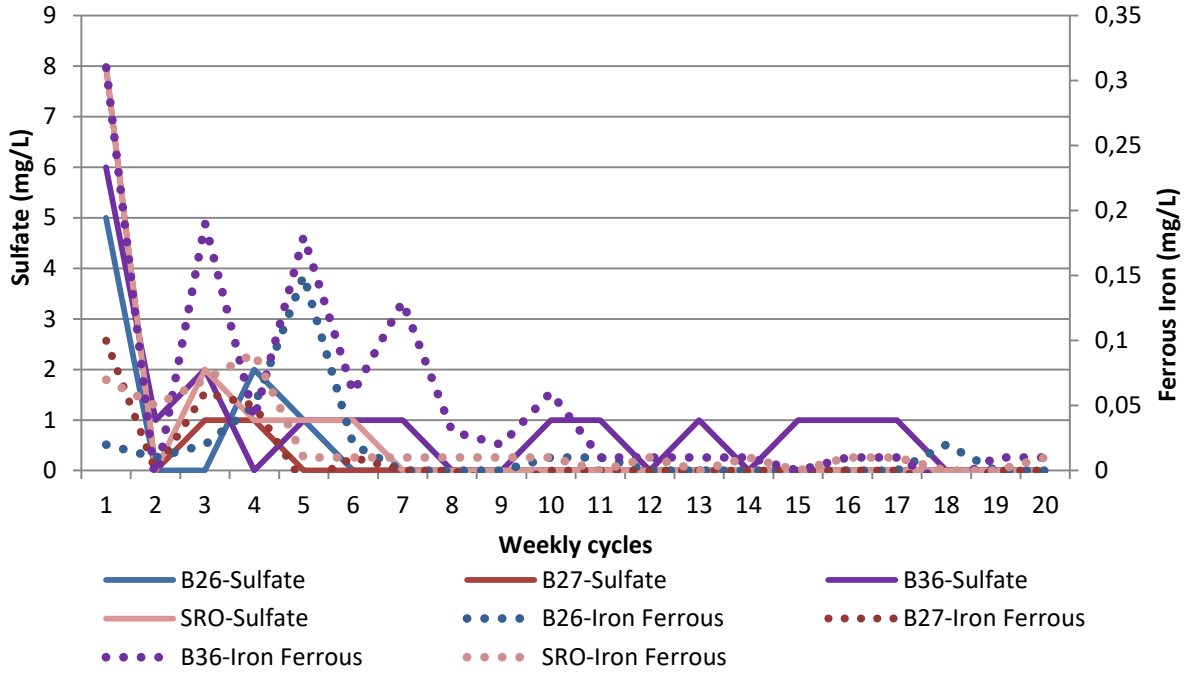

Figure 4.44: Weekly sulfate and ferrous iron trends for all the boreholes and surface rock specimens for the entire 20 weeks.

The kinetic test experiment that was run for 20 weeks showed no potential for acidic conditions, in this, five samples were selected with the highest EC values including the control sample. The selected samples were analysed with ion chromatography (IC) to determine the anions and cations. This was conducted for an express analysis to see the need for full analysis, the outcomes showed low concentrations of anions and cations, this was in line with the fact that there is no potential for acid generation within the selected period as also supported by the water quality parameters (pH and EC), alkalinity, acidity, sulfate and ferrous iron (Table 4.18).

Table 4.18: Ion chromatography analysis results in mg/L

Parameter	CON1	B27-1807-C01	B27-1909-C10	B26-1010-C13	B27-2410-C15
Cl	0.13	5.78	0.80	0.34	0.64
PO_4	0.33	0.19	0.10	0.52	0.16
SO_4	0.01	11.02	1.69	0.96	2.05
F		0.44	0.20	0.65	0.15
NO_2		0.02	0.03	0.03	0.05
NO_3		3.35	0.36	0.08	0.89
Br		0.03			
Li	0.08	0.32	0.13	0.15	0.21
Na	0.61	10.21	1.87	2.17	2.37
Mg		0.12	0.88	1.10	0.97
K		3.53	1.55		
Ca		0.33	8.58	4.34	6.66
HN_4		0.73	0.52	0.22	0.41

4.2 Discussion

Sulfide-bearing deposits are generally expected to produce acid mine drainage. This is because sulfide minerals are the major contributors to AMD generation, a process started by di-sulfides such as pyrite. According to Wilson & Anhaeusser (1998), the geological settings of some gold deposits are related or share geological traits with some silver deposits, thus, silver mining might also have a potential to produce AMD. Bigham and Cravotta (2016) stated that very acidic AMD is a mine effluent with a pH of 2 to 3. These effluents have elevated electrical conductivities surpassing the 500 mg/L limit which is in line with high metal loading into the river (Bigham and Cravotta, 2016). The post mining stage is expected to yield AMD in many cases, if there is no routine maintenance and a lack of buffering minerals.

The current status of mine drainage at Albert silver mine is stable with less threat to AMD production as proven by the outcomes of the study. The field measured pH of the Moses river is circum neutral and ranges from 7.0 and 7.78. Most of the EC values were below the aquatic standards (500 µS/cm), with an exception of sample MI3 with readings slightly above the standards (520 µS/cm). According to the South

African Water Quality Guidelines, the Moses River is not affected in relation to the TDS and salinities since they fall within recommended values (200–1100 mg/L). The elemental concentrations of Zn, Cu and Pb were also within the guidelines, however, As was found to exceed the guidelines. The water chemistry results indicate a low risk of AMD in the Moses River, which usually is characterized by elevated acidity, high sulfate concentrations and metals such as Fe, Cu, Zn, Co, Cr, Mn, Pb, Cd (Nieto *et al*., 2007).

The overall effects of AMD are highly dependent on the local conditions and varied widely depending on the geomorphology, the climate and the extent and distribution of the AMD generating minerals (McCarthy, 2011). The elemental concentrations of this study are in line with those noted by Dlamini *et al*. (2013), who noted that Pb (0.0554 ppm) was the least abundant ion and that Cu and Zn concentrations were below the maximum permissible limit as set by WHO 2008. According to McCarthy (2011), post-mining AMD rates increase due to ceased pumping but Wolkersdorfer (2008) reports that mine flooding usually improves the water quality after the first flush period, which is in line with the outcomes of this study with lower acid mine drainage rates because the shafts were fully rehabilitated.

AMD discharge introduces severe, long term effects on water quality and stream ecology in affected stream sections due to the active relationship to potentially toxic metals (Singer *et al*. 2018). The geomorphology of the tailings dam area also influences the tailings erosion to the nearby water body, therefore influencing the stream sediments geochemistry. The geochemistry of the rocks has direct influence on the drainage chemistry; the rock geochemistry is useful in the interpretation and confirmation of the mineralogical and kinetic test results (Price, 2009). It is expected that the stream sediment geochemistry be related to the tailings geochemistry if there is evidence of erosion and the rock geochemistry to be related to the drainage chemistry.

There is a positive correlation between the geochemistry of the tailings to that of the surface rocks, which was confirmed by the selected major oxides which were SiO_2, Fe_2O_3, Al_2O_3 and K_2O. The metal concentrations also supported the correlation as noted by the concentration of metals such as Pb, Cu, As to Zn. The correlation led to the confirmation that the surrounding rocks are the host rocks. The evidence of

tailings erosion prompted the investigation to deduce the influence of the tailings on stream sediments geochemistry. Comparison of the tailings and stream sediments geochemistry proved that the tailings have an influence since the metal concentration ranged from Pb, Cu, As to Zn in both. The kinetic test experiment did not reach the acidic conditions, therefore there was no metal leaching, which seems to be a contradiction when comparing the rock geochemistry and the drainage chemistry. Yet, as the water in the kinetic tests stayed circum-neutral, the metals and metaloids in the rock samples could not be mobilized.

According to Bailie and Robb (2004), the Albert silver deposit is type III: Sulfide-carbonate ore bodies (base- and precious metal rich). This criterion was developed by Crocker (1979) and Crocker *et al*. (2001). The Cu-Pb-Zn-Ag-carbonate association is the major part of the criteria; this criterion supported the correlations done in the study to compare the geochemistry of the affected geological materials. Bailie and Robb (2004) further stated that the fine-grained granite around the Albert silver mine is enriched in Al_2O_3, Fe_2O_3 and it is depleted in SiO_2 which complimented the outcomes of the study. The work done by Lusunzi *et al*. (2017) showed that SiO_2 was the dominant oxide in both the mine tailings and the source rocks followed by Fe_2O_3 and Al_2O_3. Novhe *et al*. (2014) noted that Fe, Mn, Al, As, Cr, Cu, Ni, Pb are likely potential pollutants that may negatively affect the water quality, and that the key leachable (semi-)metals include As, Cr, Cu, Ni, Pb. This was in line with the expected outcomes of the kinetic column leach test if the acidic conditions were met and metal leaching occurred.

The mineralogical information is a very important component of the AMD prediction as it determines the weathering rates and the geochemical stability of the geological materials (Price, 2009). The expected sulfide minerals that are responsible for acid mine drainage are pyrite, pyrrhotite, chalcopyrite and marcasite. Calcite and dolomite are the dominant acid neutralising carbonate minerals. According to Weber *et al.* (2004) and Weisener and Weber (2010), framboidal, disseminated pyrite minerals have a high potential to produce acid, which is due to their large surface area.

The sulfide minerals observed by XRD are pyrite, chalcopyrite, arsenopyrite and galena; these minerals were found in only three samples (B26T16, B27T7 and B27T8) out of the nine selected core samples and surface rocks samples which

makes 33.33% of the samples. Calcite was the only carbonate mineral identified and it was detected in only one sample (B27T8). Petrographic investigation of the core samples (B26T16, B27T7 and B27T8) portrayed paragenetic relationships between pyrite, chalcopyrite, galena, arsenopyrite, hematite and magnetite, which was also observed on the XRD mineral phases.

The whole rock geochemical data analysis conducted corresponds well with the outcomes of the XRD analysis. The high values of Al_2O_3 (%) and SiO_2 (%) proves that B26T12, B26T16, B36T22 and FG1 are altered and unaltered fine-grained porphyritic granite. The high values of Fe_2O_3 (%) and SiO_2 (%) in B26T16, B27T7, B27T8 and VS1 proved that these are from the mineralised and unmineralized quartz-hematite veins. The high values of Cu (ppm), Zn (ppm), As (ppm), Pb (ppm) and S (ppm) proves that B26T16, B27T7 and B27T8 are from the mineralised quartz veins of the Albert load. This is further confirmed by the deficiency of these elements from the other samples. The XRD results are also corresponding with the findings by Bailie and Robb (2004), Champion (1970) and Maulenbeld *et al*. (2014).

Pyrite was the major investigated sulfide mineral in this study, and the samples contained an equivalent euhedral and framboidal morphological pyrite grains. The grain surface area determined using IMAGEJ showed that framboidal pyrite grains have larger surface areas than the euhedral pyrite grains, which is due to its morphology.

The study conducted by Balci and Demirel (2017) also shows the paragenic relationship of pyrite, chalcopyrite, hematite and magnetite, and furthermore they found that the framboidal pyrite grains were more abundant than the euhedral grains and concluded that it has positive influence towards the formation of AMD. Lusunzi *et al*. (2017) also found that the low carbonate minerals on the samples has high potential to the formation of acid mine drainage which was contrary to this study.

The ABA is conducted to classify the geological material in terms of its potential to produce acid, the major classifications are in terms of computing the NNP and NPR using the pre-determined NP and AP (Skousen *et al*., 2002). The NAG test is also conducted to further classify the geologic material; this is also compared to the ABA results to improve the prediction confidence (see section 2.7.1. and 4.1.4.1. for the classification criterion). Sulfide bearing deposits are expected to have results that

confirm acid potential. The outcome of the static test in this investigation showed that most of the samples are non-acid generating. The comparison between the ABA (NNP and NPR) and the NAG test (NAG_{pH}) showed that most of the samples are uncertain in terms of its potential to produce acid.

The NNP and NPR classification results showed that 80% of the samples are non-acid generating. The NAG test ($NAG_{pH7.0}$) showed that 85% of the total number of samples is non-acid generating in terms of their acid generating potential. The comparison between the NAG_{pH} and the NNP showed that 60% of the total number of samples is uncertain in terms of their potential to generate acid and the comparison between the NAG_{pH} and the NPR showed that 70% of the total number of samples is uncertain in terms of their potential to generate acid. The NAG test was useful to further improve the classification since it showed that more samples are uncertain in terms of their potential to generate acid which prompted for kinetic tests.

Kotelo (2013) noted that single addition NAG test contains high level of uncertainties in terms of the sample potential to produce acid, therefore it was suggested that the sequential addition NAG test and the Kinetic test can alleviate these uncertainties. Findings made by Balci and Demirel (2017) supported the outcomes of this evaluation as they noted that majority of the samples had higher NP than AP which led to the computation of a non-acid generating NNP, furthermore they concluded that if site-specific geochemical and mineralogical conditions are well investigated and the results of the ABA and NAG tests merged this can be enough to conclude the acid potential of a geologic material.

The drainage chemistry for acid generating material is expected to yield a pH value below 5.6 and an EC above 1000 µS/cm. The acidity of the drainage is expected to be rising over the course of the kinetic test experiment with the alkalinity remaining constant to prove an acid generating condition (Price, 2009). As the experiment progress the sulfate, ferrous iron and metal concentrations should be increasing since this is directly proportional to the acidity and inversely proportional to the pH changes. The outcomes of the 20 weekly cycles showed non-acid generation.

The leachate pH over the 20 weekly cycles did not reach the acidic condition, rather it stayed circum-neutral. The electrical conductivity reading over the 20 weeks cycle

ranged below the set standard of 200–1000 µS/cm; in this the highest reading was found in B36 cycle number 1 and it was 148 µS/cm, which results from rock dust particles in the first cycle and the lowest reading was found in sample SRO (14 µS/cm). The acidity values were constant from all the columns throughout the experiment with values ranging below 0.3 mmol/L, whereas alkalinity showed a gradual increase in two columns which were B26 and B27; this gradual increase implied an acid neutralising condition. The alkalinity readings were in line with the NP readings because these two boreholes were the ones having high carbon values.

According to the pH values and the acidity readings, the leachate did not reach acidic conditions and there was no leaching of (semi-)metals, since leaching usually occurs at low pH. Therefore no metal analysis from the leachate samples was conducted. The results are supported by the low sulfate and ferrous iron concentrations. Five samples with higher EC readings were selected for IC analysis to identify any potential for metal leaching. The leachate analysis results were important for the evaluation of the potential for acid mine drainage as part of the purpose of the study and showed once more no (semi-)metal leaching potential.

Matsumoto *et al*. (2018) conducted a 40 weeks column leach test that is comparative to the setup of this evaluation, in this there were wetting and drying cycles, the experiment yielded acidic pH values but low EC values. According to Qureshi *et al*. (2016), kinetic tests on highly acidic rock samples yield high values of SO_4^{2-}, Fe and other metals, less acid rock samples yield low values, the latter correspond to the outcome of this evaluation. Bouzahzah *et al*. (2013) modified the kinetic test setup to fully correspond with the static test.

5. CHAPTER FIVE: CONCLUSIONS AND RECOMMENDATIONS

5.1 Conclusions

The study was conducted to evaluate the AMD potential at the Albert Silver Mine in Mpumalanga Province. The overall outcome of the study showed that the rocks at the Albert silver mine have a very low to negligible AMD formation potential. The following are the specific conclusions:

- Pyrite, arsenopyrite, chalcopyrite and galena were the only sulfide minerals identified, with pyrite being the primary acid generating mineral amongst the selected samples. Only three samples contained these sulfide minerals, the majority of the pyrite being framboidal in morphology, disseminated and with a large surface area. This, usually, contributes to the acid mine drainage potential,
- The XRD showed calcite in one sample with 5.6 wt%,
- There is no threat of AMD at the Moses river in terms of the current status since the water quality results yielded circum neutral pH values, EC values below 500 µS/cm and very low metal concentrations below the WHO and South African water quality guideline, and
- The rocks have a high potential to neutralise acid, since the majority of the samples yielded NNP values higher than 20 kg $CaCO_3$/t, NPR values higher than 1 and $NAG_{pH7.0}$ values below 5. This conclusion was further supported by the kinetic (column) test results that yielded circum neutral pH values, very low EC (below 148 µS/cm), constant acidity readings, a gradual increase of alkalinity, low sulfate and low ferrous iron concentrations over the 20 weeks experiment.

5.2 Recommendations

This study has shown that further techniques can be used to improve the evaluation of AMD. Specific recommendations arising from this study include:

- The use of QEMSCAN to identify the carbonate minerals,
- Use of PHREEQC to model the potential for AMD generation.

6. REFERENCES

Aphane, V. and Vermeulen, P. (2015). Acid Mine Drainage and its Potential Impact on the Water Resources in the Waterberg Coalfield, South Africa. *South African Journal of Geology,* 118(1), pp.55-70.

Bailie, R. and Robb, L. (2004). Polymetallic mineralization in the granites of the Bushveld Complex - examples from the central south-eastern lobe. *South African Journal of Geology*, 107(4), pp.633-652.

Balci, N. and Demirel, C. (2017). Prediction of Acid Mine Drainage (AMD) and Metal Release Sources at the Küre Copper Mine Site, Kastamonu, NW Turkey. *Mine Water and the Environment*, 37(1), pp.56-74.

Bhavtosh, S. and Shweta T. (2013). Simplification of Metal Ion Analysis in Fresh Water Samples by Atomic Absorption Spectroscopy for Laboratory Students. *Journal of Laboratory Chemical Education*, 1(3), pp.54-58.

Blowes D.W., Ptacek C.J., Jambor, J.L. and Weisener C.G. (2003). The geochemistry of acid mine drainage. In: Holland, H.D. and Turekian, K.K. (Eds.) *Treatise on Geochemistry.* Elsevier, Oxford, pp.131-190.

British Columbia AMD Task Force (1989). Draft Acid Rock Drainage Technical Guide, Vol. Crowd Publications, Victoria, B.C.p.274

Brodie, M.J., Broughton, L.M. and MacG, A. (1991). A Conceptual Rock Classification System for Waste Management and a Laboratory Method for ARD Prediction From Rock Piles. In*: Second International Conference on the Abatement of Acidic Drainage*. Canada: Montreal. p.352.

Bouzahzah, H., Benzaazoua, M., Bussiere, B. and Plante, B. (2013). Prediction of Acid Mine Drainage: Importance of Mineralogy and the Test Protocols for Static and Kinetic Tests. *Mine Water and the Environment*, 33(1), pp.54-65.

Cairncross, B. and Dixon, R. (1995). *Minerals of South Africa*. The Geological Society of South Africa, Linden, Johannesburg, p.290.

Capricco, F.T., Geidel, G., and Pelletier, M. (1981). Occurrence and prediction of acid drainages. J. Energy Div. Amer. Soc. Civil Engineers, 107(1). pp. 167-178.

Cawthorn, R.G. and Walraven, F 1987. *The Bushveld Complex: A time to fill and a time to cool*. EGRI Information Circular, University of the Witwatersrand, p.307.

Champion, A.T. (1970). *The Mineralogy and Related Geology of the Albert Silver Mine, Bronkhorstspruit – Transvaal* (unpublished). Master of Science. University of Natal, Durban, p.89.

Craig, J. and Vaughan, D. (1995). *Ore Microscopy and Ore Petrography*. 2nd ed. New York: Wiley, p.434.

Crocker, I. T., Eales, H. V. and Ehlers, D. L. (2001). The fluorite, cassiterite and sulphide deposits associated with the acid rocks of the Bushveld Complex. *Memoir of the Council for Geoscience, Pretoria,* 90, p.151.

Crocker, I. T. (1979). Metallogenic aspects of the Bushveld granites: fluorite, tin and associated rare-metal carbonate mineralization. *Special Publication of the Geological Society of South Africa*, 5, pp. 275-295.

Davis, G.B. And Ritchie, A.I.M. (1986). A model of oxidation in pyretic mine wastes, 1, Equations and approximate solutions. Appl. Math. Model. pp.314-322.

De Bruiyn, H. (1980). The geology of the acid phase of the Bushveld Complex, north of Pretoria – a geochemical/statistical approach*. Unpublished PhD thesis, University of the Orange Free State, Bloemfontein*, *South Africa,* pp.175.

Dlamini, C., Fadiran, A. and Thwala, J. (2013). A Study of Environmental Assessment of Acid Mine Drainage in Ngwenya, Swaziland. *Journal of Environmental Protection*, 4(11), pp.20-26.

Dold, B. (2014). Evolution of Acid Mine Drainage Formation in Sulphidic Mine Tailings. *Minerals*, 4(3), pp.621-641.

Dold, B. (2017). Acid rock drainage prediction: A critical review. *Journal of Geochemical Exploration*, 172(1), pp.120-132.

El Amari, K. and Hibti, M. (2019). A comparison between kinetic test results and natural weathering: The Abandoned Kettara Mine Tailings Pond. *Mine Water and the Environment.39(1).* pp.157-161.

Ferguson, K.D. (1986). Static and Kinetic Methods to Predict acid mine drainage. Proceedings: Fundamental and Applied Biohydrometallurgy, Eds. R.W. Lawrence, R.M.R. Branion and H.G. Ebner, Elsevier, Amsterdam, pp.486-488.

Ferguson, K.D. and Erikson, P.M. (1987). Will it generate AMD? An Overview of Methods to Predict Acid Mine Drainage. Proceedings Acid Mine Drainage Workshop, Halifax, Nova Scotia, March 23-26, Environment Canada, pp.41-70

Ferguson, K.D., and Morin, K. A. (1991). The Prediction of Acid Rock Drainage – Lessons from the Database. In: *Second International Conference on the Abatement of Acidic Drainage*, Canada: Montreal, pp.2-11.

Ferguson, K.D. and P.M. Erickson, (1988). Pre-Mine Prediction of Acid Mine Drainage. In: *Dredged Material and Mine Tailings*. Berlin: Springer, pp.24-43.

Ferré, E. C., Wilson, J. and Gleizes, G. (1999). Magnetic susceptibility and AMS of the Bushveld alkaline granites, South Africa. *Tectonophysics*, 307(1), pp.113-133.

Fleisher, M. and Mandarino, J.A. (1995). *Glossary of Mineral Species,* Mineralogical Record, Tucson, p.280.

Foose, M.P.; Zientek, M.L., and Klein, D.P. (1995). Magmatic Sulfide Deposits. In: Bray, E. *Preliminary Compilation of Descriptive Geoenvironmental Mineral Deposit Models.* Denver, CO: U.S. Geological Survey, pp.1-9.

Gibbs, R. (1973). Mechanisms of Trace Metal Transport in Rivers. *Science*, 180(4081), pp.71-73.

Grantham, G., 2012. *Structural Study of The Albert Silver Mine And Environs*. [image] Available at: http://www.lerama.co.za/projects/albert-silver-mine [Accessed 13 March 2020].

Hamilton, Q., Lamb, H., Hallett, C. and Proctor, J. (1999). Passive Treatment Systems for the Remediation of Acid Mine Drainage at Wheal Jane, Cornwall. *Water and Environment Journal*, 13(2), pp.93-103.

He, B.B., (2009). *Two-Dimensional X-ray Diffraction*. Wiley, Hoboken, N.J. pp.1-140.

Jacobs, J., Lehr, J. and Testa, S. (2014). *Acid mine drainage, rock drainage, and acid sulfate soils*. Hoboken, New Jersey: Wiley & Sons, pp.1-8.

Jambor, J.L., Nordstrom, D.K. and Alpers, C.N. (2000). Metal-sulfate salts from sulfide mineral oxidation. *Rev. Mineral. Geochem.* 40 (1), pp.303–350.

Kikkert, J. (1983). Practical geochemical analysis of samples of variable composition using X-ray fluorescence spectrometry. *Spectrochimica Acta Part B: Atomic Spectroscopy*, 38(5-6), pp.809-820.

Kinnaird, J.A. (2005). The Bushveld Large Igneous Province. Review Paper. The University of the Witwatersrand, Johannesburg, p.39.

Kleeman, G. J. and Twist, D. (1989). The compositionally zoned sheet-like granite pluton of the Bushveld Complex: evidence bearing on the nature of A-type magmatism. *Journal of Petrology*. 30(6), pp.1383-1414.

Kotelo, L. (2013). *Characterising The Acid Mine Drainage Potential Of Fine Coal Wastes*. MSc. University of Cape Town, p.166

Lapakko, K. (1994). Evaluation of Neutralization Potential Determinations for Metal Mine Waste and a Proposed Alternative. *Journal American Society of Mining and Reclamation*. 1994(1), pp.129-137.

Lawrence, R.W., Poling, G.P. and Marchant, P.B. (1986). Investigation Predictive Techniques for Acid Mine Drainage. Report on DSS Contract No. 23440-79178/01-SQ, Energy Mines and Resources, Canada, MEND report 1.16.1(a).

Lawrence, R.W. (1990). Prediction of the behaviour of mining and processing mining wastes in the environment. Proceedings, Western Regional Symposium on Mining and Mineral Processing Wastes, Ed. F.M. Doyle, May 30-june 1, Berkeley, CA, AIME/ SME Publication, Littleton, CO, pp.115-121.

Lerama Resources (2013). Geological Map of the Farm Roodepoortjie 250JR. [image] Available at: http://www.lerama.co.za/wp-content/uploads/2013/11/albert_silver_mine_31.png [Accessed 12 October 2018].

Lichtner, P., Steefel, C. and Oelkers, E. (1996). *Reactive Transport in Porous Media*. Washington, DC: Mineralogical Society of America, p.438.

Lishman, K.L. (2009). *The Acid Mine Drainage Potential of the Platreef, Northern Limp of the Bushveld Complex, South Africa.* Master of Science, University of the Witwatersrand, pp.70.

Lusunzi, R., Gumbo, J., Yibas, B. and Novhe, O. (2017). Geochemical and Mineralogical Characterization of Gold Mine Tailings for the Potential of Acid Mine Drainage in the Sabie-Pilgrim's Rest Goldfields, South Africa. In: *9th Int'l Conf. on Research in Chemical, Agricultural, Biological & Environmental Sciences (RCABES-2017)*. [online] Parys: pp.272-275. Available at: https://www.researchgate.net/publication/321483999_Geochemical_and_Mineralogical_Characterization_of_Gold_mine_tailings_for_the_potential_of_acid_mine_drainage_in_the_Sabie-Pilgrim's_Rest_Goldfields_South_Africa [Accessed 9 Feb. 2020].

Maiyana, A. (2003). *Evaluation and Validation of Geochemical Prediction Techniques for Underground Coal Mines in the Highveld Regions: Mineralogical Characterization of Pyrite for Long Term Prediction of Acid Rock Drainage in S7 Compartment, Brandspruit Colliery Sasol Secunda*. Master of Earth Sciences. University of Venda. p.70.

Makiese, J., Cukrowska, E., Tutu, H., Chimuka, L. and Weiersbye, I. (2015). Prediction of Acid Neutralizing Potential of Wetlands Affected By Gold Mining in a Semi-Arid Area. [online] 10th ICARD IMWA2015, p.11. Available at: https://www.imwa.info/docs/imwa_2015/IMWA2015_Lusilao-Makiese_027.pdf [Accessed 14 Jan. 2019].

Matsumoto, S., Ishimatsu, H., Shimada, H., Sasaoka, T. and Kusuma, G. (2018). Characterization of Mine Waste and Acid Mine Drainage Prediction by Simple Testing Methods in Terms of the Effects of Sulfate-Sulfur and Carbonate Minerals. *Minerals*, 8(9), p.403.

McCarthy, T. (2011). The Impact of Acid Mine Drainage in South Africa. *South African Journal of Science*, 107(5-6), pp. 1-7.

Meulenbeld, P., Grote, W. and Verryn, S. (2014). The Albert Silver Mine and Trippkeite Occurrence, Mpumalanga, South Africa. *Rocks & Minerals*, 89(5), pp.416-423.

Meteoblue (2018). *Climate Kwamhlanga*. [online] meteoblue. Available at: https://www.meteoblue.com/en/weather/forecast/modelclimate/kwamhlanga_south-africa_1105727 [Accessed 15 October 2018].

Nengovhela, A., Yibas, B. and Ogola, J. (2007). Characterisation of gold tailings dams of the Witwatersrand Basin with reference to their acid mine drainage potential, Johannesburg, South Africa. *Water SA*, 32(4), pp.499-506.

Nengovhela, A., Yibas, B. and Ogola, J. (2009). An investigation into the availability and role of oxygen gas in gold tailings dams of the Witwatersrand basin with reference to their acid mine drainage potential. *Water SA*, 33(2), pp.271-274.

Nieto, J.M., Sarmiento, A.M., Olias, M., Canovas, C.R., Riba, I., Kalman, J., Angle, D.T. (2007). Acid mine drainage pollution in the Tinto and Odiel rivers (Iberian pyrite belt, SW Spain) and bioavailability of the transported metals to the Huelva Estuary. *Environ Int,* 33(4). pp.445–455.

Novhe, N.O., Yibas, B., Netshitungulwani, R., and Lusunzi, R. (2014). Geochemical and Minerological Characterization of Mine Residue Deposits in the Komati/Crocodile Catchment, South Africa: an Assessment for Acid/Alkaline Mine Drainage. In: *Annual International Mine Water Association Conference – An Interdisciplinary Response to Mine Water Challenges*. [online] At Xuzhou, China: Sui, Sun & Wang, pp.359-365. Available at: https://www.imwa.info/docs/imwa_2014/IMWA2014_Novhe_359.pdf [Accessed 9 Feb. 2020].

Nordstrom, D.K and Southam, G. (1997). Geomicrobiology of Sulfide Mineral Oxidation. *Rev. Mineral.* 35(1), pp. 361–390.

Park, C.F. and McDiarmid, R.A. (1963). *Ore Deposits*. Freeman, 530pp.

Parker, G.K. and Robertson, A. (1999) Acid Drainage, AMEEF Occasional paper no 11. *Australian Minerals and Energy Environment Foundation*, Melbourne, pp. 101-117

Potop, V. and Soukup, J. (2008). Spatiotemporal characteristics of dryness and drought in the Republic of Moldova. *Theoretical and Applied Climatology*, 96(3-4), pp.305-318.

Potts, P. and Webb, P. (1992). X-ray fluorescence spectrometry. *Journal of Geochemical Exploration*, 44(1-3), pp.251-296.

Price, W.A., Errington, J, Koyanagi, V., (1997). Guidelines for the prediction of acid rock drainage and metal leaching for mines in British Columbia: part I. General procedures and information requirements. In: *Proc, 4th ICARD, Natural Resources Canada*, Ottawa, vol. 1, pp. 1–14.

Price, W.A. (2009). *Prediction manual for drainage chemistry from sulphidic geologic materials,* Canadian MEND report 1.20.1, Natural Resources Canada, p.579.

Pugh, C., Hossner, L. and Dixon, J. (1981). Pyrite and Marcasite Surface Area as Influenced by Morphology and Particle Diameter. *Soil Science Society of America Journal*, 45(5), p.979.

Qureshi, A., Maurice, C. and Öhlander, B. (2016). Potential of coal mine waste rock for generating acid mine drainage. *Journal of Geochemical Exploration*, 160, pp.44-54.

Reeks, G.W. (2012). *A History of Silver Mining in the greater Pretoria region, 1885 – 1999.* (Unpublished). Master of Arts, University of South Africa, Pretoria, p.213.

Robb, L.J., Robb, V.M. and Walraven, F. (1994). The Albert Silver Mine revisited: towards a model for polymetalic mineralization in granites of the Bushveld Complex, South Africa. *Exploration and Mining Geology,* 3(1), pp. 247-262.

Robinson, J., Frame, E. and Frame, G. (2005). *Undergraduate instrumental analysis*. 6th ed. New York: Dekker, p.1264.

Schippers, A. (2004). Biogeochemistry of metal sulfide oxidation in mining environments, sediments and soils. In: Amend JP, Edwards KJ, Lyons TW (eds) *Sulfur biogeochemistry*—past and present, vol 379. Geological Society of America, Boulder, pp. 49–62

Schmitz-Antoniak, C. (2013). Characterisation of FePt nanomagnets by X-ray absorption spectroscopy. *physica status solidi (a)*, 210(7), pp.1298-1304.

Schweitzer, J. K., Hatton, C. J. and de Waal, S. A. (1995). Regional lithochemical stratigraphy of the Rooiberg Group, Upper Transvaal Supergroup: a proposed new subdivision. *South African Journal of Geology*, 98(3), pp.245-255.

Schweitzer, J. K., Hatton, C. J. and De Waal, S. A. (1997). Link between the granitic and volcanic rocks of the Bushveld Complex, South Africa. *Journal of African Earth Sciences*, 24(1-2), pp.95-104.

Singer, D., Jefferson, A., Traub, E. and Perdrial, N. (2018). Mineralogical and geochemical variation in stream sediments impacted by acid mine drainage is related to hydro-geomorphic setting. *Elementa Science of the Anthropocene*, 6(1), p.31.

Skoog, D., Holler, F. and Crouch, S. (2007). *Principles of instrumental analysis*. 6th ed. Canada: Brooks/Cole, p.1056.

Skousen, J., Simmons, J., McDonald, L.M. and Ziemkiewicz, P. (2002). Acid – Base Accounting to Predict Post-Mining Drainage Quality on Surface Mines. *Journal of Environmental Quality*, 31(6), pp. 2034-2044.

Smart, R., Skinner, B., Levay, G., Gerson, A., Thomas, J., Sobleraj, H., Schumann, R., Welsner, C., Weber, P. (2002). Prediction of Kinetic control of Acid Mine Drainage, AMIRA International, ARD Test Handbook Project P387A.

Sobek, A.A., Schuller, W.A., Freeman, J.R. and Smith, R.M. (1978). Field and laboratory Methods Applicable to Overburdens and Minesoils, EPA 600/2-78-054, p.203.

Sobek, A. (2004). *Field and Laboratory Methods Applicable to Overburdens and Minesoils*. Denver: WRCC, OSM. pp.189-195

U.S. Environmental Protection Agency (1994). *Acid Mine Drainage Prediction*. Washington, DC: Office of Solid Waste, p.48.

Usher, B.H. (2003). Development and Evaluation of hydrogeochemical Prediction Techniques for South African Coalmines. Unpublished Ph.D thesis, University of Free State. p.329.

Van Zijl, J.S.V. (1965). *A Geological-Geophysical Investigation of the Albert Silver Mine North of Bronkhorstspruit, Transvaal*. *Bulletin 43 of the Geological Survey of South Africa*. Government Printer, Pretoria, p.84.

Viljoen, M.J. (2016). The Bushveld Complex – Host to the World's Largest Platinum, Chromium and Vanadium Resources. *Episodes*, 39(2), pp. 239-268.

Walraven, F. (1987). Textural, geochemical and genetic aspects of the granophyric rocks of the Bushveld Complex. Memoir 72, Geological Survey South Africa, p.145.

Walraven, F. (1997). Geochronology of the Rooiberg Group, Transvaal Supergroup, South Africa. *Information Circular of the Economic Geology Research Unit, University of the Witwatersrand*, *Johannesburg*, 316(1), p.18.

Weber P.A, Stewart, W.A, Skinner, W.M, Weisener, C.G, Thomas, J.E, Smart R.S.C. (2004). Geochemical effects of oxidation products and framboidal pyrite oxidation in acid mine drainage prediction techniques. *Appl Geochem* 19(1), pp.1953–1974.

Weisener, C.G., Weber, P.A. (2010) Preferential oxidation of pyrite as a function of morphology and relict texture. *N Z J Geol Geophys* 53(2–3), pp.167–176.

Wilson, M. G. C. & Anhaeusser, C. R. (1998): The Mineral Resources of South Africa, 6 edn. Silverton (Council for Geoscience), p.740.

Wolkersdorfer, C. 2008. Water Management at Abandoned Flooded Underground Mines – Fundamentals, Tracer Tests, Modelling, Water Treatment. Heidelberg: Springer, p.465.

APPENDICES

A.1 Ethical Clearance Certificate

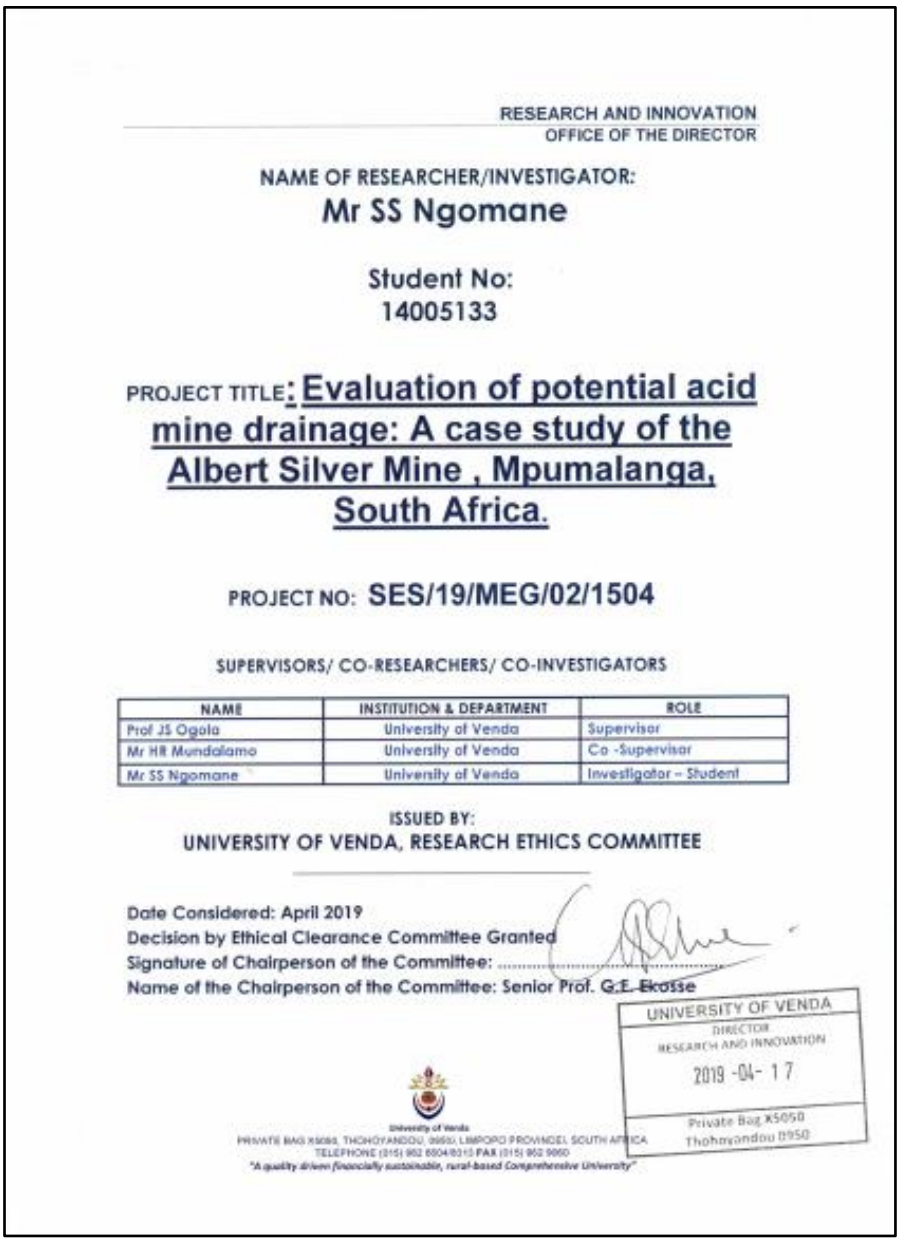

RESEARCH AND INNOVATION
OFFICE OF THE DIRECTOR

NAME OF RESEARCHER/INVESTIGATOR:
Mr SS Ngomane

Student No:
14005133

PROJECT TITLE: **Evaluation of potential acid mine drainage: A case study of the Albert Silver Mine , Mpumalanga, South Africa.**

PROJECT NO: **SES/19/MEG/02/1504**

SUPERVISORS/ CO-RESEARCHERS/ CO-INVESTIGATORS

NAME	INSTITUTION & DEPARTMENT	ROLE
Prof JS Ogola	University of Venda	Supervisor
Mr HR Mundalamo	University of Venda	Co -Supervisor
Mr SS Ngomane	University of Venda	Investigator – Student

ISSUED BY:
UNIVERSITY OF VENDA, RESEARCH ETHICS COMMITTEE

Date Considered: April 2019
Decision by Ethical Clearance Committee Granted
Signature of Chairperson of the Committee: .....
Name of the Chairperson of the Committee: Senior Prof. G.E. Ekosse

UNIVERSITY OF VENDA
DIRECTOR
RESEARCH AND INNOVATION
2019 -04- 17
Private Bag X5050
Thohoyandou 0950

University of Venda
PRIVATE BAG X5050, THOHOYANDOU, 0950, LIMPOPO PROVINCE, SOUTH AFRICA
TELEPHONE (015) 962 8804/8313 FAX (015) 962 9660
"A quality driven financially sustainable, rural-based Comprehensive University"

A.2 Permission to remove samples from MINTEK

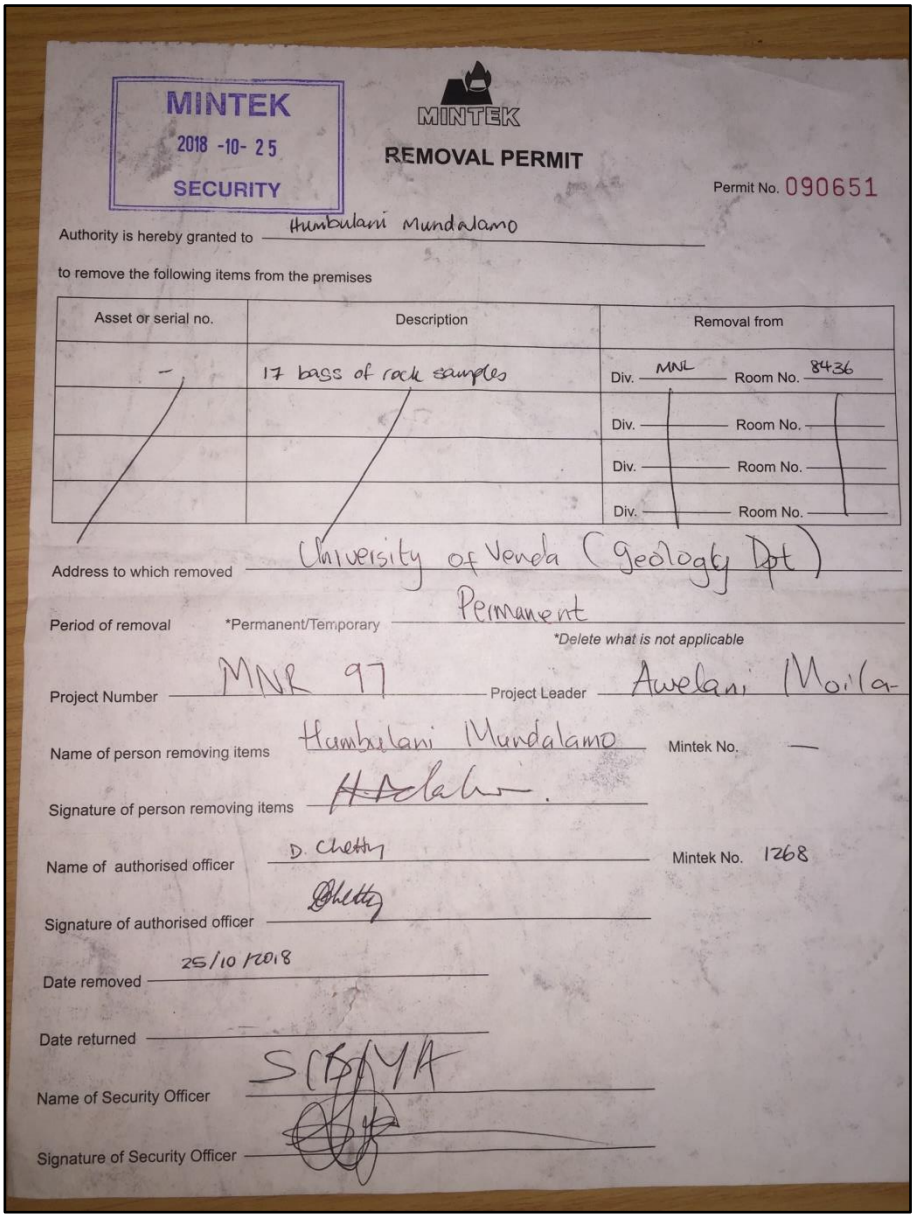

MINTEK
2018 -10- 25
SECURITY

MINTEK

REMOVAL PERMIT

Permit No. 090651

Authority is hereby granted to Humbulani Mundalamo

to remove the following items from the premises

Asset or serial no.	Description	Removal from
–	17 bags of rock samples	Div. MNL Room No. 8436
		Div. Room No.
		Div. Room No.
		Div. Room No.

Address to which removed University of Venda (Geology Dpt)

Period of removal *Permanent/Temporary Permanent

*Delete what is not applicable

Project Number MNR 97 Project Leader Awelani Moila

Name of person removing items Humbulani Mundalamo Mintek No. —

Signature of person removing items

Name of authorised officer D. Chetty Mintek No. 1268

Signature of authorised officer

Date removed 25/10/2018

Date returned

Name of Security Officer SIBUYA

Signature of Security Officer

A.3 Column Leach Test Experiment Properties

The following table consist of all the experimental parameters, the figure below shows the experimental setup.

Table A.1: Column leach test experiment properties

Columns dimensions	**Columns dimensions**	**Pumps properties**
Column diameter: 7 cm Column height: 50 cm Sample height: 20 cm	Column diameter: 7 cm Column height: 50 cm Sample height: 20 cm	Pump name: Heidolph pumpdrive 5006 (SP Standard) Peristaltic pumps. Pumping speed: 50 rpm Pumping direction: Anti-clockwise direction
Pipes properties	**Insulation and screening**	
Pipe type: rubber flexible Pipe length: 1 m Pipe diameter: 0.65 cm	Insulation type: hydrophobic insulator Insulation dimensions: 2 cm height by 7 cm diameter Screening type: Fly net Screening location: on the water input and output areas Screening dimensions: 4 × 4 cm	

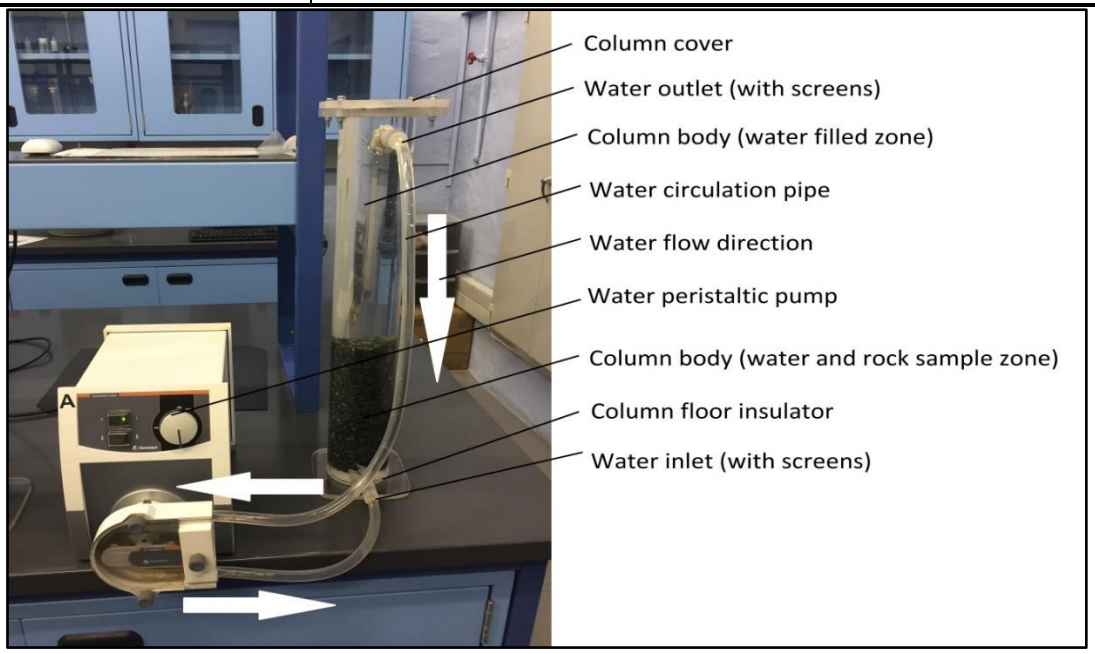

A.4 Diffraction Peak Patterns for Sample B26T12

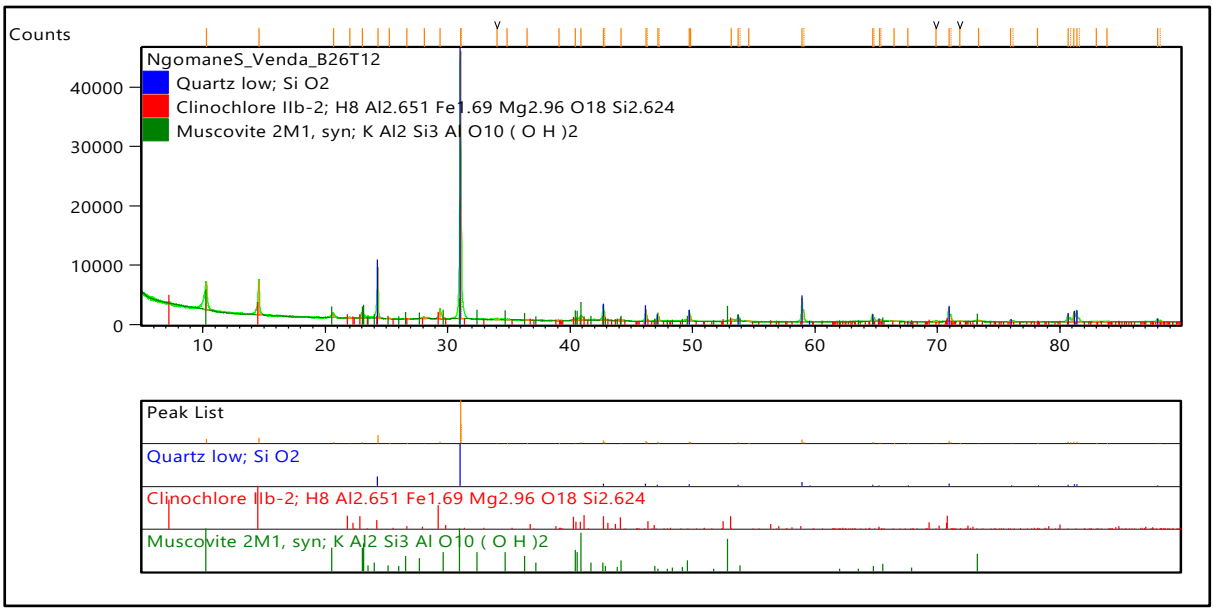

A.5 Diffraction Peak Patterns for Sample B26T16

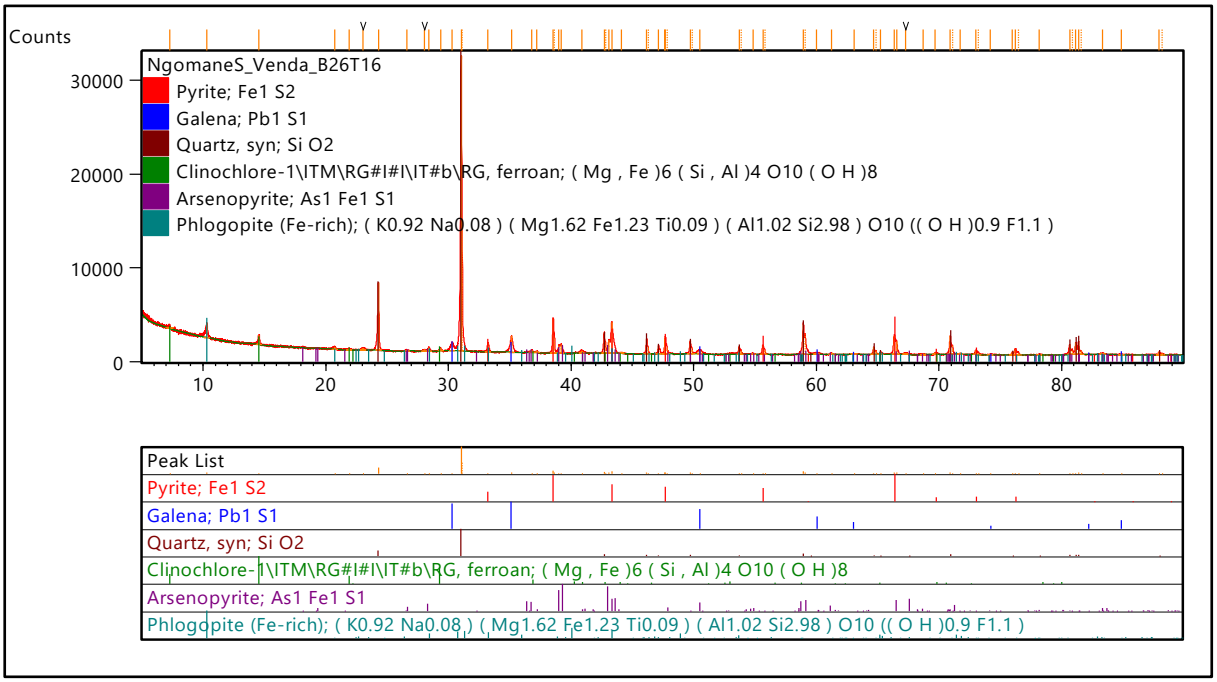

A.6 (d) Diffraction Peak Patterns for Sample B27T7

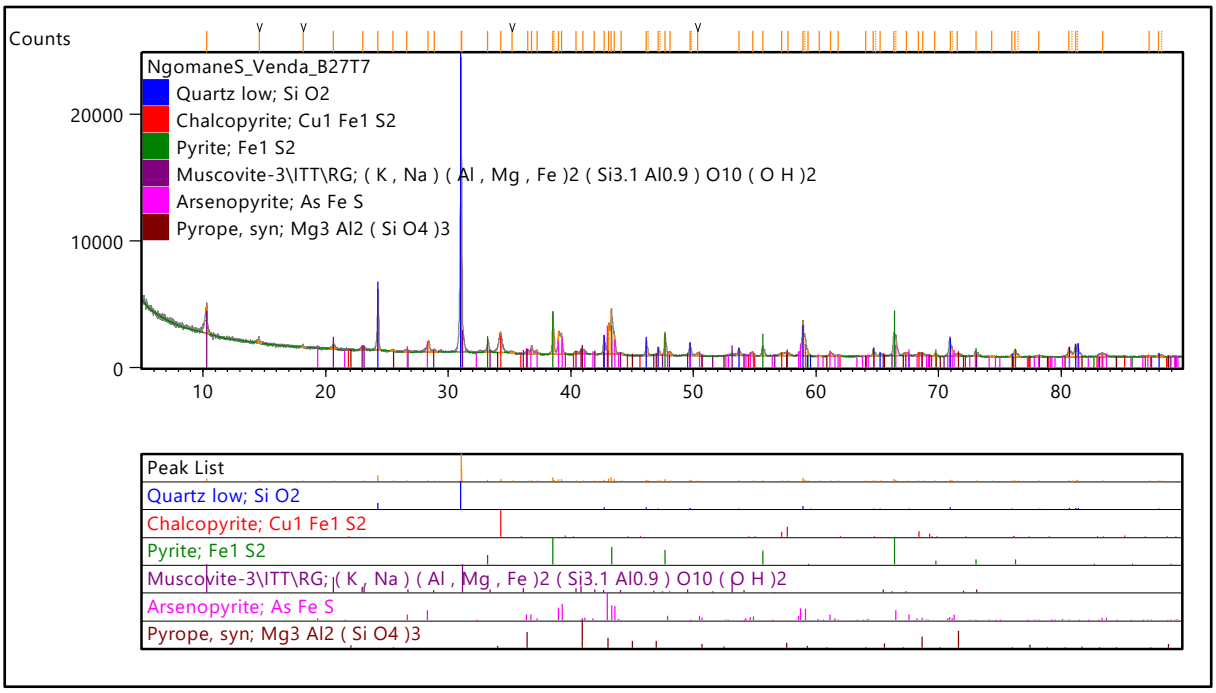

A.7 Diffraction Peak Patterns for Sample B27T8

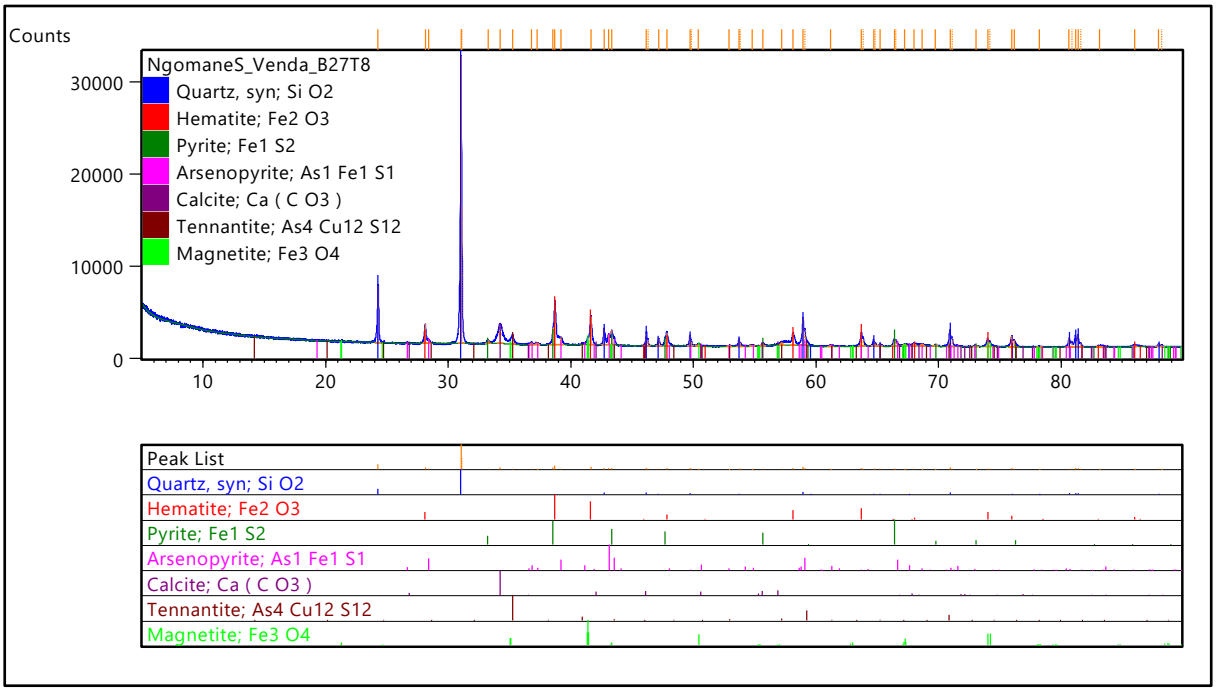

A.8 Diffraction Peak Patterns for Sample B36T17

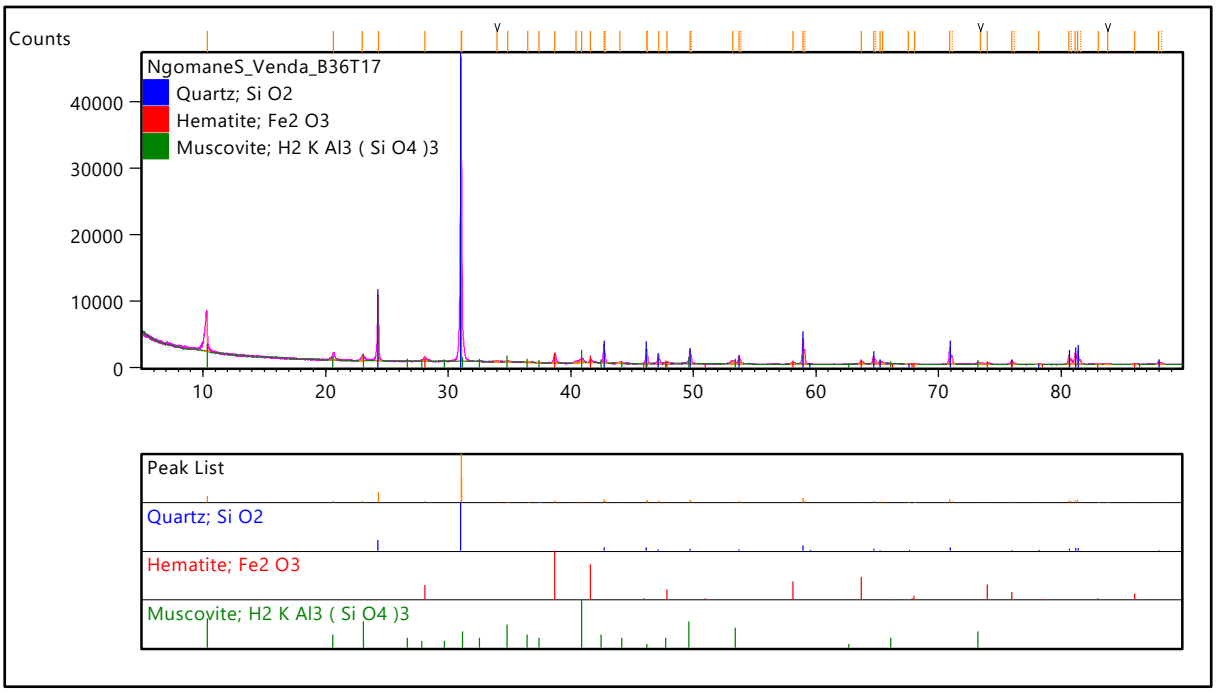

A.9 Diffraction Peak Patterns for Sample B27T8

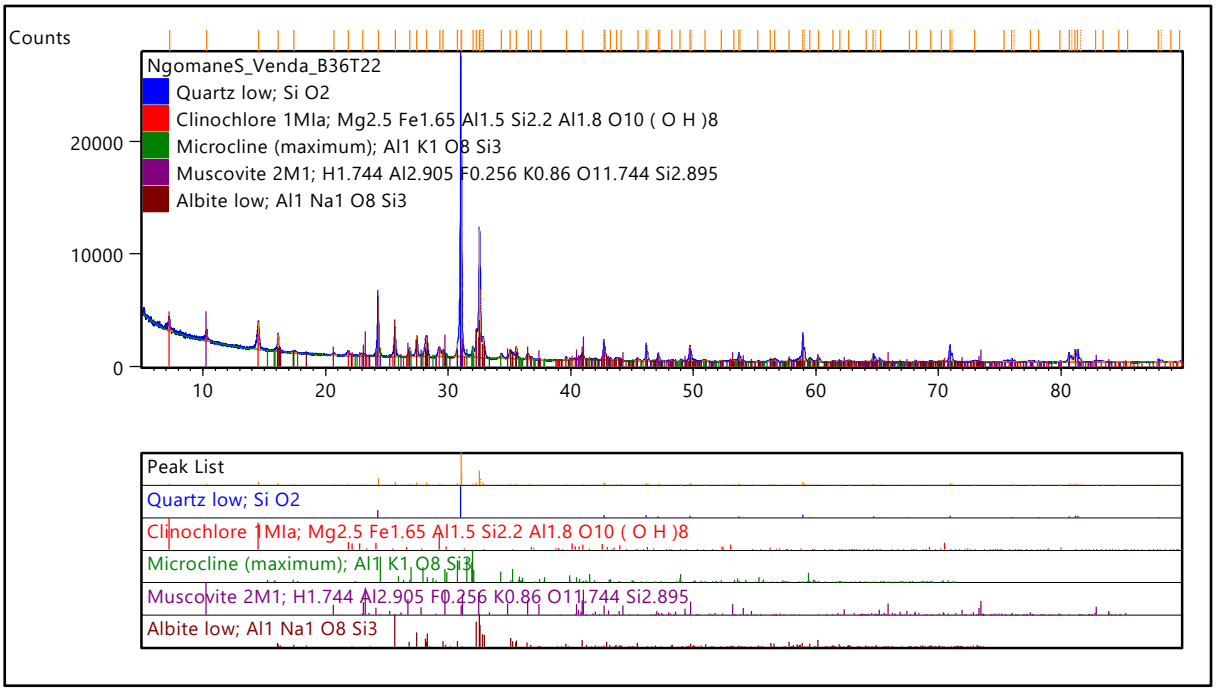

A.10 Diffraction Peak Patterns for Sample VS1

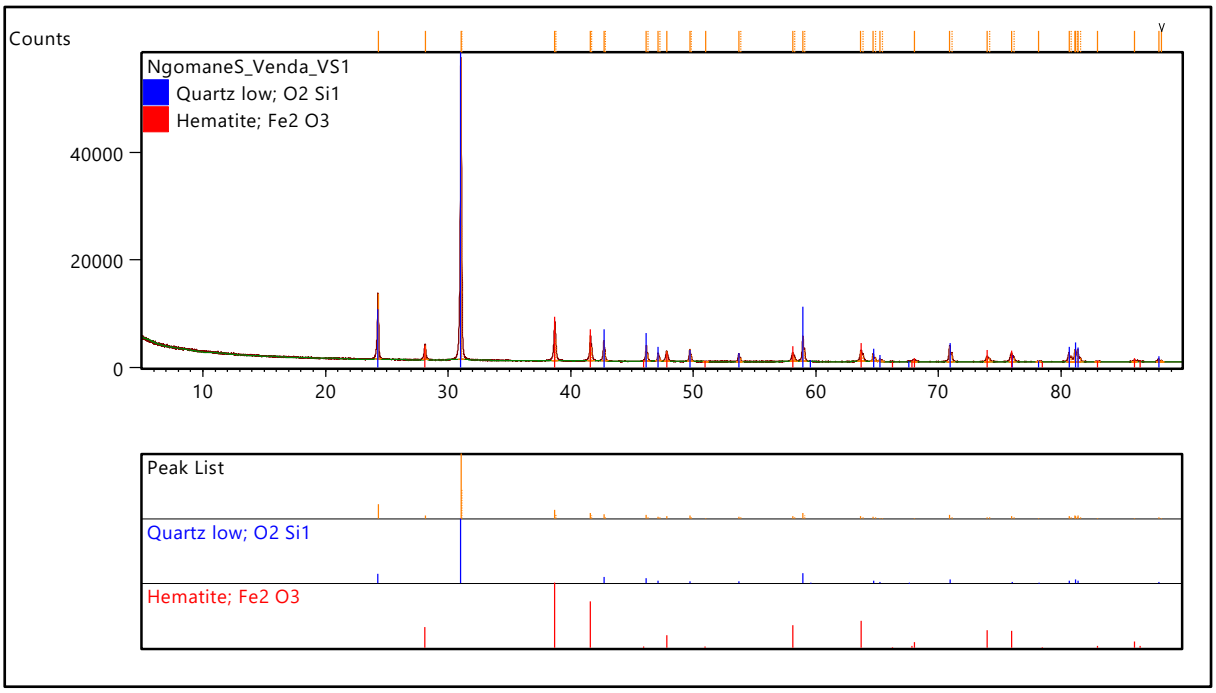

A.11 Diffraction Peak Patterns for Sample FG1

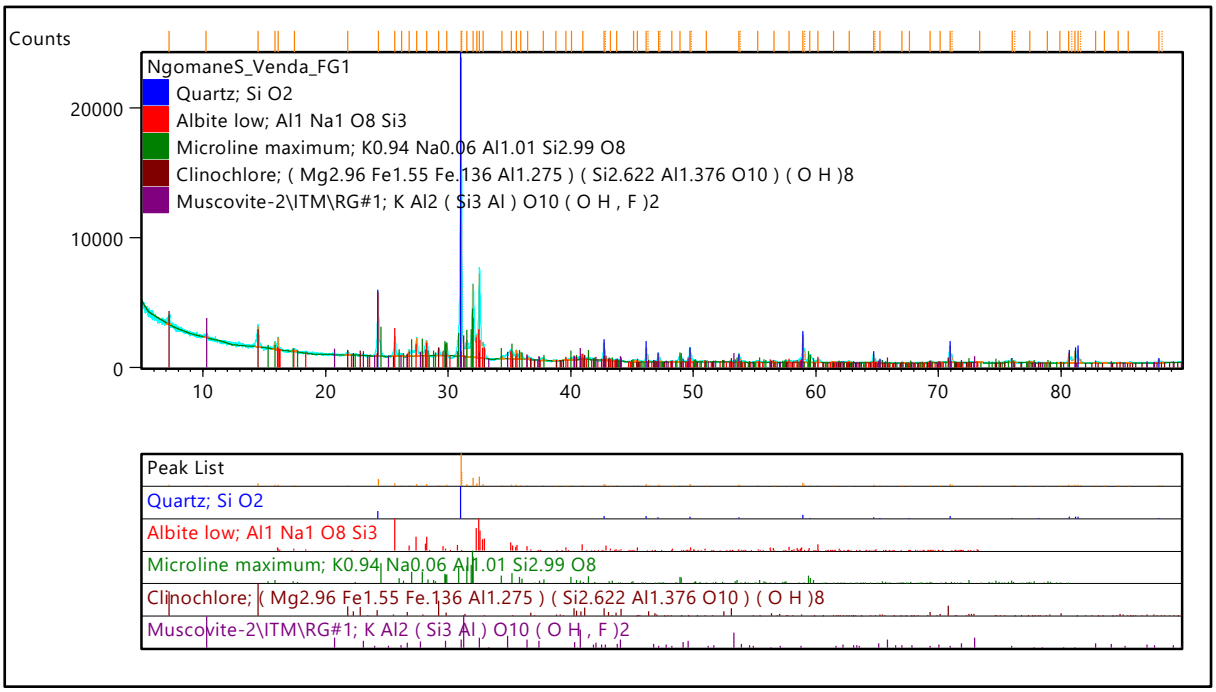

A.12 Diffraction Peak Patterns for Sample DS1

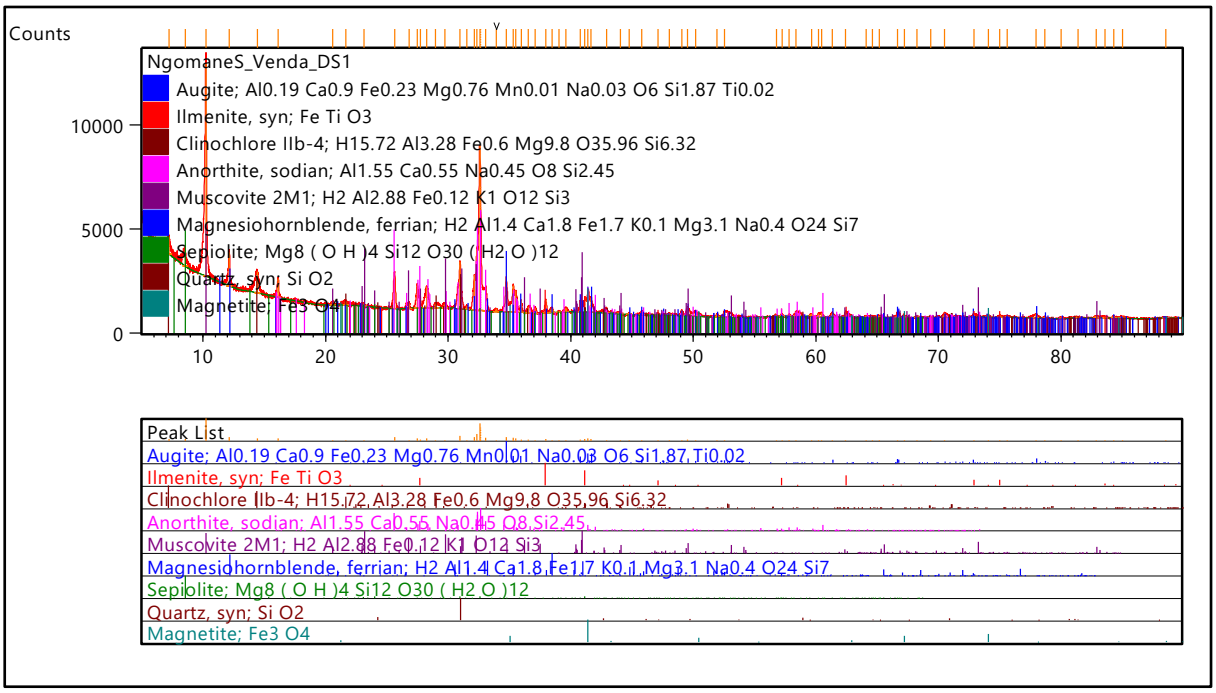

A.13 Neutralisation Potential (NP) Input Data, Results and Titration Curves; Acid (HCl) and Base (NaOH) normality always 0,0972 N

Sample ID	Re-action	Fizz Rating	Acid, mL	Base, mL	Acidity, mmol/L	NP, kg $CaCO_3$/t
B26-T12	None	0	20	5.1173	12.43	36.165
B26-T13	None	0	20	5.0937	12.373	36.2223
B26-T14	None	0	20	5.2676	12.795	35.7997
B26-T15	None	0	20	5.2321	12.709	35.886
B26-T16	None	0	20	5.1576	12.528	36.067
B26-T17	None	0	20	5.23	12.703	35.8911
B26-T18	Slight	1	40	3.9831	9.675	87.5211
B27-T7	None	0	20	5.1591	12.531	36.0634
B27-T8	None	0	20	5.1535	12.518	36.077
B27-T9	Slight	1	40	8.8107	21.401	75.78
B36-T16	None	0	20	5.1212	12.439	35.1555
B36-T17	None	0	20	5.206	12.645	35.9494
B36-T18	None	0	20	4.7972	11.652	36.9428
B36-T19	None	0	20	5.15	12.509	36.0855
B36-T20	None	0	20	5.1901	12.607	35.9881
B36-T21	None	0	20	5.2123	12.661	35.9341
B36-T22	None	0	20	4.8879	11.873	36.7224
FG1	None	0	20	5.0938	12.373	36.2221
VS1	None	0	20	5.4195	13.164	35.4306
DS1	None	0	20	3.8003	9.231	39.3653

B26-T12

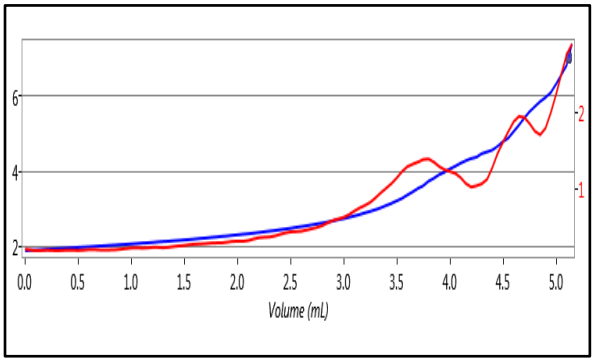

B26-T13

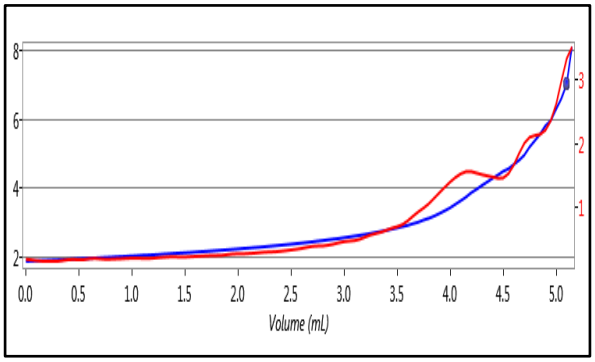

B26-T14

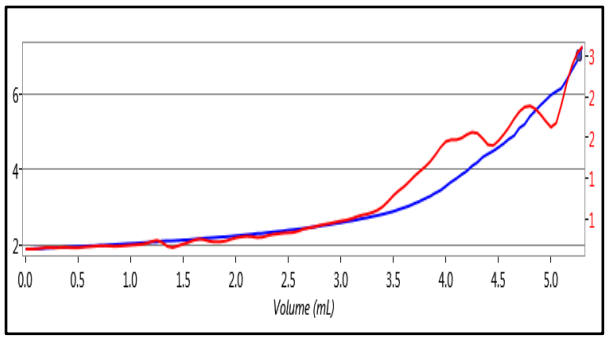

B26-T15

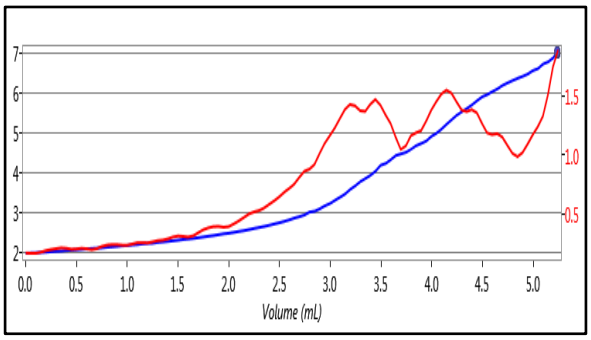

B26-T16

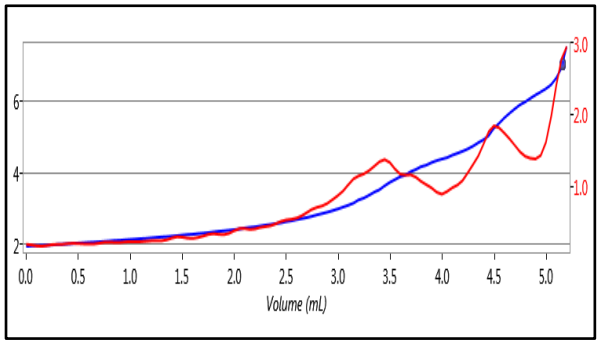

B26-T17

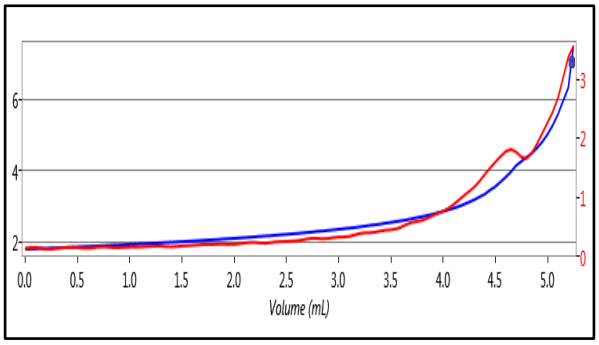

B26-T18

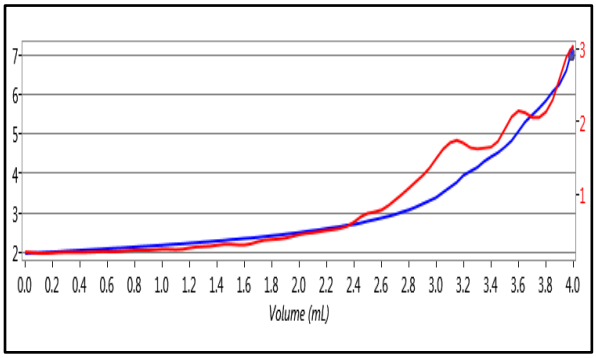

B27-T7

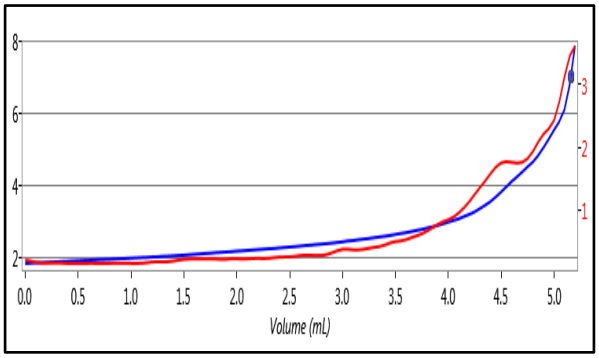

B27-T8

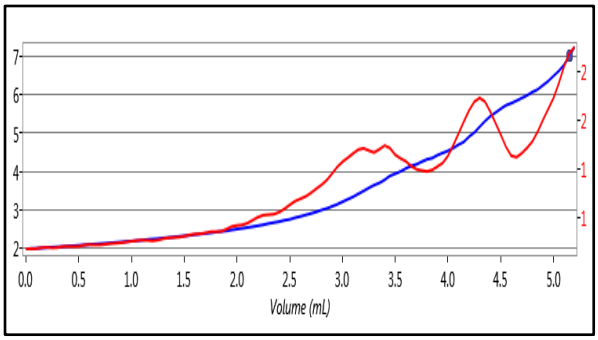

B27-T9

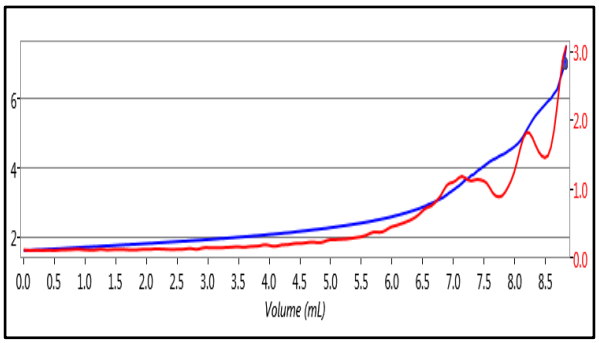

B36-T16

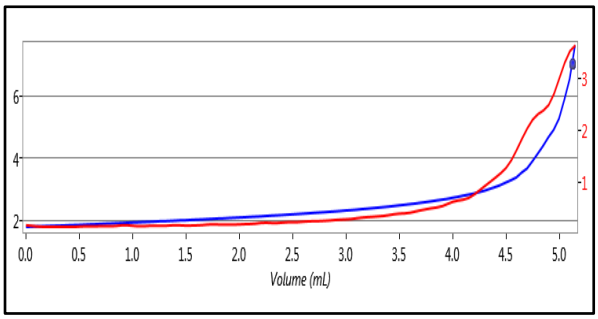

B36-T17

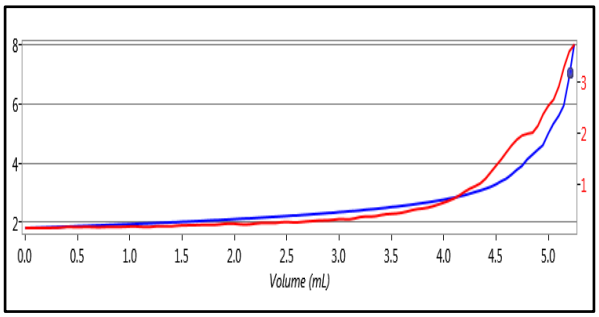

B36-T18

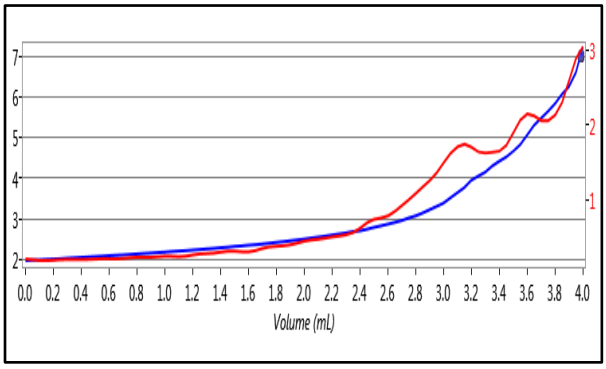

B36-T19

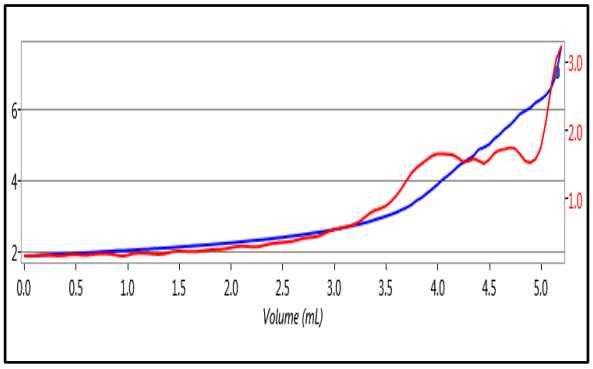

B36-T20

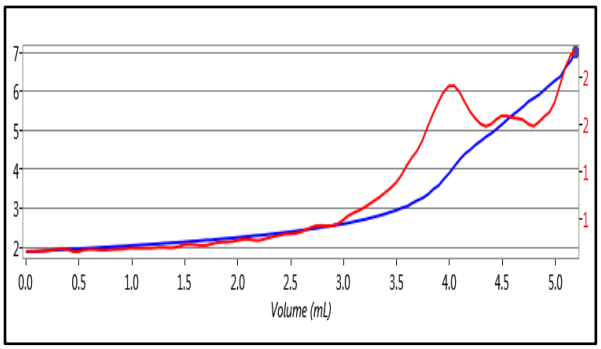

B36-T21

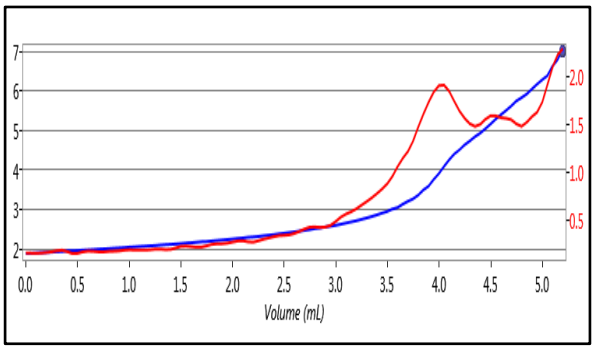

B36-T22

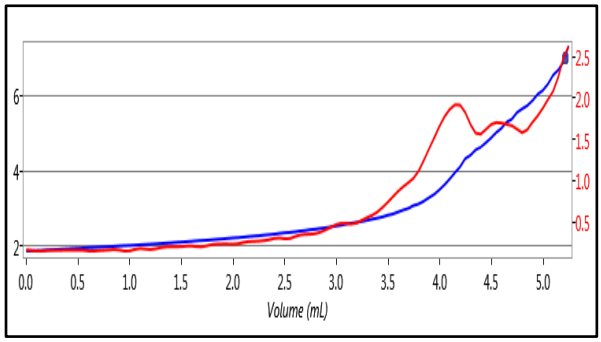

FG1

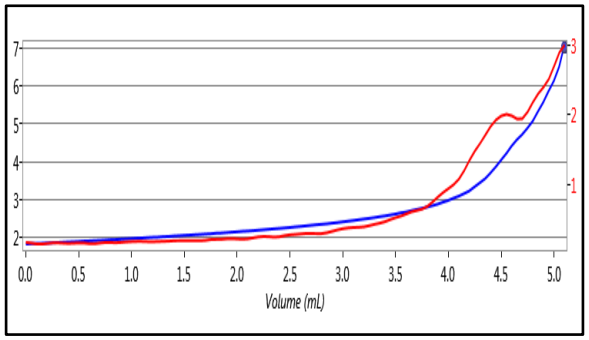

VS1

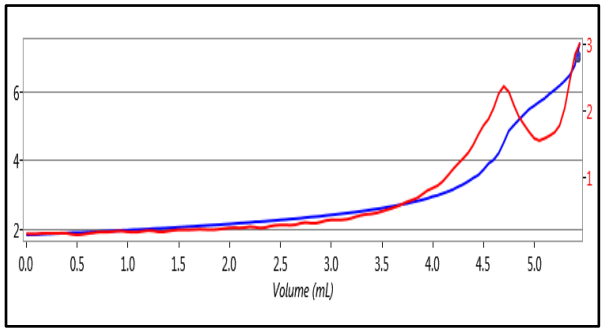

DS1

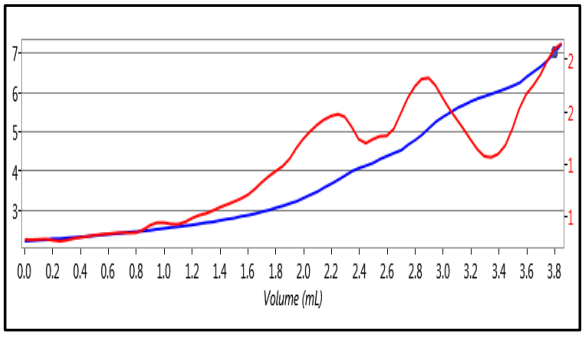

A.14 Net Acid Generation (NAG) Input Data, Results and Titration Curves; Base: NaOH

Sample ID	Preboil pH	NAG_{pH}		$NAG_{pH4.5}$		$NAG_{pH7.0}$	
		pH	EC	Base, mL	NAG	Base, mL	NAG
B26-T12	3.16	3.59	369	0.2	0.3756	0.5773	1.0842
B26-T13	3.65	3.75	327	0.2	0.3756	0.6913	1.2983
B26-T14	2.55	2.83	915	0.7499	1.4083	1.2511	2.3496
B26-T15	2.68	2.90	1118	0.65	1.2207	2.0916	3.928
B26-T16	2.39	2.52	1633	1.6999	3.1924	2.2862	4.2935
B26-T17	2.43	2.39	1947	2.2498	4.3196	2.7273	5.2364
B26-T18	4.76	5.62	426	0	0	0.05	0.096
B27-T7	3.35	4.21	344	0.05	0.096	0.3828	0.735
B27-T8	2.34	2.37	2759	2.6998	5.1836	6.4478	12.378
B27-T9	3.29	2.69	1322	0.9499	1.8238	1.4743	2.8307
B36-T16	3.87	3.67	269	0.2	0.3936	0.8221	1.6179
B36-T17	3.44	3.62	338	0.15	0.2952	0.5525	1.0873
B36-T18	2.63	3.22	751	0.4	0.7872	1.2771	2.5133
B36-T19	2.39	2.36	2247	2.64	5.1955	3.6107	7.1059
B36-T20	2.59	2.96	982	0.55	1.0828	1.4689	2.8908
B36-T21	2.75	3.46	590	0.2	0.3792	0.737	1.3974
B36-T22	4.36	4.88	303	0	0	0.3763	0.7135
FG1	4.42	3.98	248	0.2	0.372	0.7657	1.4518
VS1	3.26	5.37	259	0	0	0.1042	0.1976
DS1	4.02	5.36	367	0	0	0.1048	0.1987

B26-T12

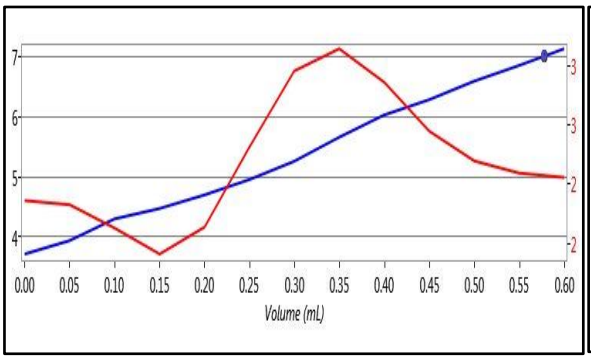

B26-T13

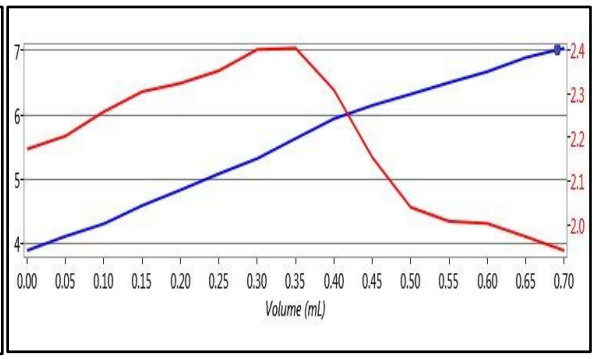

B26-T14

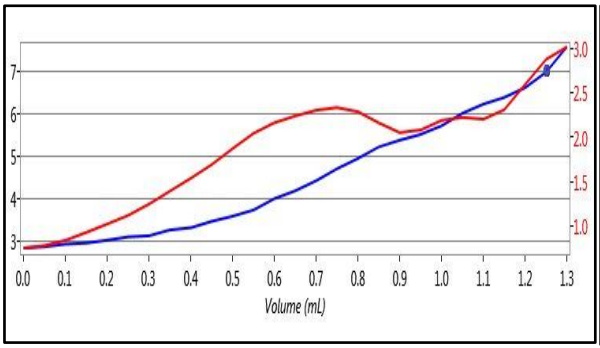

B26-T15

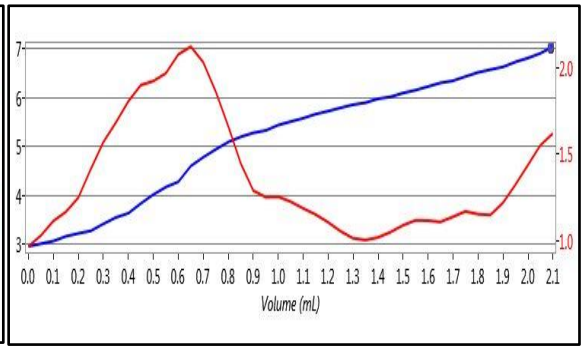

B26-T16

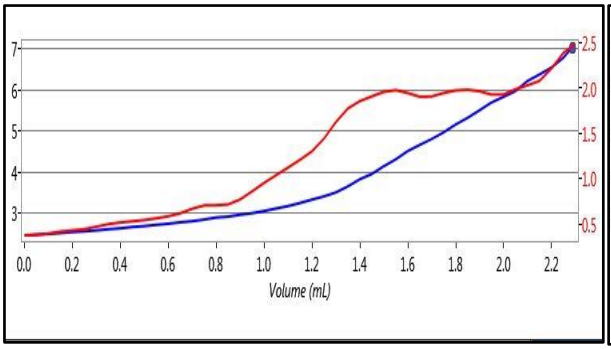

B26-T17

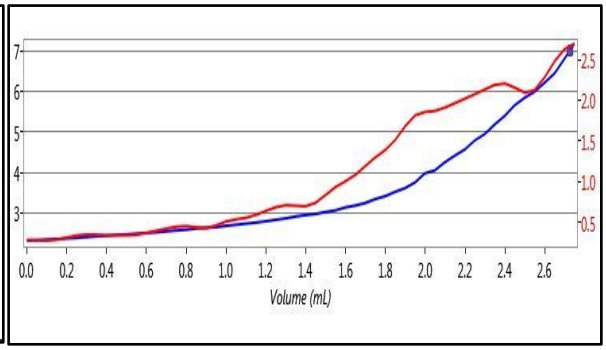

B26-T18

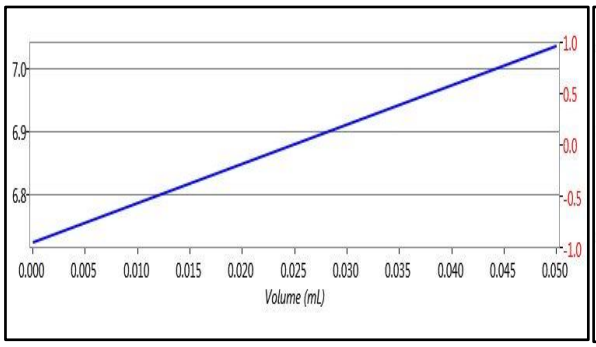

B27-T7

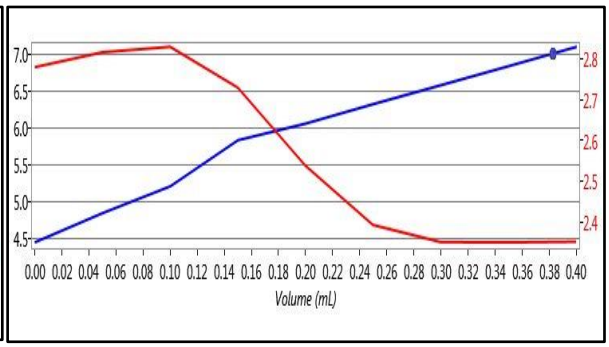

B27-T8

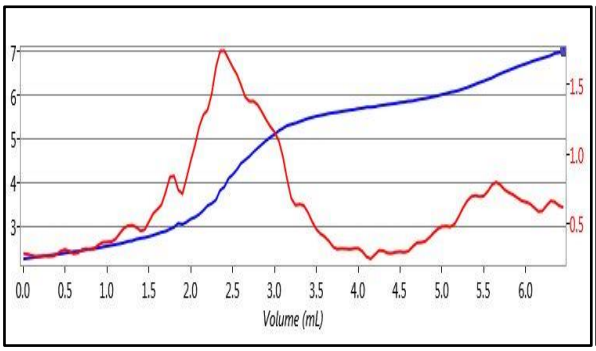

B27-T9

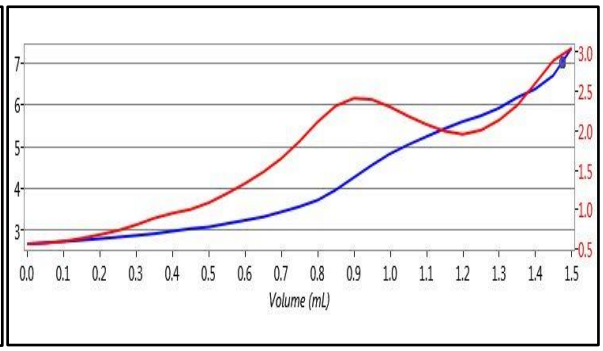

B36-T16

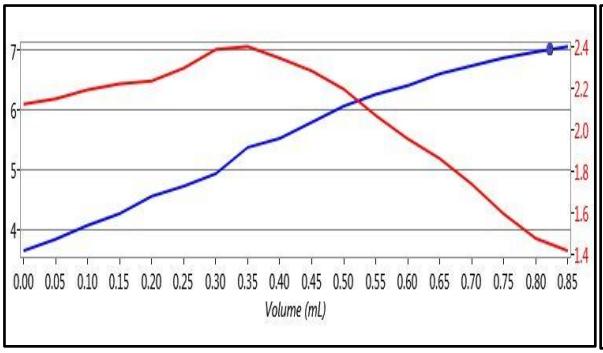

B36-T17

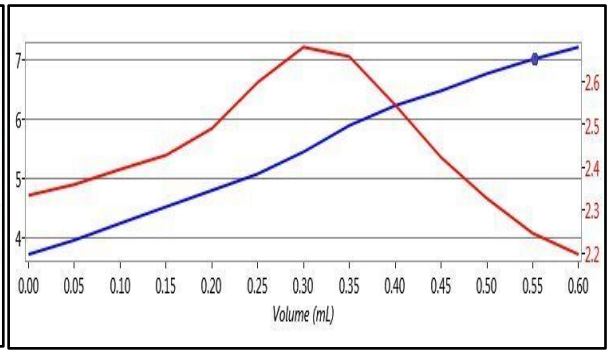

B36-T18

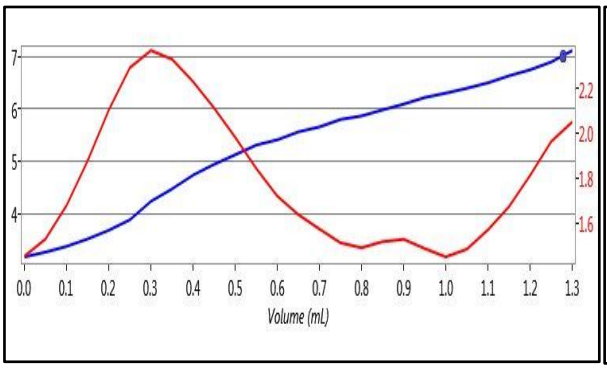

B36-T19

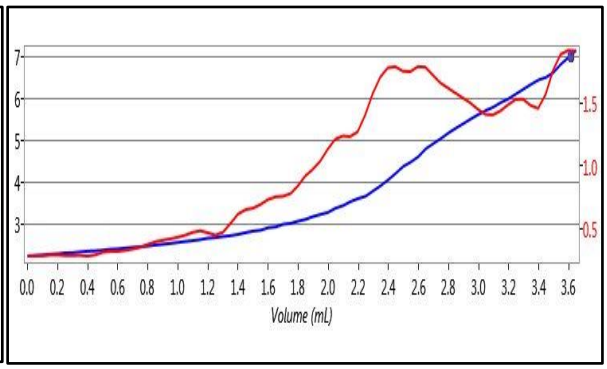

B36-T20

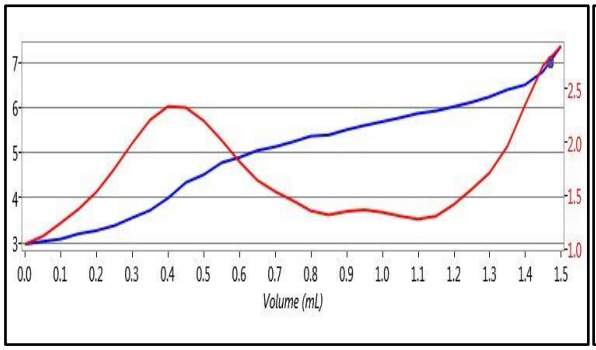

B36-T21

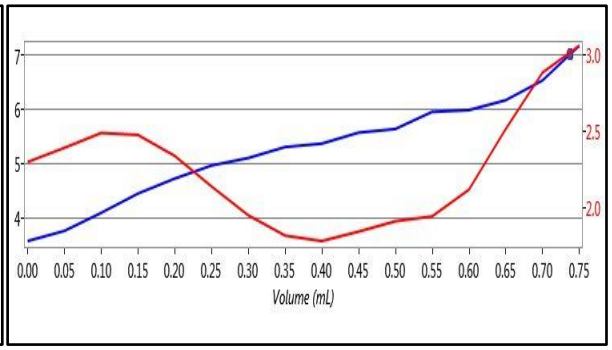

B36-T22

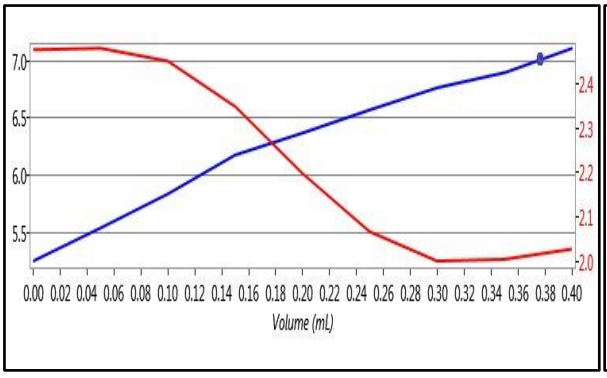

FG1

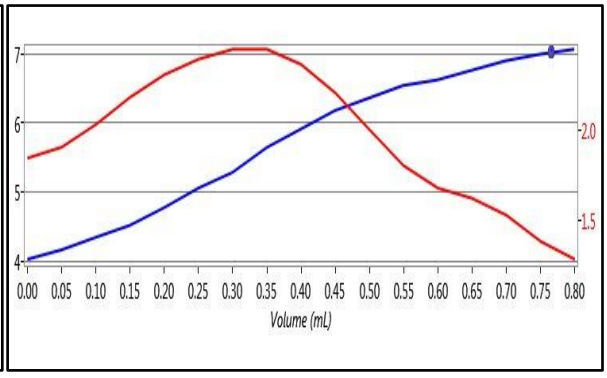

VS1 **DS1**